Wissenschaftlich-Technische Berichte
FZR-432
August 2005

U. Rohde, T. Höhne, S. Kliem, M. Scheuerer,
B. Helmström, T. Toppila, T. Dury, J. Klepac, J. Remis,
P. Mühlbauer, L. Vyskocil, I. Farkas, Y. Bezrukov,
A. Aszodi, I. Boros, J. A. Lycklama a Nieholt

The European project FLOMIX-R: Fluid mixing and flow distribution in the reactor circuit Final Summary report

Editor: U. Rohde

Bibliothek FZ Rossendorf
01287950

Forschungszentrum
Rossendorf

EUROPEAN COMMISSION
5th EURATOM FRAMEWORK PROGRAMME 1998-2002
KEY ACTION : NUCLEAR FISSION

FLOMIX-R

FIKS-CT-2001-00197

Deliverable D13

Final Summary report (extended version)

Dissemination level :
PU: public

Authors

Forschungszentrum Rossendorf (FZR)
U. Rohde, T. Höhne, S. Kliem

Gesellschaft für Anlagen- und Reaktorsicherheit (GRS)
M. Scheuerer

Vattenfall Utveckling
B. Hemström

Fortum Nuclear Services
T. Toppila

Paul Scherrer Institute
T. Dury

VUJE Trnava
J. Klepac, J. Remis

NRI Rez
P. Mühlbauer, L. Vyskocil

AEKI Budapest
I. Farkas

EDO Gidropress
Y. Bezrukov

TU Budapest
Aszodi, I. Boros

NRG Petten
J. A. Lycklama a Nieholt

Manuscript prepared by

U. Rohde

Contents

	Executive Summary	**5**
A	**Objectives and Scope**	**6**
B	**Work Programme**	**7**
C	**Work performed and Results**	**7**
C.1	**Identification of the key mixing phenomena (WP 1)**	**10**
C.2	**Slug mixing (WP 2)**	**15**
C.2.1	**Description of the test facilities**	**15**
C.2.2	**Results of slug mixing tests**	**20**
C.2.3	**Experiments on buoyancy driven mixing**	**29**
C.3	**Steady state mixing and flow distribution (WP 3)**	**36**
C.3.1	**Introduction**	**36**
C.3.2	**ROCOM steady-state mixing experiments**	**37**
C.3.3	**Measurements at NPP**	**41**
C.4	**CFD code validation (WP 4)**	**43**
C.4.1	**Introduction**	**43**
C.4.2	**Application of the Best Practice Guidelines**	**45**
C.4.3	**Post-test calculations of ROCOM steady-state mixing tests**	**49**
C.4.3.1	CFX results	**49**
C.4.3.2	FLUENT results	**54**
C.4.3.3	Conclusions on CFD calculations for ROCOM steady-state mixing tests	**57**
C.4.4	**CFD calculations for the ROCOM slug mixing tests**	**58**
C.4.4.1	CFX-4 calculations	**59**
C.4.4.2	CFX-5 calculations	**62**
C.4.4.3	FLUENT couterpart calculations	**70**
C.4.5	**Quantitative comparison of CFD results with measurement data for the ROCOM non-buoyant experiments**	**73**
C.4.5.1	Methodology of comparison	**73**
C.4.5.2	Comaprison for the steady-state experiment ROCOM-stat01	**75**
C.4.5.3	Comparison for the slug mixing experiment ROCOM-02	**77**
C.4.6	**Simulation of ROCOM buoyant mixing experiments**	**83**
C.4.7	**CFD calculations for Vattenfall experiments**	**88**
C.4.7.1	Description of CFD calculations	**88**
C.4.7.2	Comparison with measurements	**91**

C.4.8	**CFD calculations for the Fortum PTS experiments**	**99**
C.4.8.1	Description of the CFD simulations	**99**
C.4.8.2	CFD results and comparison with measurements	**102**
C.4.9	**CFD calculations for the Gidropress experiments**	**106**
C.4.9.1	Description of the calculations	**106**
C.4.9.2	Results of Gidropress slug mixing calculations	**107**
C.4.10	**CFD simulation of mixing tests at Paks NPP (VVER-440 reactor)**	**110**
C.4.10.1	Decsription of the CFD calculations	**110**
C..4.10.2	Results of the CFD analyses	**114**
C.4.11	**Summary and conclusions from CFD code validation**	**118**
C.4.11.1	Conclusions from sensitivity tests according to the BPG	**118**
C.4.11.2	Comparisons with measurements	**121**
C.4.11.3	Development needs	**123**
D	**Conclusion**	**125**
	References	**127**

Executive Summary

The project was aimed at describing the mixing phenomena relevant for both safety analysis, particularly in steam line break and boron dilution scenarios, and mixing phenomena of interest for economical operation and the structural integrity. Measurement data from a set of mixing experiments, gained by using advanced measurement techniques with enhanced resolution in time and space were used to improve the basic understanding of turbulent mixing and to provide data for Computational Fluid Dynamics (CFD) code validation. Slug mixing tests simulating the start-up of the first main circulation pump have been performed with two 1:5 scaled facilities: The Rossendorf coolant mixing model ROCOM and the VATTENFALL test facility, modelling a German Konvoi type and a Westinghouse type three-loop PWR, respectively. Additional data on slug mixing in a VVER-1000 type reactor gained at a 1:5 scaled metal mock-up at EDO Gidropress are provided. Experimental results on mixing of fluids with density differences obtained at ROCOM and the FORTUM PTS test facility were made available.

Concerning mixing phenomena of interest for operational issues and thermal fatigue, flow distribution data available from commissioning tests (Sizewell-B for PWRs, Loviisa and Paks for VVERs) have been used together with the data from the ROCOM facility as a basis for the flow distribution studies. The test matrix on flow distribution and steady state mixing performed at ROCOM comprises experiments with various combinations of running pumps and various mass flow rates in the working loops.

Computational fluid dynamics calculations have been accomplished for selected experiments with two different CFD codes (CFX-5, FLUENT). Best practice guidelines (BPG) were applied in all CFD work when choosing computational grid, time step, turbulence models, modelling of internal geometry, boundary conditions, numerical schemes and convergence criteria. The BPG contain a set of systematic procedures for quantifying and reducing numerical errors. The knowledge of these numerical errors is a prerequisite for the proper judgement of model errors. The strategy of code validation based on the BPG and a matrix of CFD code validation calculations have been elaborated. Besides of the benchmark cases, additional experiments were calculated by new partners and observers, joining the project later.

Based on the “best practice solutions”, conclusions on the applicability of CFD for turbulent mixing problems in PWR were drawn and recommendations on CFD modelling were given. The high importance of proper grid generation was outlined. In general, second order discretization schemes should be used to minimise numerical diffusion. First order schemes can provide physically wrong results. With optimised “production meshes” reasonable results were obtained, but due to the complex geometry of the flow domains, no fully grid independent solutions were achieved. Therefore, with respect to turbulence models, no final conclusions can be given. However, first order turbulence models like K-ε or SST K-ω are suitable for momentum driven slug mixing. For buoyancy driven mixing (PTS scenarios), Reynolds stress models provided better results.

A. Objectives and Scope

Several various mixing phenomena characterize the various operating conditions of Pressurized Water Reactors (PWR) and influence the safety analyses of the pertaining plant operating states. Turbulent mixing at low flow velocities is governed by the buoyancy forces that are created by the temperature and boron concentration differences. At higher velocities turbulent mixing is governed by the velocity differences of different flow streams. Computational Fluid Dynamics (CFD) is the main tool to study such phenomena. Since there are still large uncertainties in the proper application of turbulence models in various cases, in the suppression of numerical diffusion and in optimum time step selection and mesh size definition, the validation of CFD codes for reactor applications requires well-defined experiments. Such requirements were discussed in a profound manner during the EUBORA Concerted Action focusing on mixing and transport of diluted slugs during boron dilution transients. The conclusion was that it would be beneficial to employ existing 1/5-scale facilities for statistical experiments, combined with the data from the commissioning testing of the plants. The measurement data were used to develop the CFD code capabilities for the determination of the flow distribution to the reactor core and to the different loops as well as for turbulent mixing in the case of slug transport and cold emergency core cooling water.

- The first objective of the project was to obtain complementary and confirmatory data for the resolution of the local boron dilution transients after restart of a RCP. The local boron dilution is considered as potentially leading to a most serious reactivity transient in the PWRs and VVERs. The most important mitigative mechanism is mixing before the slug enters the reactor core. The aim was to carry out experiments in order to understand in sufficient detail, how the slug mixes before it enters the reactor core, and to validate the CFD codes for plant application.
- The second objective was to use the experimental data to justify application of various turbulence and turbulent mixing models for various flow conditions, to suppress numerical diffusion and to decrease grid, time step and user effects in the CFD analyses.
- The third objective was to utilize the experience from the mixing experiments and the plant commissioning test data to justify the application of CFD to determine the primary circuit flow distribution and the effect of thermal mixing phenomena in the context of the structural integrity assessment.

B. Work Programme

The work in the project was performed within five Work Packages.

WP 1: Identification of the key flow mixing and distribution phenomena for the safety analyses and structural integrity applications

Since the aim was to cover mixing phenomena relevant for both safety analysis, particularly in steam line break and boron dilution scenarios, and mixing phenomena of interest for economical operation and the structural integrity, the first work package is focussed on the key phenomenology of various applications. The common features and differences were identified. Test matrices for the experiments and a CFD code validation strategy have been elaborated.

WP2: Slug mixing experiments

Slug mixing experiments were carried out in two existing 1:5-scale facilities of partners FZR and Vattenfall. ROCOM (Rossendorf Coolant Mixing Model) is a test facility modelling a German KONVOI type reactor. The RPV model is made of transparent acryl enabling velocity measurements using LDA techniques. ROCOM is equipped with one fully controllable pump in each of the four loops giving the possibility to perform tests in a wide range of flow conditions. The VATTENFALL facility is a mock-up of the Westinghouse PWR at NPP Ringhals. The un-borated water slugs are modelled in both facilities by means of a salt water tracer solution. Conductivity is measured to determine the mixing of the tracer. CFD calculations performed to analyse the scaling of the models have shown, that under forced flow conditions (high Reynolds numbers), the scaling of 1:5 to the prototype meets both physical and economical demands. The experiments were performed in order to complement the existing data base with the following new information:

- statistical experiments, i.e. 5 similar runs in order to reveal the chaotic behaviour of the swirls in the downcomer,
- experiments with emphasis on velocity measurements that are mainly missing,
- effect of scaling, i.e. Reynolds versus Strouhal scaling and Froude scaling.

Improved measurement techniques being capable of providing data on turbulent mixing phenomena with enhanced resolution in time and space have been employed. To investigate the Reynolds versus Strouhal scaling, the height, the slope and the length of the start-up ramps were varied from normal pump start-up conditions down to parameters typical for the start-up of natural circulation. Additional data on slug mixing in a VVER-1000 type reactor gained at a 1:5 scaled metal mock-up at EDO Gidropress have been provided.

Besides of slug mixing data, experimental results on buoyancy driven mixing of fluids with density differences obtained at ROCOM and the FORTUM PTS test facility have been made

available. Buoyancy driven mixing is relevant for PTS scenarios. Froude number scaling was considered for experiments with density differences.

WP 3: Flow distribution in the primary circuit

Experiments on the flow distribution in the 4-loop PWR with running RCPs were carried out at ROCOM allowing the operation with different controlled mass flow rates in the various loops. Salt water plugs are injected near the cold leg outlet nozzles. The degree of mixing is determined from conductivity measurements by the help of high resolution wire mesh sensors.

Additional test data awee made available for the project by Paks NPP, based on the commissioning tests, typical for VVER conditions. The tests performed at the plant addressed mixing among coolant loop flows in the downcomer and up to the core inlet in forced flow conditions. For that purpose one or more loops were running at temperatures different from that of the other loops and the core outlet temperature distribution was recorded at 212 fuel assemblies out of a total of 349. The test scenario is important for the "classical" VVER-440 design, with typical cold leg and main circulating pump design. There are earlier experiments aimed for determination of the mixing factors for VVER-440 reactors, too. These experiments were performed at zero reactor power in Loviisa VVER-440 NPP.

Computational Fluid Dynamics (CFD) methods were used for the simulation of the flow field in the primary circuit of the operating reactors. Computed results were compared to available measurement data, and conclusions were drawn concerning the usability and modelling requirements of CFD methods for that kind of application.

WP 4: Validation of CFD codes based on the mixing experiments

The experimental results from the mixing experiments were used to evaluate the quality and trust of different CFD modelling approaches for reactor applications. The objectives were to

- examine the effect of mesh size, time step, boundary conditions and detail in description of geometry,
- define appropriate numerical schemes which allow to reproduce physically real solutions and show appropriate convergence behaviour,
- examine the applicability of different turbulence models for a number of different fluid mixing and flow distribution situations.

A limited set of benchmark tests for CFD code validation was derived from the experiments. The ERCOFTAC and ECORA “Best Practice Guidelines” are referenced [BPG, Men02]. Systematic studies concerning numerical errors and model errors have been performed according to the BPG. Efforts were made to calculate steady-state mixing and flow

distribution, slug mixing tests and buoyancy induced mixing cases. The codes used were CFX and FLUENT, which allow accurate and flexible modelling of geometry and inclusion of various physical models. The experience from the applications was compiled in a final report and will be used as recommendations for using CFD to different mixing cases.

WP 5: Evaluation of the results, reporting and co-ordination

Information on the status of experimental and CFD code applications has been collected and compared from the various Work Packages.

The main results of the project are:

- an unique experimental data base on steady state flow distribution, slug mixing and buoyancy driven mixing with enhanced resolution in time and space gained from test facilities representing various European reactor types,
- conclusions on flow distribution and temperature fluctuations in NPPs under normal operation conditions being important for economical operation and the estimation of thermal fatigue,
- the recommendations for the CFD applications concerning applied turbulence modelling features, concerning geometrical modelling, meshing and time step, numerical solution schemes, and turbulence modelling features.

The final reports on the work packages 2 (slug mixing), 3 (flow distribution) and 4 (CFD code validation) are public to support the dissemination of the results of the project [D09], [D10], [D11]. An overview on the experimental data base gained within FLOMIX-R is given in [Roh05].

C Work performed and results

C.1 Identification of the key mixing phenomena (WP 1)

The identification of the key phenomena is elaborated in [D02], mainly based on the final report of the EUBORA Concerted Action on boron dilution [Eub99].

The objectives of WP1 were:

- identification of the key phenomena important for slug mixing (forced and buoyancy induced),
- identification of the key phenomena important for overcooling transients and normal operation conditions,
- planning of work to be performed for CFD code validation,
- elaboration of the test matrix for the slug mixing experiments.

The main objective of the investigations was to understand in sufficient detail, how water of different quality mixes in the cold leg and in the downcomer of a PWR before it enters the reactor core. These different quality might be different temperatures, different densities and/or different concentrations of additives. The most relevant additive to the primary coolant in PWR is boron acid used for the control of reactivity. In some cases, dependent on the scenario of the transient, both temperature and boron acid concentration might be different in the slug mixed with ambient water, in some cases density differences due to temperature gradients can be neglected with respect to mixing.

The mixing of lower borated slugs with water of higher boron concentration is the most mitigative mechanism against serious reactivity accidents in local boron dilution transients, and therefore, is one of the most important, nuclear safety related issues of mixing. Significant advantage in boron dilution transient analysis can be achieved, if realistic mixing data are used [Gru94], [Kli04].

Local or heterogeneous boron dilution refers to all events that could lead to formation of partially diluted or completely un-borated slugs in the primary system. In the FLOMIX-R project, emphasis was put on heterogeneous dilution considering the transport and turbulent dispersion of a slug of lower borated water which might be formed in the primary circuit by various mechanisms.

Lower borated slugs can be formed in the primary circuit of a PWR due to external or inherent boron dilution events. An external dilution refers to the cases where diluted or pure water slug is created by injection from outside of the primary circuit. Examples of such are an eventual injection of un-borated coolant or coolant of reduced boric acid concentration by the makeup system, and injection of un-borated pump sealing water to the primary system. Steam generators, chemical and volume control system, diluted accumulator or diluted re-fueling water storage tank and diluted containment sump are mentioned as potential sources of

diluted water. Dilution may occur during power operation, shutdown or accident conditions. The sequence of events may vary significantly in different scenarios: pure water from the secondary side may flow to the primary circuit due to maintenance errors during shutdown, reactor coolant pumps (RCP) may stop during inadvertent dilution thus initiating slug formation or inadvertently diluted accumulators may leak to primary circuit during power operation or during accident conditions.

An inherent dilution mechanism is connected with the formation of slugs of under-borated water through an inherent phenomenon during an accident. Such an inherent phenomenon can be a boiling-condensing heat transfer mode occurring inside the primary system, or back flow from the secondary system in case of primary-to-secondary leakage accidents.

In VVER-440 reactors, because of the complex geometry of the primary loops and the main gates valves in both the hot and cold legs, there are various extra aspects of slug formation and transport. Particularly, main gate valves in VVER-440 can be closed during reactor operation to isolate single loops for maintenance. The water in these isolated loops might be under-borated due to failure of the water make-up system. The nuclear consequences of transients after re-start of an isolated loop in a VVER-440 type reactor have been studied in [Roh97].

The mixing of slugs of water of different quality is also very important for pre-stressed thermal shock (PTS) situations. In emergency core cooling (ECC) situations after a LOCA, cold ECC water is injected into the hot water in the cold leg and downcomer. Due to the large temperature differences, thermal shocks are induced at the RPV wall. Temperature distributions near the wall and temperature gradients in time are important to be known for the assessment of thermal stresses.

One of the important phenomena in connection with PTS is thermal stratification, a flow condition with a vertical temperature profile in a horizontal pipe. The fluid is in single-phase regime unlike in case when the upper part of the pipe is filled with steam, which is not elaborated within this context. Typically a stratified condition builds up, when a low-velocity cold fluid enters to a low-velocity warm fluid in a horizontal pipe. Stable stratification is not particularly dangerous for the pipe itself in structural integrity sense. However, in a real process there are often disturbances that make the temperature boundary to move vertically. Velocity difference between the colder and warmer fluids may also cause wave formation in the temperature boundary. All this may cause thermal fatigue in the pipe. Besides of thermal fatigue, a single thermal shock can also be relevant for structural integrity, if it is large enough, especially in the case, that the brittle fracture temperature of the RPV material is reduced due to radiation embrittlement. Therefore, additional to the investigations of slug mixing during re-start of coolant circulation, the mixing of slugs or streams of water with higher density with the ambient fluid in the RPV were performed. The aim of these investigations was to study the process of turbulent mixing under the influence of buoyancy forces caused by the temperature differences. Heat transfer to the wall and thermal conductivity in the wall material have not been considered.

Another objective of the investigations was to utilize data from steady state mixing experiments and plant commissioning test data to determine the primary circuit flow distribution and the effect of thermal mixing phenomena in the context of the improvement of normal operation conditions and assessment of overcooling transients. Overcooling scenarios are mainly connected with steam line breaks. Inadvertent opening of turbine valves or other valves in the secondary circuit of a NPP are characterized by the same consequences and phenomena.

Steam line breaks can be classified by different criteria. A break at full power conditions enhances the heat transfer to the secondary side and leads to the closure of the turbine valves and the reactor trip, inserting a high negative reactivity into the core. The heat release after the trip reduces the amount of overcooling. A break at hot zero power or in the state after a reactor scram is characterised by an increase of the heat transfer to the secondary side from nearly zero to values greater than in the nominal regime of the reactor. The effects of overcooling are higher and are not reduced by a fuel heat release.

Depending on the scenario, the reactor coolant pumps can be switched-off or stay in operation during the transient. Running pumps transport the perturbation to the reactor core very quickly. In case of switching-off all RCP, a developed natural circulation establishes after running out of the pumps. A special case is the switching-off the RCP in the broken loop, only. In that case, reverse flow in this loop establishes and the perturbation is not transported to the core directly.

A break of one main steam line is characterised by an asymmetric perturbation of the primary circuit. To estimate the impact on the reactor core, the mixing of coolant of different temperature coming from the broken and intact loop has to be assessed. Different from heterogeneous boron dilution events, the change of coolant temperature and the change of flow rates in the individual loops is relatively slow (in comparison to the transport time of the temperature perturbation from the primary circuit cold legs to the core inlet). That's why, the coolant mixing can be considered as quasi-stationary with fixed temperature distribution and mass flow rates at a certain moment of time. Therefore, the mixing can be assessed based on experiments and calculations for steady-state flow situations. Nuclear analysis of main steam line break scenarios based on advanced coolant mixing modelling is reported about in [Kli99].

However, steady-state mixing and flow distribution is not only relevant for overcooling scenarios, but also for nominal operation of the reactor or operational transients. In operational transients, e.g. switching off or switching on single reactor coolant pumps during commissioning tests, the coolant temperature distribution at the core inlet is also non-homogeneous. In these cases, the pressure drop between the lower and the upper plenum of the reactor forces the coolant in the idle loops to flow through the loops in reverse direction. The coolant from the operating and non-operating loops is mixed in the lower and upper plenum of the reactor. Even for nominal operation of the NPP, flow distribution and mixing is important, because mass flow rates and cold leg temperatures of the individual loops can differ by some percent respectively degrees because of differences in the geometry of the loops including steam generators or of pump characteristics. The knowledge of the correct

temperature distribution at the core inlet is important for increasing the accuracy of reactor power estimation.

Based on the identification of the key mixing and flow distribution phenomena relevant for both safety analysis, particularly in steam line break and boron dilution scenarios, and for economical operation and the structural integrity, test matrices for the experiments are elaborated. Experiments on slug mixing have been performed at two test facilities, modelling different reactor types in scale 1:5, the Rossendorf and Vattenfall test facilities. The corresponding accident scenario is the start-up of first RCP after formation of a slug of lower borated water during the reflux-condenser mode phase of a small break LOCA. The measurement data have been made available for CFD code validation purposes. Slug mixing tests have also been performed at the VVER-1000 facility of EDO Gidropress to meet the specifics of this reactor type. Experiments on density driven mixing were carried out at the Rossendorf and the Fortum PTS facilities. The test facilities and selected results of some tests are described in section C.2 of this report.

Concerning steady-state mixing and flow distribution in the cold legs and pressure vessel of the primary circuit, commissioning test measurements performed at the Paks and Loviisa VVER-440 NPPs are used for the estimation of thermal mixing of cooling loop flows in the downcomer and lower plenum of the pressure vessel. A series of quasi steady state mixing experiments are performed at the ROCOM test facility. Description of the experimental results as well as conclusions on flow distribution are presented in section C.3.

Following aspects of mixing not yet fully covered by previous investigations were pointed out in the EUBORA report [Eub99]:

(1) velocity measurements in the downcomer and lower plenum, especially during RCP restart,

(2) Reynolds scaling versus Strouhal scaling,

(3) effects of downcomer geometry and lower plenum structures,

(4) impact of the number and the orientation of primary loops,

(5) transition from buoyancy driven to momentum driven mixing,

(6) full-scale conditions.

In the slug mixing experiments performed within the FLOMIX-R project, mainly the items (1) to (4) have been covered. These aspects were taken into account elaborating the slug mixing test matrix described in section C.2. Additional slug mixing experiments at a mock-up of a VVER-1000 reactor have been provided by EDO Gidropress. These experiments address the effect of geometry and primary loop configuration specific for VVER-1000 reactors, on the one hand, and Reynolds and Strouhal scaling on the other hand.

Considering item (5), the impact of density differences of the mixing fluids has to be considered. To address this aspect, the results of experiments on the generic investigation of the

transition between density controlled and momentum driven mixing performed at ROCOM and measurement data from PTS experiments carried out at the Fortum test facility have been made available.

Item (6), concerning full-scale conditions, could not be directly addressed within the project because only scaled test facilities were available. Conclusions on the mixing in real reactor conditions have been gained from measurement data on flow distribution from NPPs. However, no scaled counterpart tests for these measurements are available.

C.2 Slug mixing tests (WP 2)

C.2.1 Description of the test facilities

ROCOM (**Ro**ssendorf **Co**olant **M**ixing Model) is a test facility for the investigation of coolant mixing operated with water at room temperature [Pra03]. The facility models a KONVOI type reactor with all important details for the coolant mixing in a linear scale of 1:5. ROCOM is a four-loop test facility with a RPV mock up made of transparent acryl (Fig. C.2.1).

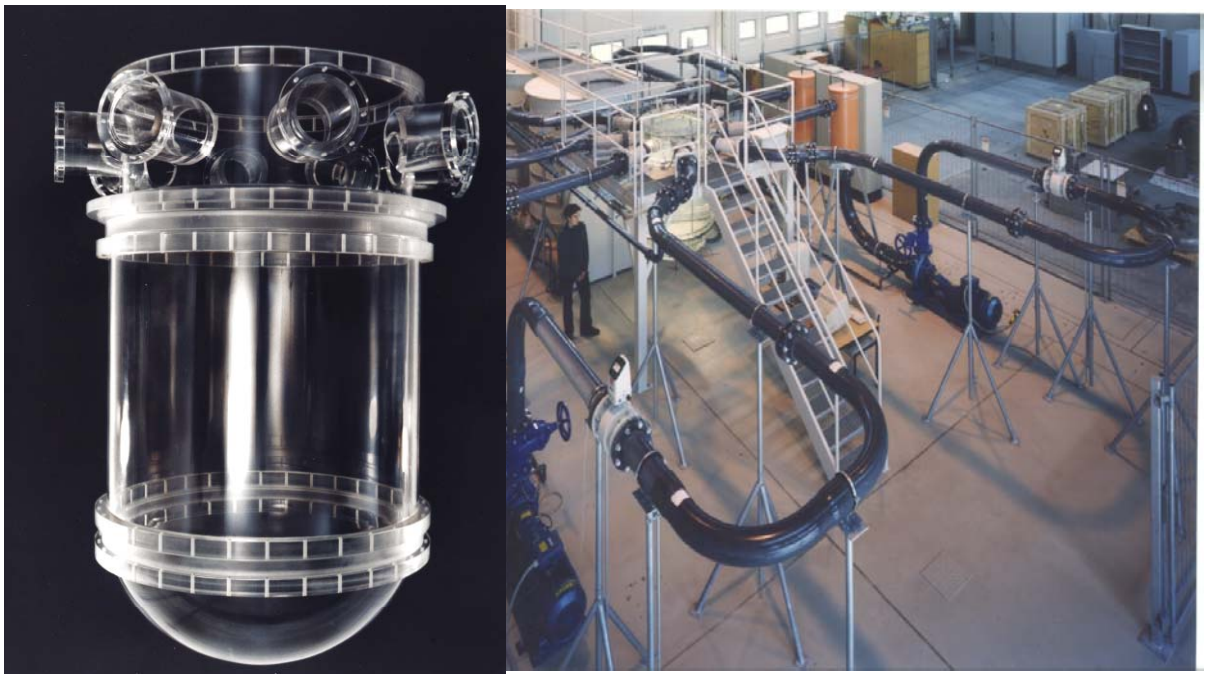

Fig. C.2.1 Acryl model of the RPV and view on the test facility ROCOM

Individually controllable pumps in each loop give the possibility to perform tests in a wide range of flow conditions, from natural circulation to nominal flow rate including flow ramps (pump start up). The transparent material for the pressure vessel allows the measurement of velocity profiles in the downcomer by laser Doppler anemometry.

Both boron concentration and temperature fields are modelled by the concentration field of a tracer solution. The disturbance is created by computer controlled injection of salted water into the cold leg of one of the loops, while the test facility is operated with de-mineralised water. The test facility is equipped with wire-mesh sensors for the electrical conductivity measurement [Pra98],[Pra02] which allow a high resolution determination of the transient tracer concentration in space and time. Four such sensors are installed in the reactor pressure vessel model with altogether about 1000 single measurement positions and a measuring frequency of up to 200 Hz. The location of the sensors in the model is shown on fig. C.2.2.

The measured conductivity values are transformed into a mixing scalar $\Theta_{x,y,z}(t)$. It is calculated by relating the local instantaneous conductivity $\sigma_{x,y,z}(t)$ to the amplitude of the conductivity change in the inlet nozzle of the disturbed loop.

$$\Theta_{x,y,z}(t) = \frac{\sigma_{x,y,z}(t) - \sigma_0}{\sigma_1 - \sigma_0} \qquad \text{(C.2.1)}$$

Θ represents the contribution of the coolant from the disturbed loop to the mixture at the given position x,y,z. The upper reference value σ_1 in (C.2.1) is the conductivity in the injected slug. The lower reference value σ_0 is the initial conductivity of the water in the test facility before the tracer is injected. The degree of mixing can be also expressed in relative boron concentration or temperature, if temperature measurement technique is applied.

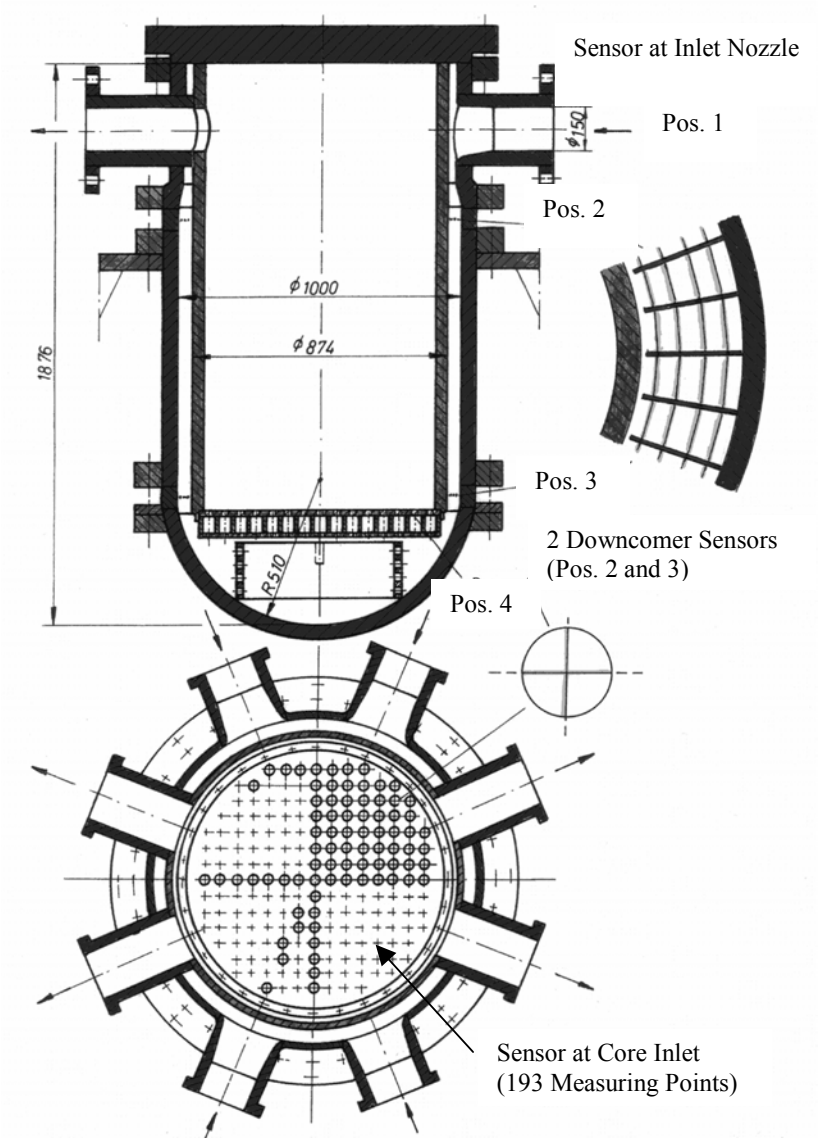

The Vattenfall mixing test facility is a 1:5 scale model of a Westinghouse PWR [Alv95]. The lower plenum and the lower 2/3 of the downcomer are made of acryl. A general view of the facility and the technological scheme of the model are shown on fig. C.2.3. Two idle loops are included in the model. The model is run with a maximum flow rate of 127 l/s and at temperatures between 20 and 50 ^{o}C. Components that can be important for mixing have been modelled, for example thermal shields, inlet pipe diffusers, structures in lower plenum, core support plates and core.

Fig. C.2.2 Positions of wire mesh sensors in ROCOM

The determination of the relative boron concentration is based on salt water tracering and conductivity measurement, too. Conductivity is measured to at 181 measurement positions close to the inlet to the core. A sampling frequency of 60 Hz has been used.

The slug is injected into an empty section of the cold leg pipe that has been isolated from the rest of the pipe (between valves V4 and V5 in figure C.2.3). The slug is released by quickly opening the two valves that encompass the slug (V4 and V5). Flow through the model is then slowly (during around 40 seconds) increased to the maximum flow rate. The increased flow rate is achieved by opening a motor gate-valve (V3) upstream of the slug. In order to minimise buoyancy effects ethanol is added to the salt water to lower the density of the salt-water to that of tap-water. The density difference is lower than 1 kg/m^3 after this adjustment.

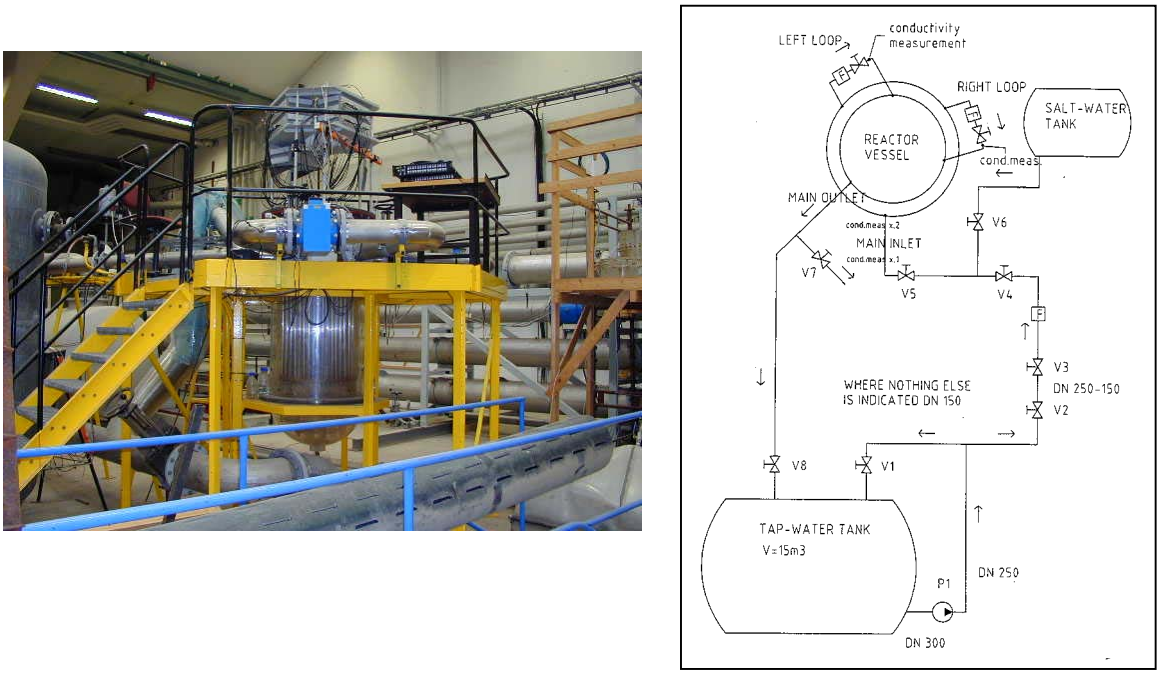

Fig.C.2.3 General view (left) and technological scheme (right) of the Vattenfall test facility

The test facility of EDO "Gidropress" [Log00] is a metal model of the Russian VVER-1000 reactor in a scale of 1:5. One loop with a loop seal and reactor coolant pump simulator is modelled. The other three loops are made short-circuit, and only the pressure loss of them is simulated. The core model has 151 fuel assembly (FA) simulators, which have the same pressure loss as the regular FA. Boron concentration change is modelled by a change in temperature (the de-borated water slug is simulated by colder water). About 100 thermocouples are placed in the lower part of the downcomer and at the core inlet to study the mixing of flows.

The Fortum PTS test facility [Tuo87] was a 1:2.56 scale model of the Loviisa VVER-440 reactor. The facility contained a half of the circumference of the reactor downcomer and

included three cold legs and perforated plate in the lower plenum. The material of the facility was transparent acryl. The middle one of the three cold legs consisted of the section between RPV and RCP including the main gate valve and bottom safety injection point. Two other cold legs were built to model side loop flows only. The choice of the transparent material restricts the tests to atmospheric pressure and to a maximum temperature of around 75 °C. Minimum injection temperature was about 10 °C and the extra buoyancy effect was induced by salt addition to injection water. The high pressure injection (HPI) rate Q_{HPI}, side loop flows Q_A and Q_C, main loop flow Q_B as well as density difference ratio between HPI and loop flow water were varied. Most of the 62 thermocouples were installed to the downcomer to measure the temperature fluctuations on the vessel wall. The thermocouples were read once in two seconds. A schematic view of the facility and locations of the thermocouples are shown in fig. C.2.4 and C.2.5.

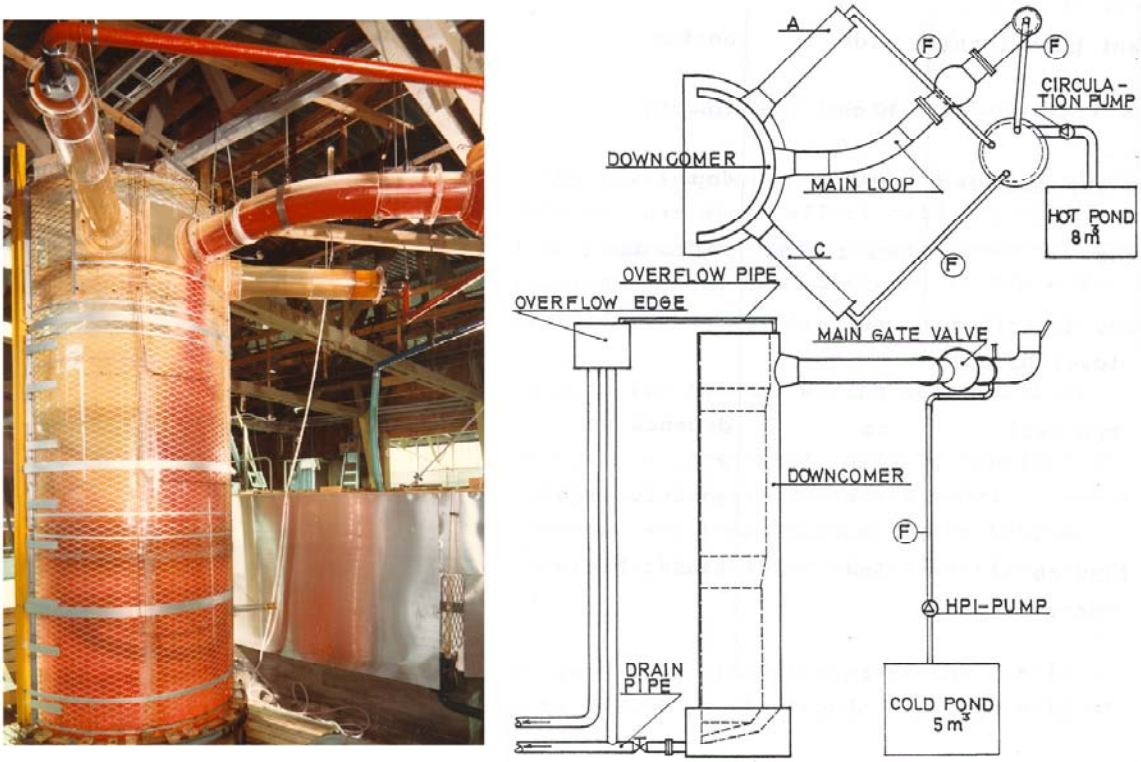

Fig. C.2.4 General view, top view and side view of the Fortum PTS test facility

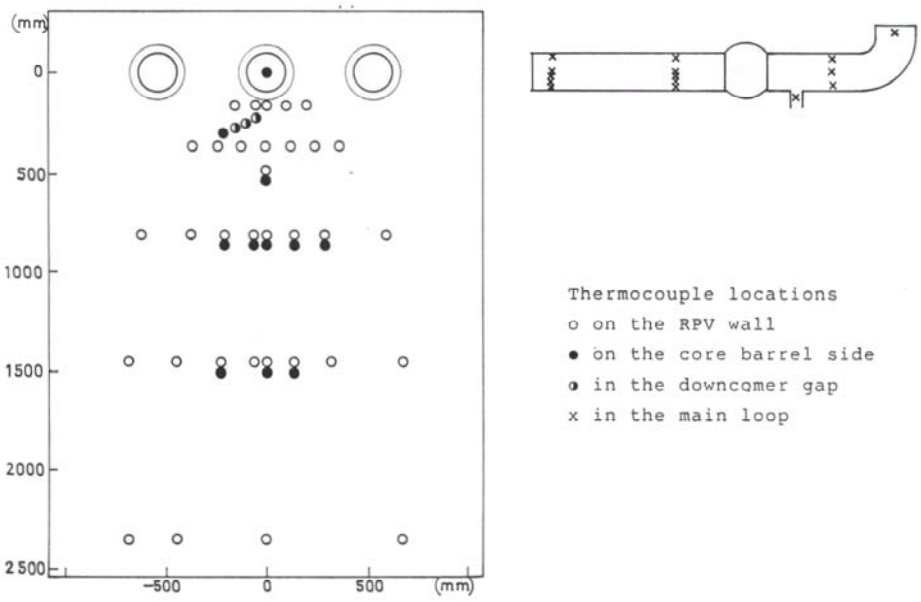

Fig. C.2.5 Measurement positions location at the Fortum PTS test facility

C.2.2 Results of the pump start-up tests

The slug mixing test matrix contains 12 experiments at ROCOM and 4 experiments at the Vattenfall facility with simulation of the start-up of the first main coolant pump (see table C.2.1).

Run	Ramp length [s]	Final volume flow rate [m^3/h]	Slug volume [m^3]*	Initial slug position [m]*	Status of unaffected loops
ROCOM-01	14	185.0	40.0	10.0	Open
ROCOM-02	14	185.0	20.0	10.0	Open
ROCOM-03	14	185.0	4.0	10.0	Open
ROCOM-04	14	185.0	4.0	2.5	Open
ROCOM-05	14	185.0	4.0	22.5	Open
ROCOM-06	14	185.0	4.0	40.0	Open
ROCOM-07	14	185.0	20.0	10.0	Closed
ROCOM-08	28	92.5	4.0	10.0	Open
ROCOM-09	56	46.3	4.0	10.0	Open
ROCOM-10	14	148.0	4.0	10.0	Open
ROCOM-11	14	222.0	4.0	10.0	Open
ROCOM-12	14	185.0	8.0	10.0	Open
VATT-01	16	429	14.0	10.0	Open
VATT-02	16	429	8.0	10.0	Open
VATT-03	16	429	4.5	10.0	Open
VATT-04	40	172.8	8.0	10.0	Open

* related to the original reactor

Tab. C.2.1
Matrix of slug mixing experiments performed at the ROCOM and Vattenfall test facilities

For the pump start-up experiments the following boundary conditions were varied:

- Length of the pump ramp
- Final mass flow rate of the loop with the starting–up pump
- Volume of the injected slug and initial position in the cold leg
- Status of the unaffected loops
- Geometry of the reactor pressure vessel

The initial position of the slug cannot be varied in the Vattenfall test facility, while it is possible in the ROCOM one. However, in the ROCOM pump start-up experiments, a concentration of the created slug decreasing in time has to be accepted. Due to the slug creation technique in the ROCOM test facility (injection of tracer with a constant volume flow rate into the loop with the starting-up pump), the concentration of the slug decreases over the length. The degree of decreasing depends on the slope of the pump ramp. These circumstances have to be taken into account in the determination of the boundary conditions for the experiments and in the interpretation of the results.

The ramp length in the ROCOM experiments is the time interval of increasing the pump frequency. The final volume flow rate establishes with a time delay due to the inertia of the fluid. In the Vattenvall experiments, the ramp length is the time interval of valve opening. The final volume flow rate of 185.0 m^3/h in the ROCOM test facility and the flow rate of 172.8 m^3/h correspond to the nominal flow rate in the real plant modelled in the scale of 1:125. For both facilities, the initial slug position is the distance in the cold leg from the entry into the reactor pressure vessel related to the real plant. The slug size is also related to the real plant. The experimental results are documented in detail in [D05], [D06].

The experiments ROCOM-02 and VATT-04 represent the basic scenarios of pump start-up for the both facilities. In that cases, the transit time for the slug, i.e. the time it takes for the slug to travel from its initial position to the inlet to the core, is the same as in the plant. The other three Vattenfall tests cases are run with a higher flow rate in order to increase the Reynolds number, and thereby decrease the Reynolds number scaling effects. Strouhal number scaling is used to determine the ramp length for these tests.

A series of experiments are made for different slug sizes (ROCOM-01; -02, -03 and –12; VATT-01; -02 and –03). The impact of the initial slug position was investigated in experiments ROCOM-04, -05 and –06 versus ROCOM-03. Strouhal scaling was considered in tests ROCOM-08 and –09 versus ROCOM-03. The final flow rate after the pump start-up was varied in ROCOM-10 and –11. ROCOM-07 was performed to estimate the influence of the status of the idle loops.

Besides of the measurements of boron concentration at the inlet to the core, laser Doppler velocimetry (LDV) measurements of vertical and tangential/circumferential velocity in the downcomer during steady state and transient conditions were performed at both test facilities. At the Vattenfall facility, additionally the following types of visualisations were made:

- local injections of dye during steady state flow and during a transient,
- visualisations of a coloured slug passing through the downcomer during a transient,
- laser sheet visualisations of a slug passing through the downcomer during a transient.

Fig. C.2.6 shows the average value and the maximum value of the mixing scalar in experiment ROCOM-02 determined over all measurement positions of the corresponding sensor. The decrease of the tracer concentration in time at the cold leg sensor position is seen

in this figure. Then, the slug enters the pressure vessel and moves through the measurement cross section of all sensors. During the transport, the slug mixes with the ambient coolant in the vessel and the perturbation reduces, as can be concluded from the decreasing maximum values reached at the different sensor positions. As it can be seen on fig. C.2.6, maximum values of the mixing scalar can exceed 1.0 (at the cold leg sensor). This is due to the fact, that the average mixing scalar value in the inlet cross section is normalized to 1.0, but higher local values can occur caused by turbulent fluctuations and in-complete mixing at the salt water injection position.

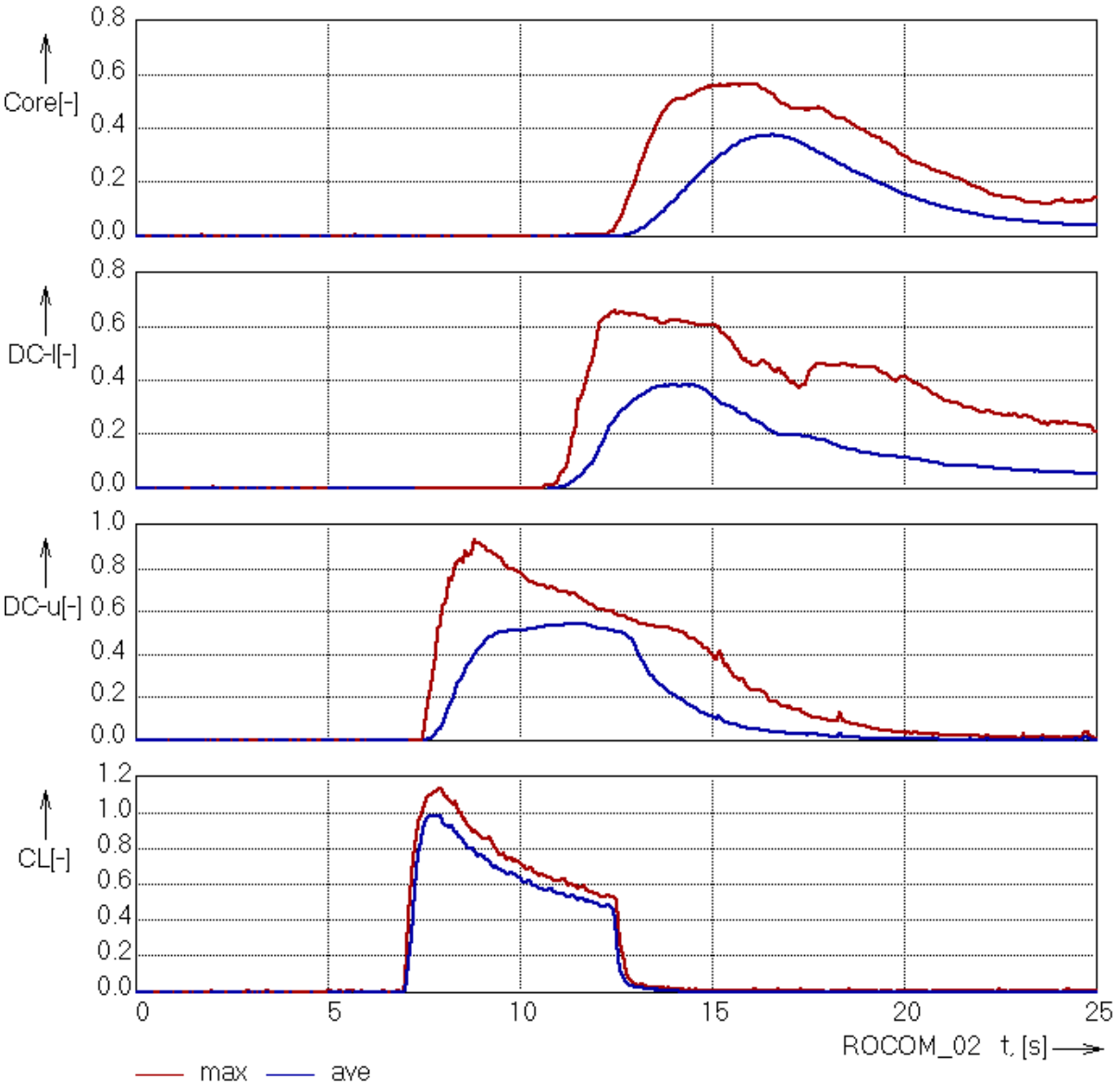

Fig. C.2.6 Time behaviour of average and maximum mixing scalar at cold leg nozzle, upper downcomer sensor, lower downcomer sensor and core inlet (from lower to upper fig.)

As it was proved during the experiments, time behaviour of the resulting mixing scalar at identical positions in the pressure vessel differ from each other when an experiment is repeated with identical boundary conditions. Fluctuations of the flow field in the reactor pressure vessel are the reason for these deviations between single realizations of one experiment. These fluctuations are due to the turbulent nature of the flow. Therefore, all experiments at ROCOM and the Vattenfall facility were repeated five times. The results of these single realizations were averaged and used for further analysis (e.g. CFD code validation). However, the data of the single realizations were used to carry out an uncertainty analysis of the obtained results [D09].

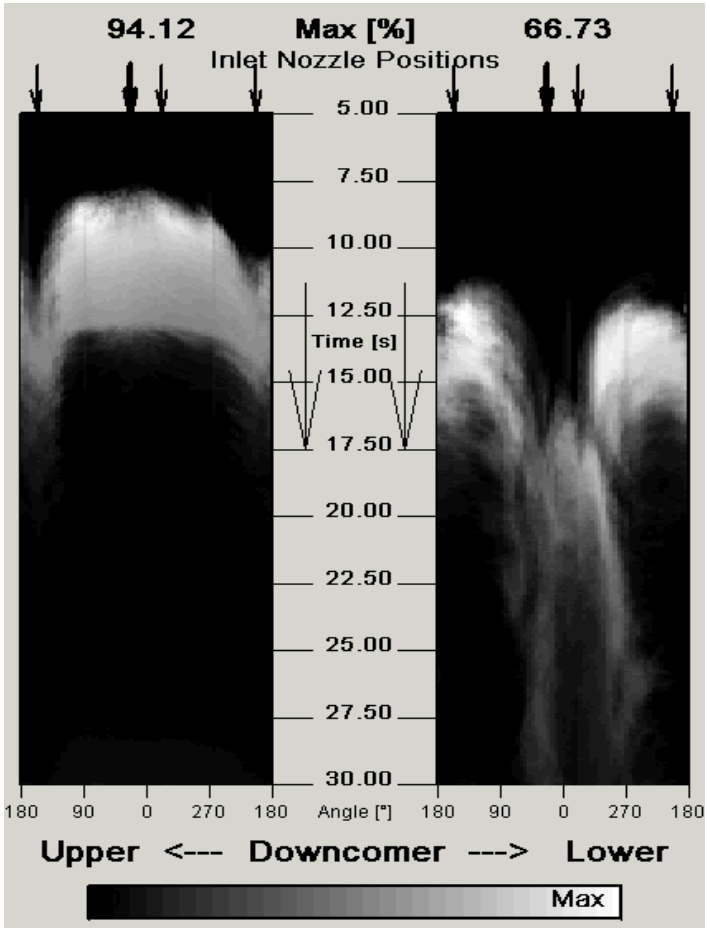

Fig. C.2.7 shows the time evolution of the mixing scalar at the two sensors in the downcomer in the experiment ROCOM-02. Both sensors are shown in an unwrapped view, the position of the loop with the starting up pump is marked by the bold arrow. From this visualization is clearly to be seen, that the de-borated coolant passes around the core barrel instead of flowing directly downstream. At the upper sensor, the tracer arrives still below the affected inlet nozzle. With growing time, the tracer spreads in the azimuthal direction. Subsequently, at the lower sensor two maximums of the tracer at azimuthal positions on the back side of the downcomer are observed.

Fig. C.2.7 Evolution of the mixing scalar distribution at upper and lower downcomer sensor position for experiment ROCOM-02

The mixing scalar distribution at the core inlet at the moment of maximum tracer concentration resp. minimum boron concentration for the experiments ROCOM-02 and VATT-02 are shown on fig. C.2.8 and C.2.9. Please note, that in the two figures the quantification of mixing degree is given in different presentations. In fig. C.2.8, the mixing scalar is shown, while in fig. C.2.9 the normalized minimum boron concentration is depicted.

The minimum boron concentration is unity minus the mixing scalar. Both figures show, that the maximum dilution is reached in the half of the core opposite to the sector where the loop with slug injection is located. However, the distribution is more asymmetric in the Vattenfall experiments. It is assumed, that this asymmetry is caused by an asymmetric velocity profile at the inlet nozzle, as it has been proved from CFD calculations. In the Vattenfall facility, a bend is existing in the cold leg pipe not far upstream from the inlet nozzle. This bend causes a distortion of the flow velocity distribution in the inlet nozzle plane leading to a velocity field deformation in the downcomer. Velocity measurements under steady-state flow conditions with one working pump in the lower part of the downcomer have shown, that the azimuthal velocity distribution along the perimeter of the downcomer is very asymmetric.

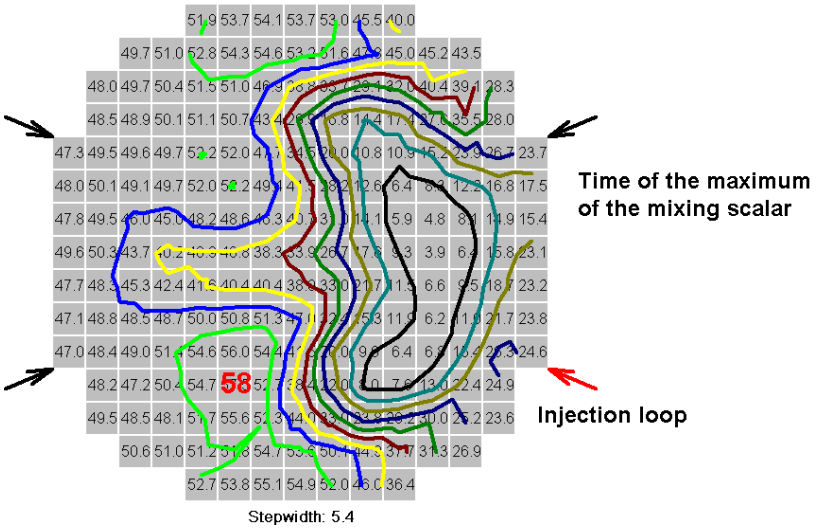

Fig. C.2.8 Maximum mixing scalar distribution at the core inlet in experiment ROCOM-02

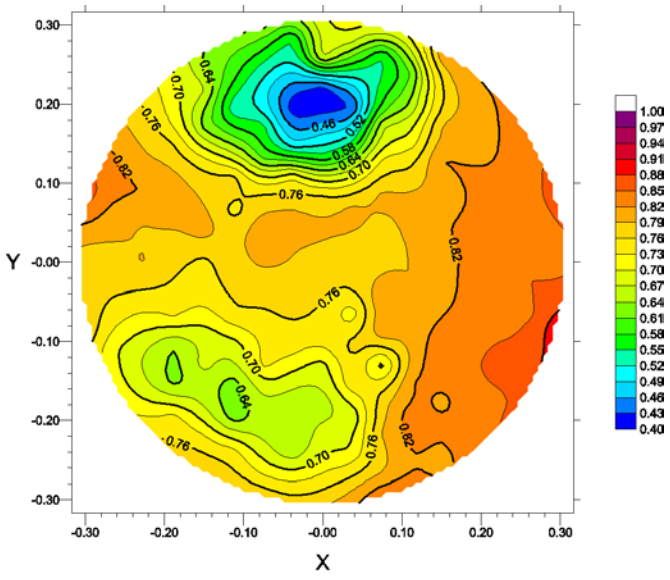

Fig. C.2.9 Maximum relative boron concentration at the core inlet in experiment VATT-02

The measurement values for vertical and horizontal velocity components at the Vattenfall facility are shown on fig. C.2.10. At the 30 degrees position, the vertical velocity component is even positive, that means there is an upwards flow. Moreover, velocity value at this position was found to be very strongly fluctuating in time. The complicated and fluctuating velocity field leads to the asymmetric, complicated mixing pattern at the core inlet.

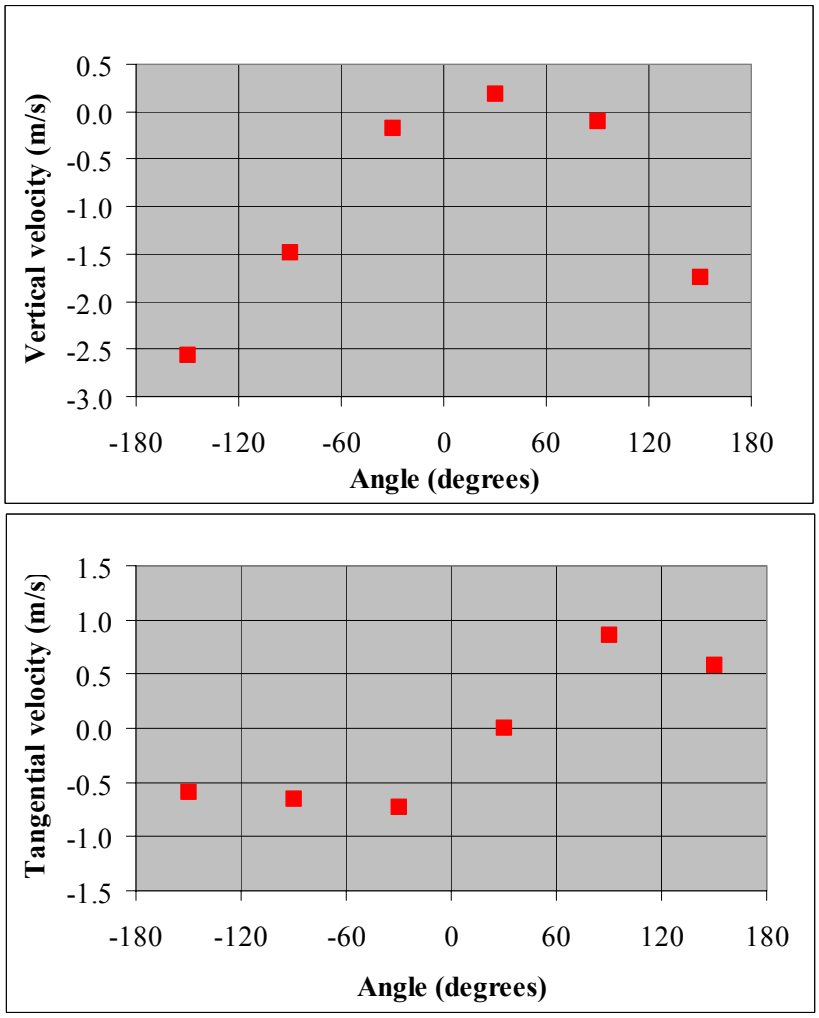

Fig. C.2.10 Vertical and horizontal velocity components in the lower downcomer measured at the Vattenfall facility

As it was mentioned above, the length of the pump ramp, final mass flow rate of the loop with the starting pump, volume of the injected slug and initial position in the cold leg as well as the status of the unaffected loops was varied in the experiments. Some aspects of the influence of these variations on the mixing will be discussed in the following only briefly in a qualitative manner.

In the experiments ROCOM-01; 02; 03 and 12, as well as in VATT-01, VATT-02 and VATT-03, the initial slug size was varied. All other boundary conditions are identical. It was

proved, that with growing slug volume, the maximum value of tracer concentration reached in the experiment is growing, too. This has been proved for both facilities. Only between ROCOM-02 (20 m^3) and ROCOM-01 (40 m^3) the maximum value is no more increasing, because due to the decreasing tracer concentration during the injection, the rear part of the slug does no more contribute to the maximum mixing scalar, in spite of the fact, that the overall salt volume input is greater.

In the experiments ROCOM-04; -05 and -06, the influence of the initial slug position was investigated. The initial distance of the slug from the pressure vessel was 2.5 m in the experiment ROCOM-04 and 40 m in the experiment ROCOM-06. Fig. C.2.11 compares the distributions at the time point of maximum mixing scalar at the core inlet for all four experiments with variation of the initial slug position.

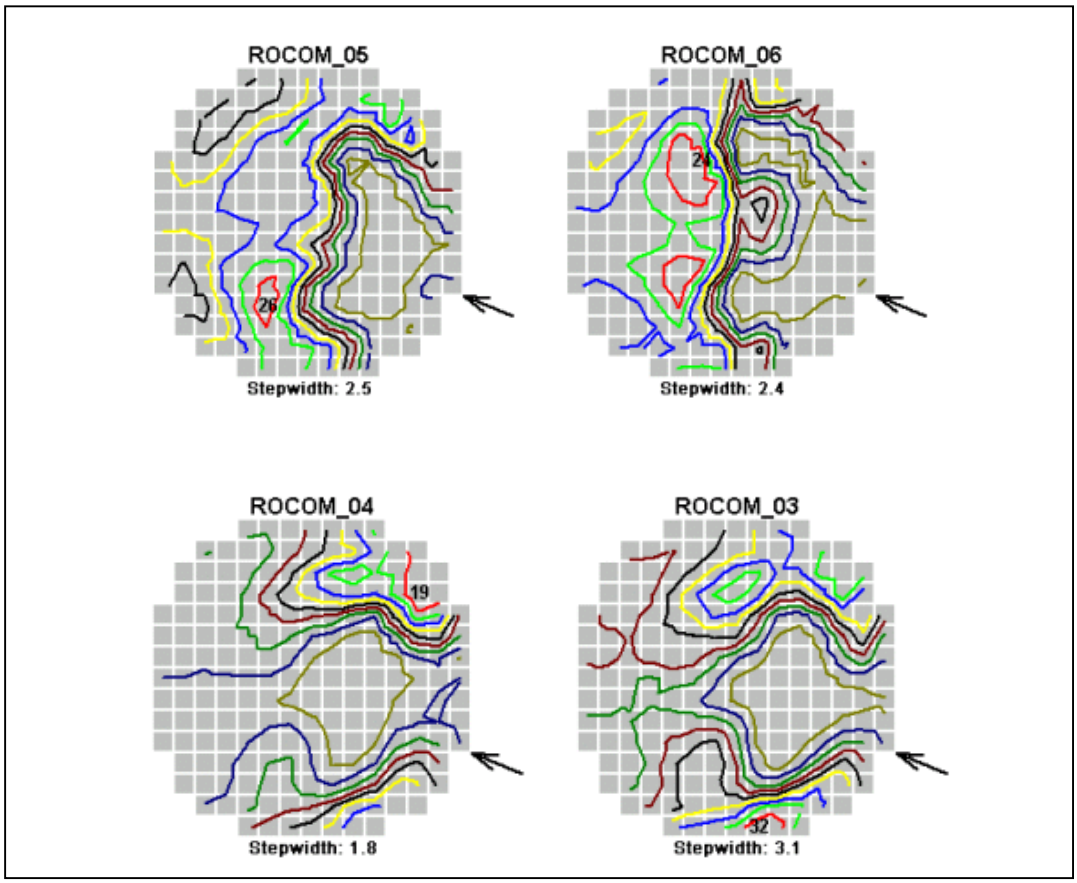

Fig. C.2.11 Core inlet distribution of the mixing scalar at the time point of maximum in the experiments with variation of the initial slug position

As it can be concluded from that figure, with increasing initial distance, the location of the maximum at the core inlet moves to the side opposite to the starting loop position. Further, the first experiment shows a significantly lower maximum value. That indicates, that a qualitative change of the flow conditions takes place during the pump start-up process. The typical velocity field, being responsible for the maximum at the opposite side of the core inlet cross section, establishes with a time delay of some seconds, only. Therefore, slugs entering the

vessel at an early stage of the process, flow more or less directly downwards, instead of flowing to the opposite side. In the initial stage of the mass flow increase, there is a slug-like movement of the whole liquid inside the RPV, while later two large vortexes are formed in the two parts of the downcomer left and right from the starting loop position.

In the experiment ROCOM-07 versus ROCOM-02, the influence of the status of the passive loops was investigated. In the experiments ROCOM-07 they are closed, so that a reverse flow is not possible. The volume flow rate in the loop with the starting up pump is practically not affected by the closed loops. The tracer is injected at the same time in corresponding experiments. The time course of the average and the maximum mixing scalar is very close between both experiments. The status of the loops has almost no influence on the mixing inside the reactor pressure vessel. The tracer arrives at the core inlet sensor slightly earlier in the experiments with closed gate valves. That is connected with a higher resulting velocity in the downcomer due to the absence of reverse flow in the idle loops.

Complementary experiments on slug mixing were performed at the VVER-1000 mixing test facility [Bez02]. A slug of low borated coolant was assumed to be accumulated in the cold leg loop seal located before the main coolant pump. The boron concentration in the reactor model was studied using the temperature method. The borated primary coolant was simulated by hot water at temperature of 65-75 ^{o}C, the un-borated slug – by cold water at temperature of 20-30 ^{o}C. The water volume in model loop seal was equivalent to 8.5 m^3 in the full-scale reactor. The circuit was heated up due to the heat released during operation of the circulation pump. After heating up, the pump was shut down and the gate valves at the loop seal inlet and outlet were closed. The hot water between the valves was replaced by colder one. The experiment was then started opening the valve in the moment of pump start-up. The mixing pattern at the core inlet was obtained from temperature measurements.

Because different from the ROCOM and Vattenfall mixing experiments, temperature differences were used at the Gidropress facility, there might be an impact of heat transfer to the walls and of density differences. However, the density difference between cold and hot water is lower than 3 % and was estimated to be negligible under pump start-up conditions with momentum dominated flow. Special experiments were performed to estimate the impact of heat transfer. Some experiments were repeated with the same boundary conditions, but varying the temperature difference between the cold and the hot water. It was concluded, that the heat exchange does not have a noticeable influence on the mixing measurements, and that the relative temperature characterises the degree of coolant dilution.

Three series of tests with final flow rates of 175; 470 and 815 m^3/h and pump start-up times of 2, 8 and 16 s and without back flow through the idle loops were carried out. Each series of the experiments consisted of five or six experiments for statistical averaging. The time behaviour of the relative temperature, averaged over the core inlet plane, is shown on fig. C.2.12. The results confirm qualitatively the findings from the ROCOM and Vattenfall tests (see fig. C.2.6 and C.4.33), but cannot directly be compared due to differences in the geometry of the facilities and in the boundary conditions of the experiments.

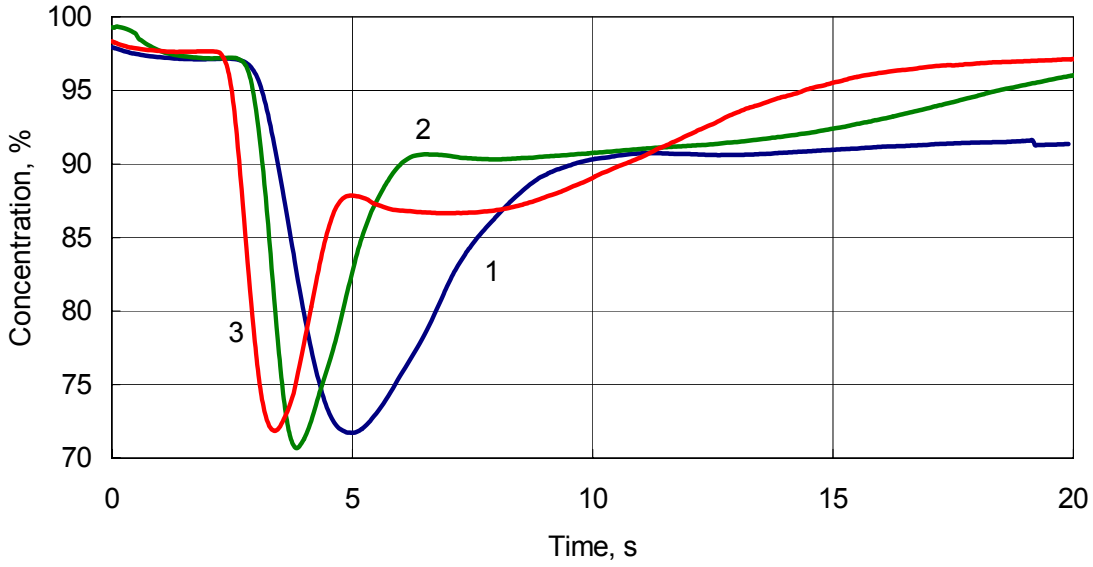

Fig. C.2.12 Relative temperature averaged over the core inlet plane for the VVER-1000 mixing tests (1 - 175 m³/h, 2 - 470 m³/h, 3 - 815 m³/h)

C.2.3 Experiments on buoyancy driven mixing

For the investigation of the influence of density effects, generic experiments have been carried out at the ROCOM test facility. It is expected, that density differences can be neglected, if the flow rates are sufficiently high, that means, if mixing is momentum controlled. The objective of these experiments was to find the conditions for transition from momentum controlled mixing, as it is typical for pump start-up scenarios, to buoyancy driven mixing, being relevant for PTS scenarios and natural circulation re-start after LOCA. Specific PTS mixing experiments has were performed at the Fortum PTS test facility.

Due to the fact, that the ROCOM facility cannot be heated up, the necessary density differences were simulated by adding sugar (glucose) to the water that is injected into the cold leg. To observe the mixing of the ECC water fed into the cold leg by the HPI system, this water was tracered by small amounts of sodium chloride, as in previous experiments. Generating density differences by high salt concentrations is not possible, because the measurement system is very sensitive and would be saturated at high salt concentrations. An accurately modelled ECC injection nozzle has been connected to one of the cold legs of ROCOM from side under an angle of 60°.

At the Fortum PTS facility, the colder water was injected from the bottom of the cold leg of the test facility. The mixing of the injection water was then observed by measuring temperatures in the downcomer and in the cold leg and visually through the transparent material of the facility. The density difference of the colder HPI water was further induced by salt addition. The density difference ratios between HPI and loop flow used in the tests was $(\rho_{HPI} - \rho_L)/\rho_{HPI} = \Delta\rho/\rho = 0.022 - 0.16$. In the ROCOM tests, a maximum density difference of 10 % was generated. Table C.2.2 gives a comparison of the features and parameters of the two facilities.

Feature	**Fortum PTS facility**	**ROCOM facility**
Measurement principle	Temperature	Conductivity
Density differences created by	Temperature (0.022) and salinity (up to 0.16)	Glucose solution (0.02 – 0.10)
Scaling	1:2,56	1:5
HPI	From bottom; Q_{HPI} = 0,1 – 4,0 l/s	From side: Q_{HPI} = 0,2 - 1,4 l/s
Flow rate in cold leg	Q_{CL} = 0 – 1,87 l/s	Q_{CL} = 0 – 12,8 l/s
Flow rate in adjacent loops	Q_{adj} = 0 – 2,0 l/s	Q_{adj} = 0

Table C.2.2
Main features and parameters of the ROCOM and Fortum PTS test facilities with respect to buoyancy driven mixing

The goal of the ROCOM experiments was the generic investigation of the influence of density differences between the primary loop inventory and the ECC water on the mixing in the downcomer. To separate the density effects from the influence of other parameters, a constant flow in the loop with the ECC injection nozzle was assumed in this study. The mass flow rate was varied in the different experiments between 0 and 15 % of the nominal flow rate, i.e. it was kept in the magnitude of natural circulation. The other pumps were switched off. The density difference between ECC and loop water has been varied between 0 and 10 %. In the Fortum PTS facility, experiments have been performed with coolant mass flow in the loops adjacent to the HPI loop. At ROCOM, only the HPI loop was operated. Table C.2.3 summarises the boundary conditions of the ROCOM experiments and selected Fortum PTS tests. In the table, only Fortum PTS tests with zero flow rate in the adjacent loops are included.

Nr	**Q_{CL}(l/s)**	**Q_{HPI} (l/s)**	**$\Delta\rho_{HPI}/\rho$**
Fortum PTS tests			
3	1.87	2.31	0.02
8	1.87	2.00	0.16
9	0	2.02	0.16
10	0	2.31	0.16
12	0	0.62	0.16
14	0.62	0.62	0.16
16	0	0.31	0.16
44; 45; 46	0	4.00	0.10; 0.16; 0.02
50	1.87	1.87	0.02
51	0	2.31	0.02
52	1.87	0.62	0.02
ROCOM buoyancy mixing tests			
3 - 8	7.72	1.00	0; 0.02; 0.03; 0.04; 0.05; 0.10
12 - 17	5.14	1.00	0; 0.02; 0.03; 0.04; 0.05; 0.10
26 - 31	2.72	1.00	0; 0.02; 0.03; 0.04; 0.05; 0.10
38, 39	0	1.00	0.05; 0.10

Table C.2.3
Selected ROCOM and Fortum PTS tests on buoyancy driven mixing with comparable boundary conditions

Altogether 20 experiments have been carried out at ROCOM. In all experiments, the volume flow rate of the ECC injection system was kept constant at 1.0 l/s. The normalised density is defined as the ratio between the density of water in the ECC loop and density of fluid in the circuit. All other boundary conditions are identical. Due to the observed fluctuations of the flow field in the RPV, each experiment was repeated five times to average over these fluctuations. In the following, the experiments are classified by the nomenclature DxMy, where x is the percentage of density difference and y is the percentage of nominal mass flow rate in the cold leg.

The experiments without density effects serve as reference experiments for the comparison. Fig. C.2.13 visualises in unwrapped views the time evolution of the tracer concentration measured at the two downcomer sensors. The downwards directed bold arrow indicates the position of the loop with the running pump, in that case delivering 10 % of the nominal flow rate. In the left figure, the results from experiment 12 according to table C.2.3 are shown. No density difference was created. At the upper downcomer sensor, the ECC water (injected in each experiment from t = 5 to t = 15 s) appears directly below the inlet nozzle. Due to the momentum created by the pump, the flow entering the downcomer is divided into two streams flowing right and left in a downwards directed helix around the core barrel. At the opposite side of the downcomer, the two streaks of the flow fuse together and move down through the measuring plane of the lower downcomer sensor into the lower plenum. Such a flow distribution is typical for single-loop operation. It is dominated by the momentum insertion due to the operating pump or high natural circulation flow rate. The maximum tracer concentration of the ECC water in the downcomer is 20 % of the injected water concentration at the upper sensor and 8 % at the lower sensor.

Fig. C.2.13 (right) shows the experiment 17, carried out at the same flow conditions, but the density difference between the injected ECC water and the primary loop coolant is now 10 %. In that case a streak formation of the water with higher density is observed. At the upper sensor, the ECC water covers a much smaller azimuthal sector. The density difference partly suppresses the propagation of the ECC water in horizontal direction. The ECC water falls down in an almost straight streamline and reaches the lower downcomer sensor directly below the affected inlet nozzle. Only later, coolant containing ECC water appears at the opposite side of the downcomer. The visualisations of the behaviour of the ECC water in the downcomer reveals that in case of momentum driven flow, the ECC water covers nearly the whole perimeter of the upper sensor and passes the measuring plane of the lower sensor mainly at the opposite side of the downcomer. When the density effects are dominating, the sector at the upper measuring device covered by the ECC water is very small. The ECC water falls down straightly and passes the sensor in the lower part of the downcomer below the inlet nozzle of the working loop. Furthermore, variations of the density were carried out to identify the transition region between momentum driven and density driven flow.

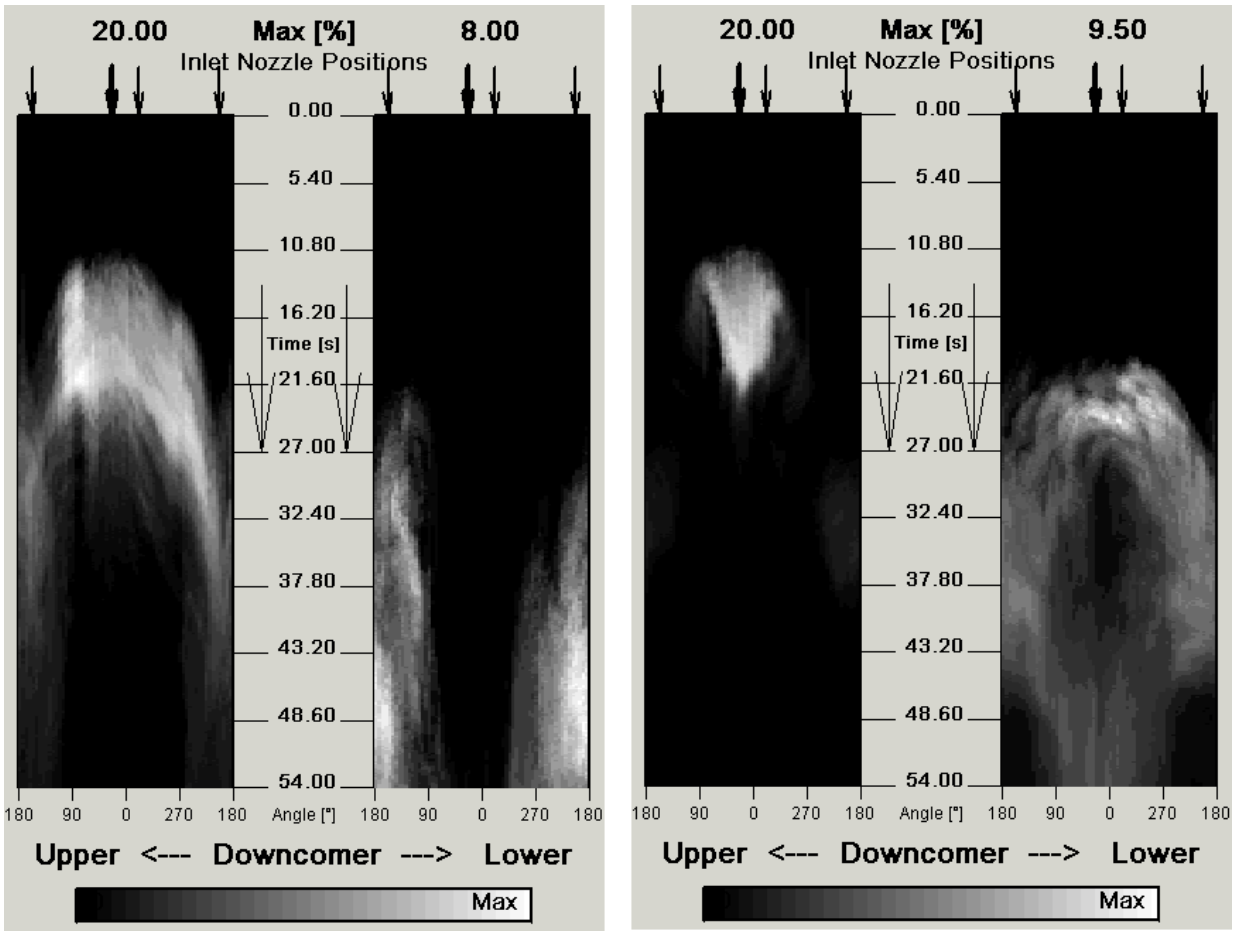

Fig. C.2.13 Mixing scalar evolution in the downcomer in ROCOM buoyancy driven mixing tests (10 % mass flow rate, left – no density difference, right - 10 % density difference)

Based on these observations, the set of experiments conducted according to table C.2.3, was divided into three groups: density dominated flow (◊), momentum dominated flow (Δ) and the transition region (*). The conditions at the inlet into the downcomer were used to calculate Froude-numbers of the experiments according to the following formula:

$$Fr_{DC} = \frac{v_{in}}{\sqrt{g \cdot H \cdot \frac{\rho_{in} - \rho_a}{\rho_{in}}}} \qquad \text{(C.2.2)}$$

where v_{in} is the velocity at the reactor inlet (combined loop and ECC flow), g is the gravitational acceleration, H is the height of the downcomer, ρ_{in} the density of the incoming flow, calculated with the assumption of homogeneous mixing between ECC and loop flow, and ρ_a the density of the ambient water in the downcomer. Lines of constant Froude-numbers calculated by means of this formula are shown in Fig. C.2.14. All experiments, identified as density dominated are located in the region left of the isoline *Fr = 0.85* and all momentum dominated points are found right of the isoline *Fr = 1.5*. Therefore, *Fr = 1* is about the critical Froude number separating the two flow regimes for the ROCOM test facility. Around this critical Froude number a transition region is located.

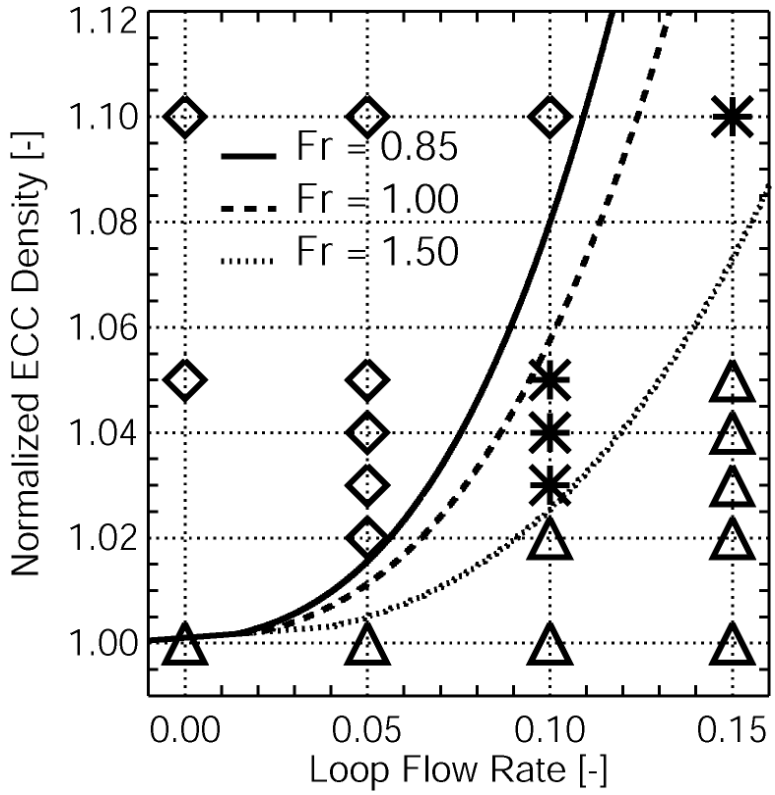

Fig. C.2.14 Classification of the ROCOM tests with density differences with respect to the downcomer Froude number (equ. C.2.2)

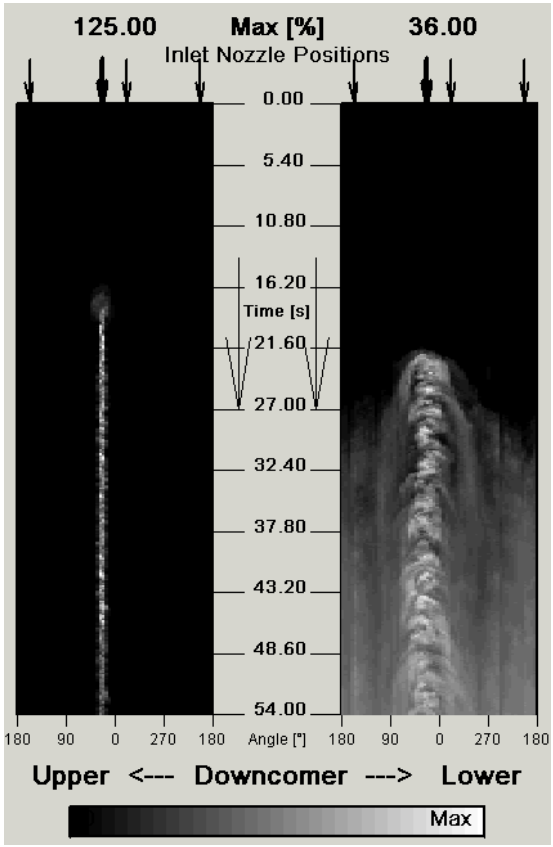

Density effects are extremely developed in an experiment with no flow in the primary loop (Fig. C.2.15), where the fluid circulation is initiated only by starting the ECC injection. At the upper sensor, the ECC water appears unmixed and covers a sector of only about 15 degrees. The data from the lower downcomer sensor show clearly buoyancy induced turbulent structures. As can be concluded from these data, the water with higher density accumulates in the lower plenum.

Fig. C.2.15 Mixing scalar evolution in the downcomer in the ROCOM buoyancy driven mixing test D10M00 (no cold leg flow rate, 10 % density difference)

Applying the same Froude scaling as it is given in equ. C.2.2, all Fortum PTS tests are located in the density driven mixing region. In the Fortum experiments, additionally the mixing in the cold leg due to the HPI injection was investigated. When the flow in the main loop is maintained by the natural circulation, nearly ideal mixing of HPI injection water is obtained. However if the loop flow is stagnant the mixing is not complete, and stratification and buoyancy driven re-circulation dominate the behaviour of the system [Tuo87]. The mixing of the HPI water in the injection point depends on the injection Froude number and the injector geometry. A quantitative criterion of this mixing is the so-called backflow ratio. The backflow ratio $Q^* = Q_h/Q_{HPI}$ is defined as the ratio between the flow rates of the stratified colder layer in the bottom of the cold leg flowing to the downcomer and the counter-flowing hot stream from the downcomer ("backflow Q_h"). Q* has been calculated from the temperature data of the experiments. Fig. C.2.16 presents the dependence of the backflow ratio from the modified Froude number [Tuo87]:

$$Fr_{CL,HPI} = \frac{Q_{HPI} / A_{CL}}{\left(gD_{CL}\Delta\rho_{HPI} / \rho\right)^{1/2}} . \qquad \text{(C.2.3)}$$

Q_{HPI} is the injection flow rate, A_{CL} the cross section of the cold leg, D_{CL} – the diameter of the cold leg, $\Delta\rho_{HPI}$ the density difference between HPI water and cold leg flow. The Froude number definition of equation C.2.3 contains characteristic parameters for the HPI injection mixing, while the Froude number according to equ. C.2.2 is related to the downcomer parameters. A high back flow ratio means strong stratification, low back flow ratio indicates better mixing. The back flow ratio is a parameter to be compared with results from the CFD validation calculations.

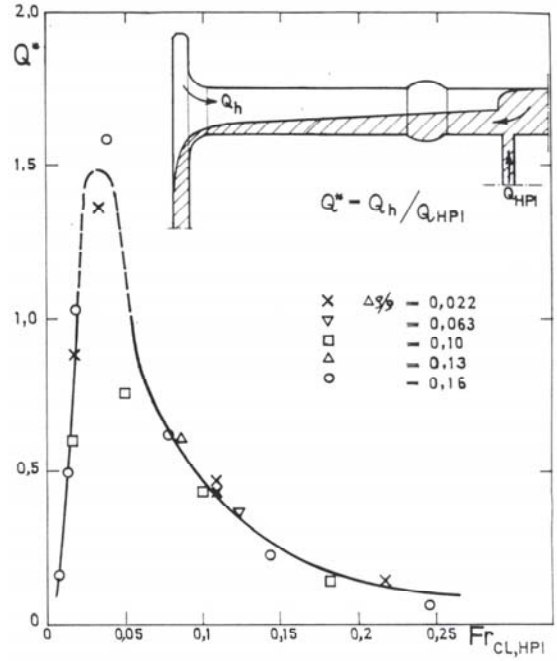

Fig. C.2.16 Measured back flow ration in the Fortum PTS tests as a function of cold leg Froude number (equ. C.2.3)

On fig. C.2.17, the time evaluation of the concentration of the HPI water averaged over all measurement points at axial position 164 mm below the inlet nozzles (see fig. C.2.5) in test 10 is shown. The comparison with analytical full mixing curve shows, that mixing in that region is weak. Comparison with CFD results will contribute to the CFD code validation.

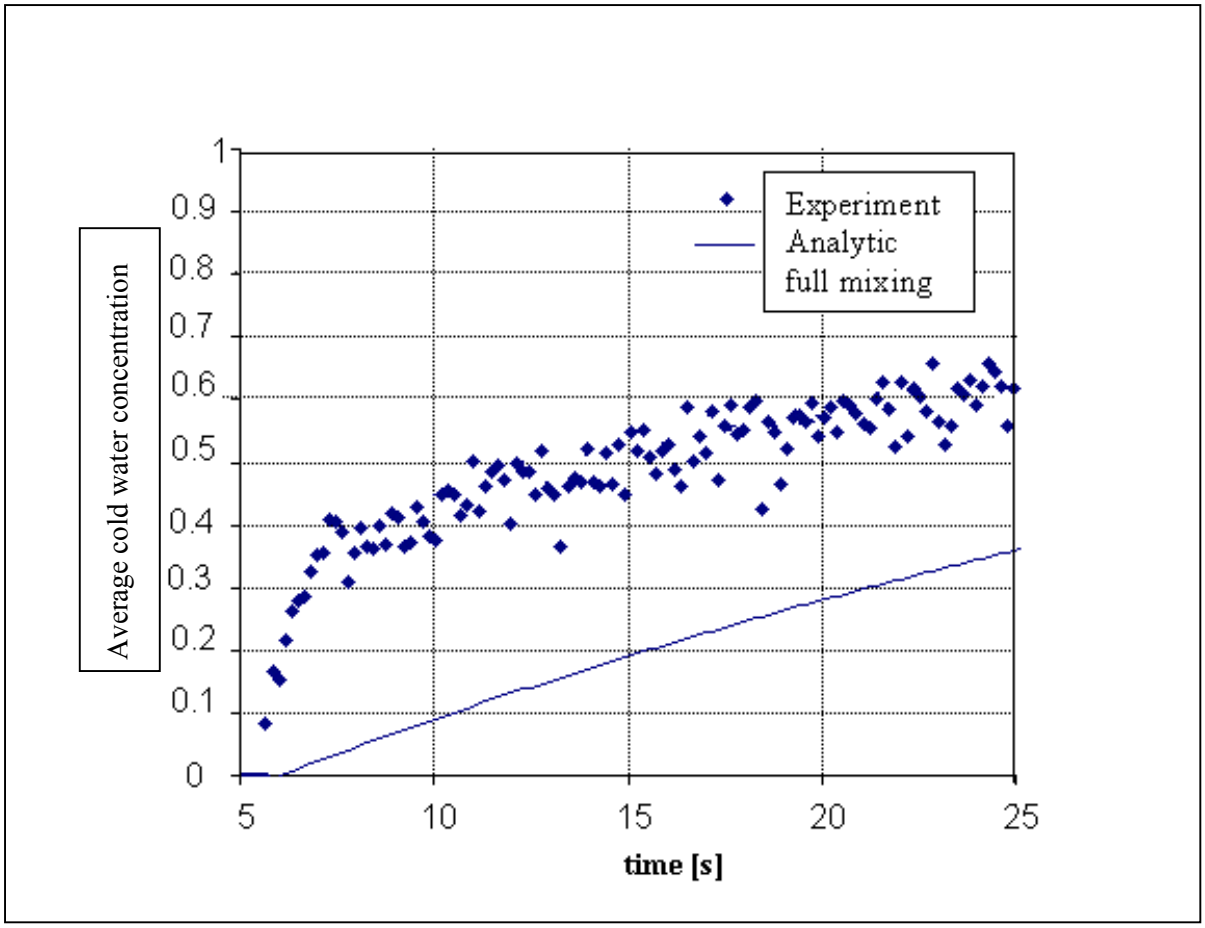

Fig. C.2.17 Average HPI water concentration at axial level z = - 164 mm (see fig. C.2.5) in Fortum PTS test 10

C.3 Steady-state mixing and flow distribution (WP 3)

C.3.1 Introduction

Flow distribution in the primary circuit of the pressurized water reactor (PWR) is an important issue connected to many operational problems. The temperature profile at the core outlet, relevant for the determination of the reactor power and thus for economical plant operation, is directly influenced by the flow distribution at the core inlet. Also the quasi-steady flow with macroscopic oscillating swirls inside the reactor vessel can cause temperature fluctuations and therefore is of importance to long-term thermal fatigue.

The flow distribution at the core inlet is influenced by the flow field in the pressure vessel and the flow distribution between the loops. The flow distribution between the loops is a particularly important factor during the asymmetric loop flow or temperature conditions. The asymmetric loop flow distribution is possible for example due to the pump operation uncertainties during power operation or due to the total pump failure during accident scenarios. The asymmetric temperature conditions are especially important in case of a steam line break. During a steam line break the overcooling of one or more primary circuit loops occurs. The mixing of the loop flows before the core inlet must be properly modeled in order to correctly predict the reactivity margin or the power excursion of the core.

Typically in the cases presented above at least some of the main coolant pumps are operating or a fully developed natural circulation is established. Therefore, a turbulent quasi steady-state flow field and a momentum controlled mixing are expected to be the relevant flow and mixing mechanisms, and were the main object of interest in the work package 3 of FLOMIX-R project reported here.

In work package 3 the primary circuit flow distribution was studied both with experimental and computational methods. The main focus was on the

- influence of the flow pattern entering the downcomer, which requires modeling of the primary circuit piping to account for effects originating from the RCP, pipe bends and steam generator exit and
- the swirl behaviour in the downcomer and the lower plenum.

The experiments were carried out at the ROCOM mixing test facility. The effect of the total flow rate, the number of the operating loops, the relative location of the operating loops and the asymmetric loop flow rates were studied with nine steady state mixing experiments. The steady state mixing experiment data was also added to the data base of FLOMIX-R for later use for the CFD code validation.

The CFD simulation of the selected ROCOM experiments was performed. The main focus was to validate and test CFD methods against the well-documented experimental data. The main varied parameters were the mesh cell number and the effect of geometric details included to the model.

The CFD simulation of the flow field and mixing in the downcomer and the bottom of the pressure vessel in VVER-440 PWR was also performed. The main focus was to test the CFD methods for simulation of a case having a real plant scale and the real power operation boundary conditions and also have a more detailed understanding about the flow field and the mixing of the loop flows. The main difference to the CFD simulation of experiments was the larger Reynolds number, typically 10^7 in the main loops, that requires more computation mesh cells and thus larger models. The calculated results were qualitatively compared to the measurement data available from NPPs.

C.3.2 ROCOM steady-state experiments

Steady state mixing and flow distribution measurements have been performed at the ROCOM test facility. The matrix of experiments is shown in table C.3.1. It comprises 9 experiments with various combinations of running pumps, while the idle loops are open for back flow, and various mass flow rates in the working loops. As it was mentioned in the introduction, the study of mixing under steady state conditions is important for overcooling transients, when all pumps are running, but the cold leg temperature is much lower in one of the loops (experiment ROCOM-stat01). To check the mixing pattern in the case of fully developed natural circulation, the mass flow rate in all loops were reduced in one experiment (ROCOM-stat02). The flow distribution in the case of different combinations of running pumps is of interest for operational states during reactor start-up procedure (ROCOM-stat03, -stat04, -stat05, stat06, -stat07). Two cases with an asymmetry of 10 % and 20 % in the flow rates between two loops are considered being of interest from the viewpoint of NPP operation, where loop flow rate differences can occur (ROCOM-stat08, -stat09).

Run	**Flow rate [m^3/h]**			
ROCOM-stat	**Loop 1**	**Loop 2**	**Loop 3**	**Loop 4**
01	185	185	185	185
02	50	50	50	50
03	185	back flow	back flow	back flow
04	185	185	185	back flow
05	185	back flow	185	back flow
06	185	185	back flow	back flow
07	185	back flow	back flow	185
08	203,5	166,5	185	185
09	222	148	185	185

Table C.3.1
ROCOM test matrix of steady state mixing experiments (The loop with the tracer solution injection in the test matrix is the loop number one).

Besides of tracer concentration measurements according to the measurement technology described in section C.2.1, measurements of the velocity field in the downcomer were performed by applying laser Doppler anemometry in most of the experiments. The measurement data was also made available for the validation of CFD methods. The steady state experiment with only one loop in operation represents the final state for the slug mixing test with start-up of the first pump.

Because mixing experiments cannot be performed under real steady-state conditions with permanent tracer injection, the following approach was applied. A sufficiently large slug of tracer solution was injected assuring "saturation" in the sense, that the tracer distribution is nearly constant at the core inlet for some time. If the injection time is too short and the tracer slug is too small, the mixing along the stream lines leads to reduction of the maximum tracer concentration in comparison with the "saturation" value. On the other hand, if the slug is too large, it will turn around the whole circuit, and the front of the slug comes back to the core inlet a second time still during continuation of the injection.

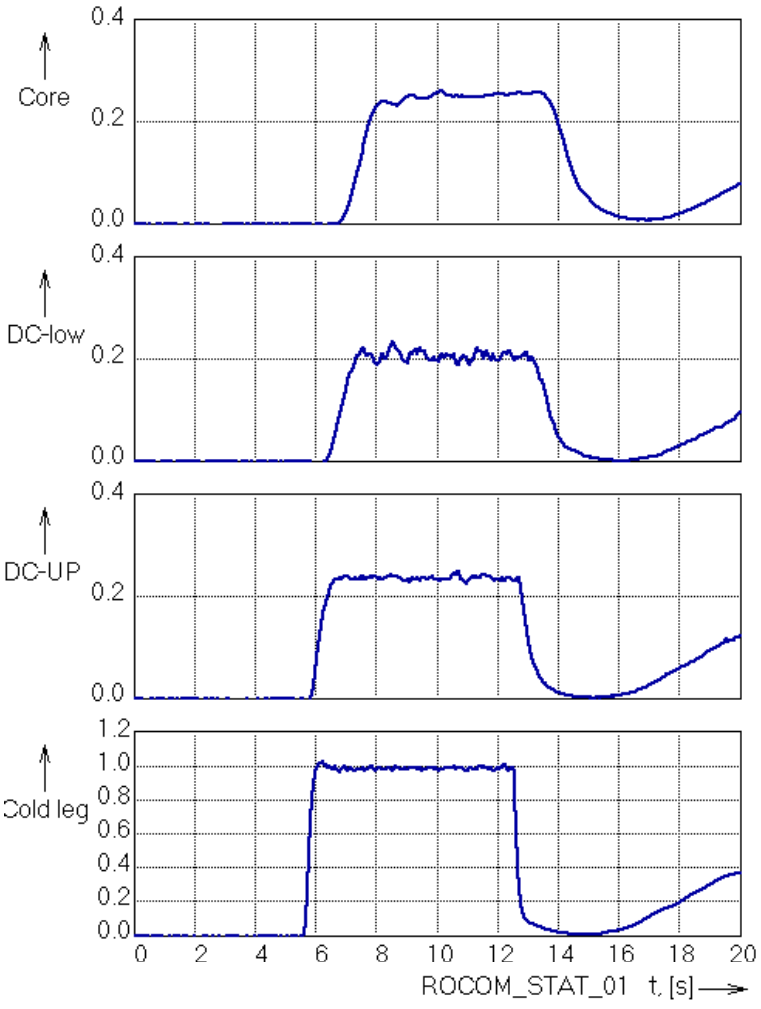

In the experiments, considerable fluctuations of the tracer concentration distribution at the core inlet have been observed. They are due to macroscopic turbulent fluctuations of the velocity field. Therefore, the measurement data from 5 repeated realizations of the same experiment were used for averaging. Fig. C.3.1 shows the time behaviour of the average mixing scalar at the inlet nozzle, upper and lower downcomer and the core inlet. The averaging was performed individually for all four sensors over the time interval, when the mixing scalar was nearly constant at plateau level. In case of the core inlet, averaging was made between t = 8.5 s and t = 13.2 s.

Fig. C.3.1
Time-dependent average mixing scalar at the sensor positions in experiment ROCOM-stat01

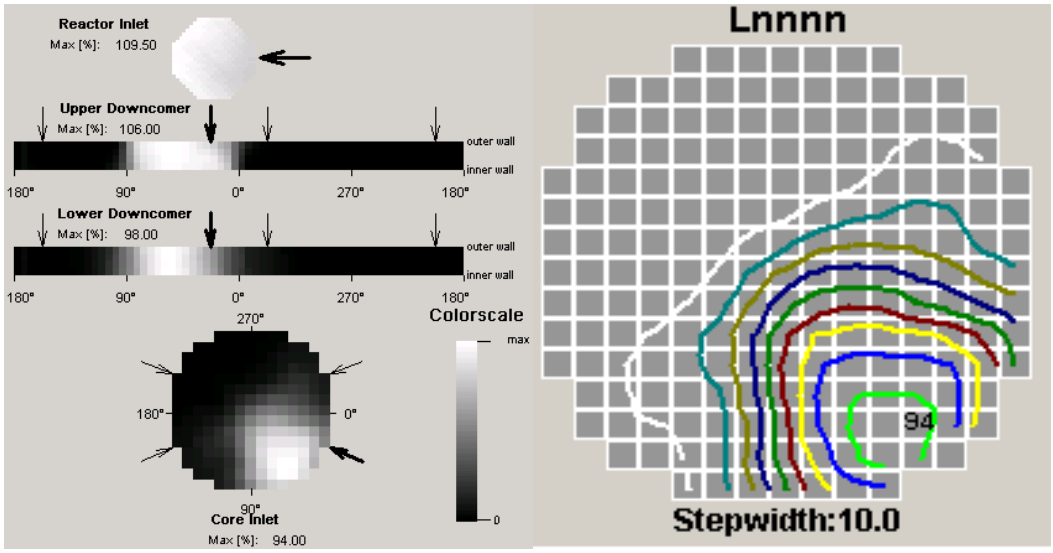

Fig. C.3.2 Plateau-averaged mixing scalar in experiment ROCOM-stat01

The averaged mixing scalar distribution in the measurement planes is shown on fig. C.3.2 (left). The mixing scalar is almost homogeneously distributed in the cold leg pipe cross section at the RPV inlet. In the downcomer and in the core inlet plane a sector formation is seen. An isoline plot of the mixing scalar is shown in fig. C.3.2 (right). The maximum mixing scalar value is 0.94.

That means, a part of the tracer reaches the core inlet plane almost un-mixed. The sector becomes more and more smeared on the way from the inlet nozzle to the core inlet. This is caused not only by turbulent dispersion in the flow, but also by turbulent fluctuations of the velocity field.

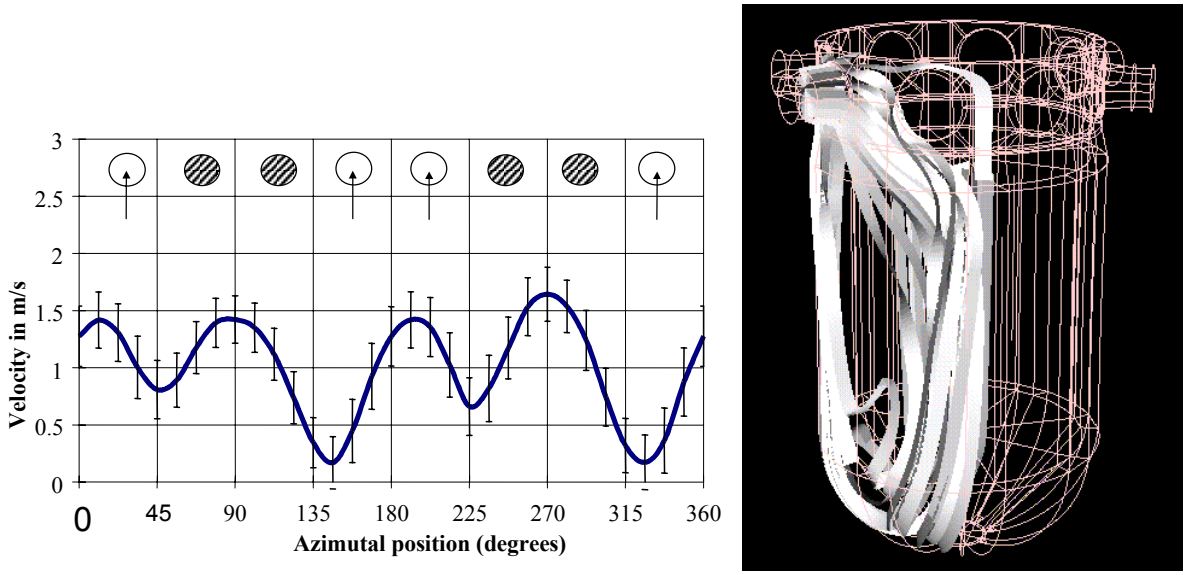

Fig. C.3.3 Velocity distribution in the downcomer under normal operating conditions – measured vertical velocity component (left) and streamlines (right)

The measured velocity distribution around the perimeter in the lower part of the downcomer is shown on fig. C.3.3 (left). An illustrative picture of the velocity field is shown in the right part of the figure. It can be seen, that there are minima of the vertical velocity component at positions below the inlet nozzles, while the maximums are located between the inlet nozzle positions. The jets from neighbouring loops impinging on the core barrel and move downwards meet at that positions. The velocity fluctuations measured by the LDV device were used to get the uncertainty band of the velocity measurement shown on the left figure.

Concerning the effects investigated in the 9 different experiments of the test matrix, only the case of asymmetric loop flow, when all pumps are running, will discussed in the following. This effect was investigated in experiments ROCOM-stat08 and ROCOM-stat09 with 10 % and 20 % asymmetry between two neighbouring loops.

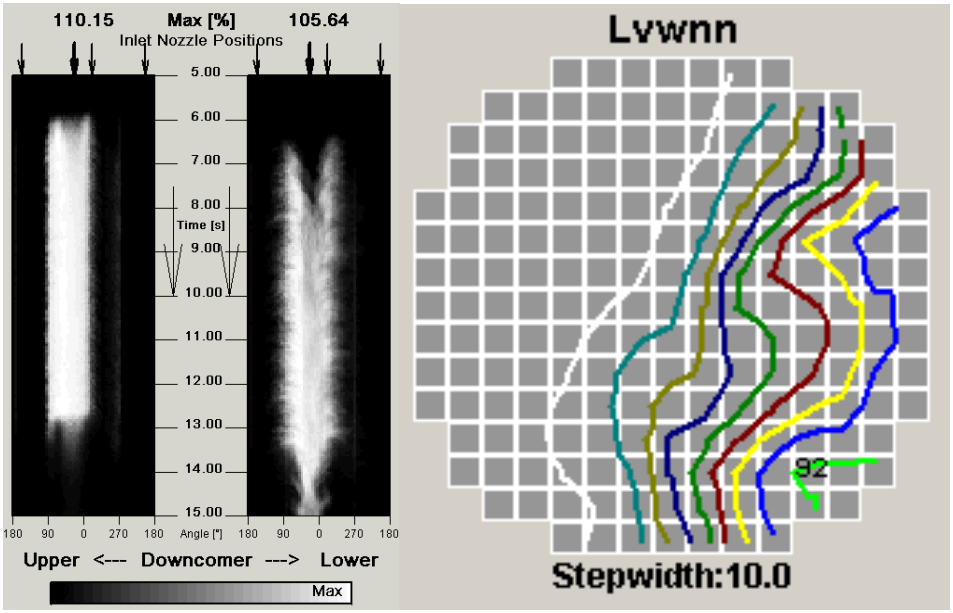

Fig. C.3.4
Time evolution of the mixing scalar in the downcomer (left) and plateau-averaged mixing scalar at the core inlet (right) in experiment ROCOM-stat09 with asymmetric loop flow rates

Fig. C.3.4 shows in the left part the time evolution of the mixing scalar in the downcomer, in the right part the mixing scalar distribution at the core inlet in experiment ROCOM-stat09. In this case of only 20 % mass flow rate asymmetry, the mixing pattern has significantly changed. The sector with high mixing scalar values is extended to more than 90 degrees, because the mass flow rate in the loop with tracer injection is higher than in the other ones. Further, at the core inlet a second maximum appears in the distribution. The splitting of the tracer already starts in the lower part of the downcomer. Due to the asymmetry in the flow rates, the distribution of the tracer is comparable with an experiment with tracer injection into two loops. The velocity field in the downcomer is responsible for this splitting. The results show, that the velocity field and the mixing pattern are very sensitive to the inlet flow boundary conditions.

C.3.3 Measurements at NPP

Experimental investigations on flow distribution and coolant mixing under steady-state conditions have also been performed at nuclear power plants. In the 70ties, first measurements were carried out at the Loviisa and Sizewell power plants (e.g. [Tsi82]. Experiments at the Paks VVER-440 NPP were carried out in 1987-1989 during commissioning tests of newly replaced safety valves of the steam generators [Elt02]. A series of 60-80 experiments was performed at about 10-15% of reactor power, where the main steam line valve of one steam generator was closed causing the heat-up of the corresponding loop. After some time, by slow increase of the reactor power, the safety valve of the steam generator was forced to open. At the moment just prior to the opening of the safety valve the cold leg temperature of the investigated steam generator were by 8-9^{o}C higher than that of the others, while the heat-up of coolant in the reactor in this cases was only 3-4^{o}C. Therefore, a significant asymmetry in the core outlet temperature distribution was caused and measured by the 210 thermocouples, located in the fuel assembly heads. Analyzing the date from 12 experiments under different conditions, where some of them have been repeated several times, mixing matrices have been derived by linear regression analysis.

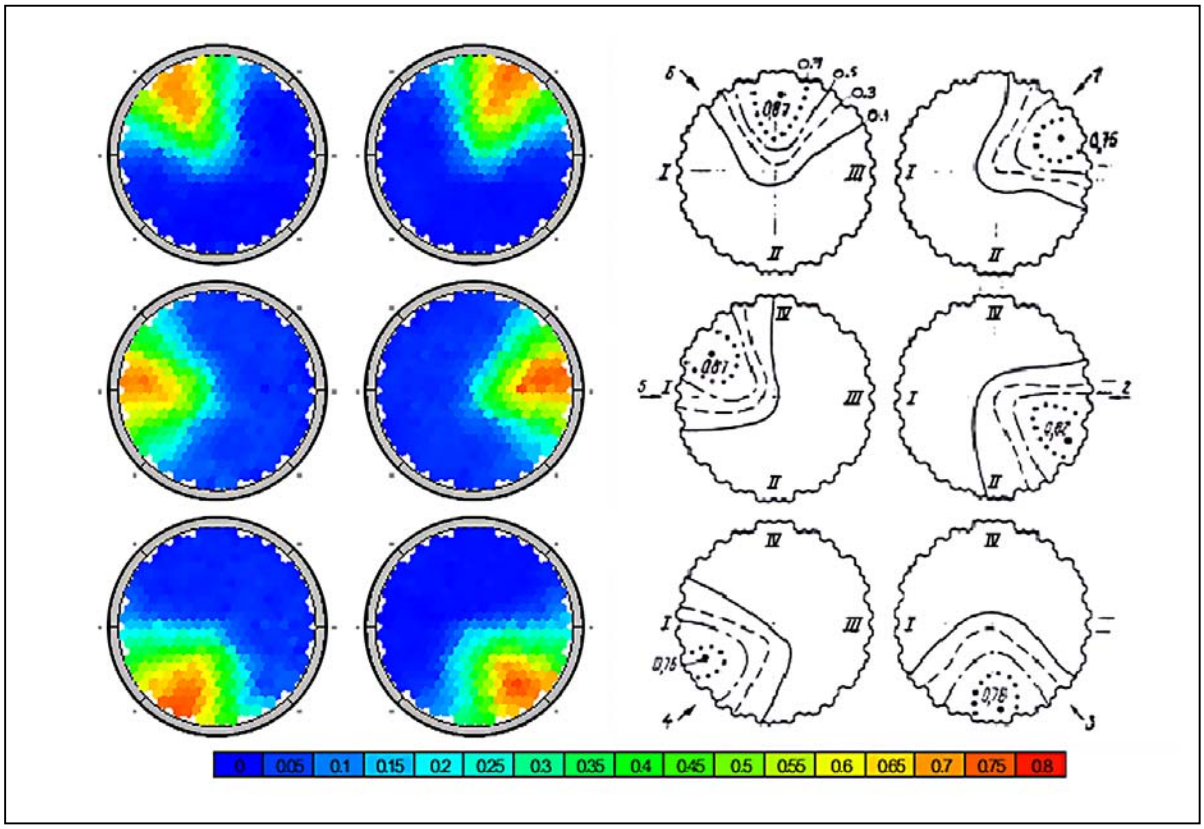

Fig. C.3.5
By-loop mixing factors at Paks leftr) and Loviisa (right) reactors
(Elter, 2002 and Tsimbalov, 1982)

These matrices describe the fraction of the perturbation of the coolant temperature in one primary circuit loop assigned to each fuel element (6 matrices - one for each loop of the VVER-440).

The maximum mixing coefficients in any case are not below 75%. The absolute error of the matrix coefficients was evaluated to about 3%. A symmetry perturbation of the mixing matrices was found caused by internal structures in the downcomer (coolant baffles aimed at directing the emergency core cooling water from the hydro-accumulators to the core). No swirling, as it as was observed in earlier experiments at the NPP Loviisa, was found in the Paks measurement results (see fig. C.3.5). This is probably due to the different constructions of the main coolant umps in both NPPs.The measurements at NPP Paks confirm qualitatively the results obtained at ROCOM, although the geometry of the RPV and its internals is quite different in the corresponding reactor types. Mixing under steady state conditions is quite incomplete. The degree of mixing is quite higher in the slug mixing case due to the high momentum insertion caused by the pump start-up.

The mixing data from the real reactor are very important, because the comparison of this data with CFD results provides information about real uncertainties in the CFD reactor calculations, which are not only due to model errors and numerical errors of the CFD code, but also due to uncertain information e.g. on boundary conditions, uncertainties of the measurement technology, uncertainties in real geometry and other uncertainties, which can be minimised in the tests at the experimental facilities, but not in the real reactor. Another advantage is the real scale of the tests. However, the measurement error is certainly higher in the real reactor.

C.4 CFD code validation (WP4)

C.4.1 Introduction

The main objective of FLOMIX-R WP4 (Work Package 4) is to investigate how well mixing during boron dilution PWRs can be modelled by Computational Fluid Dynamics codes. CFD calculations are an alternative to model tests for investigating mixing in the primary system in PWRs. This type of three-dimensional problem needs detailed three-dimensional calculations. One-dimensional system codes can therefore not be used. The category of boron dilution transient considered is characterized by a rapid start of a RCP with a slug of un-borated water present in the RCS pipe. In some model tests for which calculations are made the difference in density between the borated and un-borated water has a big influence on flow and mixing.

The competitiveness of CFD is continuously growing due the rapid developments in computer technology. Computer capacity is still, and will be for a foreseeable future, a limiting factor for the capacity for CFD calculations to produce completely accurate results. Simplified models for describing turbulence therefore have to be used and the computer capacity put restrictions on the resolution in space and time that one can use in a CFD calculation. This leads to modelling errors and numerical errors that give more or less inaccurate results. Validation of the quality and trust of different approaches in CFD calculations are therefore needed in order to get an indication on how well boron dilution transients can be modelled. In FLOMIX-R WP4 validations of CFD calculations have been made against experiments for boron dilution transients performed in four different test facilities. In FLOMIX-R WP3 (Work Package 3) additional validations have been made for steady state mixing scenarios. These are presented in FLOMIX-R D10 [D10]. The results from the validations made in FLOMIX-R are also relevant for other types of mixing cases. In particular, such recommendations will be important to those users who consider applying CFD tools for the turbulent mixing in convective and buoyancy-driven flow and for turbulence modelling of the accelerated flow in complicated geometries. In the ECORA project a broader analysis of the capabilities for CFD for simulating safety-related flows in primary system and containments in nuclear reactors was made.

The purpose of making CFD calculations of a boron dilution transient or of a mixing steady state situation is to calculate spatial and temporal variations in boron concentration, temperature and vertical velocity at the inlet to the core. These data can later be used by a reactor dynamics code to calculate what happens in the core due to the calculated variations.

For the CFD work in WP4 the ERCOFTAC Best Practice Guidelines for CFD has been used. The ERCOFTAC Best Practice Guidelines for CFD (below also called the BPG) is produced by the ERCOFTAC special interest group on “Quality and Trust in Industrial CFD” [Cas00]. The purpose of the BPG is to reduce the many sources of errors that always occur in CFD calculations (numerical errors, model errors, application uncertainties, user errors, software errors) and to give credibility to CFD calculations. In the ECORA project a set of Best

Practice Guidelines for CFD analysis of problems specific for nuclear safety has been produced [Men02].

CFD calculations need very long computation times, especially for transient and three-dimensional calculations. The computational resources are therefore limiting for the amount of work that can be made in reasonable time, which severely put restrictions on the possibilities to fully apply the BPG. The continuously increasing computing power, will, however, make a full application of the BPG more and more feasible.

Calculations in WP4 have been made by the following partners: FZR, GRS, FORTUM, PSI, Vattenfall Utveckling, NRI, VUJE, AEKI, Budapest University and NRG. The commercial CFD codes CFX4, CFX5 and FLUENT 6 have been used.

CFD calculations have been made for the following tests.

- ROCOM (Rossendorf Coolant Mixing Model) test facility (1:5 scale German Konvoi PWR).
    - Steady state mixing cases ROCOM-stat01, -stat04, -stat08 and -stat09.
    - Transient slug mixing cases ROCOM-01, ROCOM-02, ROCOM-03 and ROCOM-08
    - Transient buoyant slug mixing cases D10M05 and D05M00

- Vattenfall test facility (1:5 scale Westinghouse PWR)
    - Steady state non-mixing case VATT-02
    - Transient slug mixing case VATT-02

- FORTUM PTS test facility (2/5-scale VVER-440 PWR)
    - Buoyant steady state mixing case 20
    - Buoyant transient cases 10, 20 and 21.

- GIDROPRESS test facility (VVER 1000 PWR)
    - Buoyant transient slug mixing test 1 and 2.

- PAKS NPP tests (VVER-440 PWR)
    - Data from the commissioning tests.

Summaries from the CFD calculations made for the different test facilities are presented in the following sections. Finally, general conclusions from all calculations made in are given, including recommendations for the CFD applications concerning use of grid, geometry, time step, turbulence models etc. and suggestions on how to make CFD calculations more competitive.

C.4.2 Application of the Best Practice Guidelines for CFD

This chapter will give further background information on the contents of the Best Practice Guidelines for CFD and how it was applied in the FLOMIX-R project.

The Best Practice Guidelines divide the different types of errors in CFD simulations into the two main categories:

- Numerical errors, caused by the discretisation of the flow geometry and the model equations, and by their numerical solution
- Model errors, which arise from the approximation of physical processes by empirical mathematical models

The BPG contain a set of systematic procedures for quantifying and reducing numerical errors. The knowledge of these numerical errors is a prerequisite for the proper judgement of model errors. They contain detailed information on:

- The formalised judgement of results obtained with different CFD software packages. This includes the definition and quantification of round-off, iteration, and discretisation errors, and the assessment of modelling errors.
- The consistent use of CFD methods for reactor safety problems. The corresponding guidelines relate to geometry and grid generation, boundary and initial condition specification, selection of suitable physical models, and handling of solution algorithms.
- The judgement of experiments regarding their use for verification and validation of CFD methods in nuclear reactor safety. The guidelines include criteria for checking global mass, momentum, and energy balances, consistency checks for field data, and plausibility checks. Experiments are grouped in a hierarchy ranging from laboratory studies (verification and validation tests) to industrial demonstration tests.

The BPG are built on the concept of an error hierarchy. This concept implies that numerical errors are quantified and reduced to an acceptable level, before comparison with experimental data is made. The separation of numerical errors from model errors then allows valid conclusions on model performance. The types of procedures and advice provided in the BPGs for performing CFD simulations are as follows:

- The first step is the selection of representative and solution-sensitive target variables. These can, for instance, be maximum variable values or integrated quantities like efficiencies or heat transfer coefficients (or one-dimensional distributions like wall heat transfer along a space or time coordinate).
- These target variables are then monitored in the iterative solution of a problem. The convergence criterion is set low enough so that the target variables are no longer affected by it.

- Then the discretisation errors are quantified by either performing grid or time-step refinement or by calculating the same problem with a different discretisation scheme and comparing target variables.
- The next issue is uncertainties arising from insufficient information about the problem definition and setup. These uncertainties can be quantified by performing calculations with variations on the unknown parameters and by a subsequent statistical analysis on the influence of these parameters.
- At this stage, the numerically certified solution can be compared with experimental data. The remaining differences are the model errors. They can only be reduced by applying more accurate models.

The application of the guidelines and procedures described in the BPG is especially important for the validation of CFD codes for nuclear reactor safety as there must be a strong emphasis on reliability and quality of the computational results. Reactor safety-critical flows are a special challenge for CFD simulations due to the complex geometry and transient flow conditions in real reactor scenarios that require very large computing resources. However, even for these cases, important information on the uncertainties in the simulation and the comparison with the data could be obtained. For the simulation of the ROCOM test cases with CFX, it was shown in a sensitivity study that the detailed geometric modelling of the lower plenum provides better results than the use of a porous media approach. The resulted in a stabilization of the simulations. The tests with different spatial and temporal discretisation schemes showed the sensitivity of the simulations to the details of the numerical formulation and confirmed that only after the numerical errors are quantified, the influence of the physical models can be analysed and effective model improvements can be made.

The Best Practice Guidelines for CFD were used as a basis for the work made in FLOMIX-R WP4, in the aim for making reliable high quality CFD calculations.

The tests that were chosen for validation were the ones with most relevance for the plant owners and also challenging from a modelling point of view. Great care was taken to get a correct description of the geometry and boundary conditions for the tests and to get the data required to compare CFD calculations with experimental data. The target variables were carefully selected to meet the purpose of a CFD calculation of a boron dilution transient, i.e. to calculate boron concentration and vertical velocity at the inlet to the core. Comparison criteria to be used for quantitative comparisons between CFD calculations and experiments were developed. These were tailored to be relevant for this specific application. These comparison criteria are presented in detail in Appendix 10 of Deliverable D11 [D11].

Sensitivity tests, i.e. to check to what extent the results from CFD calculations are sensitive to different model settings and assumptions, such as grid size and turbulence model, are a very important part of the Best Practice Guidelines. It was therefore decided to spend a lot of time and resources on sensitivity tests. Instead of making calculations for a large number of tests, focus was put on making sensitivity tests for a quite limited number of validation tests (e.g.

ROCOM-02, VATT-02 and one buoyancy mixing case from ROCOM and Fortum models). Only if sensitivity tests are made the solution errors and model errors can be quantified and only then you can get an indication on how good your CFD calculations are. Sensitivity tests for the following aspects were considered:

- Grid size
- Convergence criteria
- Round-off error
- Time-step size
- Turbulence model
- Inlet boundary position and inlet boundary condition
- Outlet boundary position
- Internal geometry
- Code

Summaries of how these sensitivity tests were made are presented below.

Grid size

The aim was to make CFD calculations that gave grid-independent solutions, i.e. results that do not change when the grid is refined further. A grid-independent solution can be defined as a solution that has a solution error that is within a range that can be accepted by the end-user, in view of the purpose of the calculations. According to the BPG, calculations must be made with at least three different grids in order to be able to quantify the grid-dependence of the calculations. The two finer grids should be made using a complete refinement of the nearest coarser grid, which means that the finest grid of the three grids should have 64 times as many cells as the coarsest grid. It soon became obvious that the limited computer resources available made it impossible to strictly follow this procedure. A quantification of the discretisation error could therefore not be made for any of the CFD calculations made in FLOMIX-R WP4. However, to get an indication of the magnitude of the discretisation error, grid-sensitivity test were still made. Different strategies for grid refinements were applied for these sensitivity tests.

As transient calculations for the slug-mixing tests are very CPU-demanding (the transient calculations made in FLOMIX-R WP4 required computation times of around one week or more, even when using fast PC clusters) it was decided to perform some sensitivity tests for the steady state flow situation instead of for the actual transient. This was done in spite of important differences between the steady state flow situation and the transient flow situation, especially for those cases where the flow still accelerates during the same time as the slug travels through the downcomer and lower plenum.

To minimize the discretisation error, second order schemes were used, both in space and time. Due to convergence problems, second order schemes could not, however, be applied for all calculations.

Another way to get an indication on the magnitude of the discretisation error is to make calculations with both first and second order schemes. This was made for some tests.

Convergence criteria

Care was taken to ensure that the calculations were converged to a level that would give the prescribed accuracy for the target variables.

Round-off error

Sensitivity tests were made for round-off error, i.e. using single or double precision.

Time-step size

Sensitivity tests were made for time-step size.

Turbulence model

Model errors should be evaluated only after solution errors have been quantified. As described above, quantification of discretisation errors was not possible to perform due to limited computer resources. However, sensitivity tests for turbulence model were still made.

The turbulence model is responsible for the quite dominating part of the model errors. Only RANS models (two-equation models (e.g. the standard k-ε model) and Reynolds stress models) were used in the work in WP4. Sensitivity tests were also made for different types of wall functions. Wall functions were used for all calculations.

Inlet boundary position and inlet boundary condition

The choice of inlet boundary position and inlet boundary condition (turbulence level, variation in inlet velocity field in space and time) can have a big influence on the flow pattern far downstream from the inlet. Therefore, either the inlet boundary was put very far upstream or sensitivity tests were made for inlet boundary position and conditions. The same procedure was applied for the position of the outlet boundary.

Internal geometry

Internal geometry can either be modelled in detail, be simplified or be totally omitted. One type of simplifying model that was used, especially for structures in the lower plenum, is a porous media model, with distributed resistances. A porous media model can greatly reduce the required CPU time for a calculation compared to when a detailed model is used, but it had to be verified through sensitivity tests that it gives the same results as a detailed model.

Code

The commercial codes CFX4, CFX5 and Fluent 6 were used [CFX4], [CFX5], [FLU], [FLU03]. For comparisons between codes exactly the same grid and models were used, as far as was possible.

C.4.3 Post-test calculations of ROCOM steady state mixing tests

C.4.3.1 CFX results

A baseline steady-state calculation of ROCOM-stat01 using CFX-5.6 was performed by GRS. The main aim of this calculation was to investigate systematically numerical and model errors by analyzing the mesh influence, different discretisation schemes, the location of the flow boundaries, the flow resistance in the lower plenum and different turbulence models. Details of the results are given in Appendix 2 of Deliverable D11 [D11]. The results of the base line parameter variations and sensitivity analysis are summarized in Table C.4.1.

Table C.4.1: Parameter variations and sensitivity analysis

Parameter	**Function / Value**	**Conc.**	**Velocity**
Round-off	Single / double precision	no	no
Grid variation	Grid width / adaptation	yes	yes
Discretisation	1st / 2nd order	yes	yes
Steel plate	Detailed model / porosity	yes	yes
Sieve barrel	32000 / 64000 [kg/m4]	yes	no
Turbulence model	k-ε / SST model	no	no
Turbulence intensity	3.7 / 7.4 [%]	no	no
Diffusivity	1.E-09 / 1.E-06 / 1.E-02 [m²/s]	yes	no

In the table it is indicated, wether the parameter or model variation has a significant impact on the target values. According to Best Practice Guidelines, the following target variables were chosen:

- Boron concentration at a position below the injection pipe and at the lower end of the downcomer
- Velocity distribution at the lower end of the downcomer

Then the influence of numerical and model parameters on the target variables was investigated [Gra03]. Round-off errors have no influence on the concentration or velocity distribution. The grid refinement steps included calculations on unstructured grids with 350 000, 500 000, 750 000 and 1 000 000 elements. Grid width has a strong influence on concentration and velocity distribution, as well as the discretisation schemes and the details of the modelled geometries. Figure C.4.1 shows the convergence of the calculated velocity distribution in the downcomer with mesh refinement. Second order upwind discretisation scheme (UDS) was used in these calculations.

The pressure loss across the sieve barrel was doubled and influence was found only on the concentration distribution. Turbulence model and turbulence intensity at the inlet showed no significant effect on the results. The value of molecular diffusivity between water and salt solution has also some uncertainty. The most likely value is $3 \times 10\text{-}6$. There was little change

between values of 1e-09 to 1e-06; however, when the diffusivity was further increased to 0.01, the concentration profiles were strongly influenced.

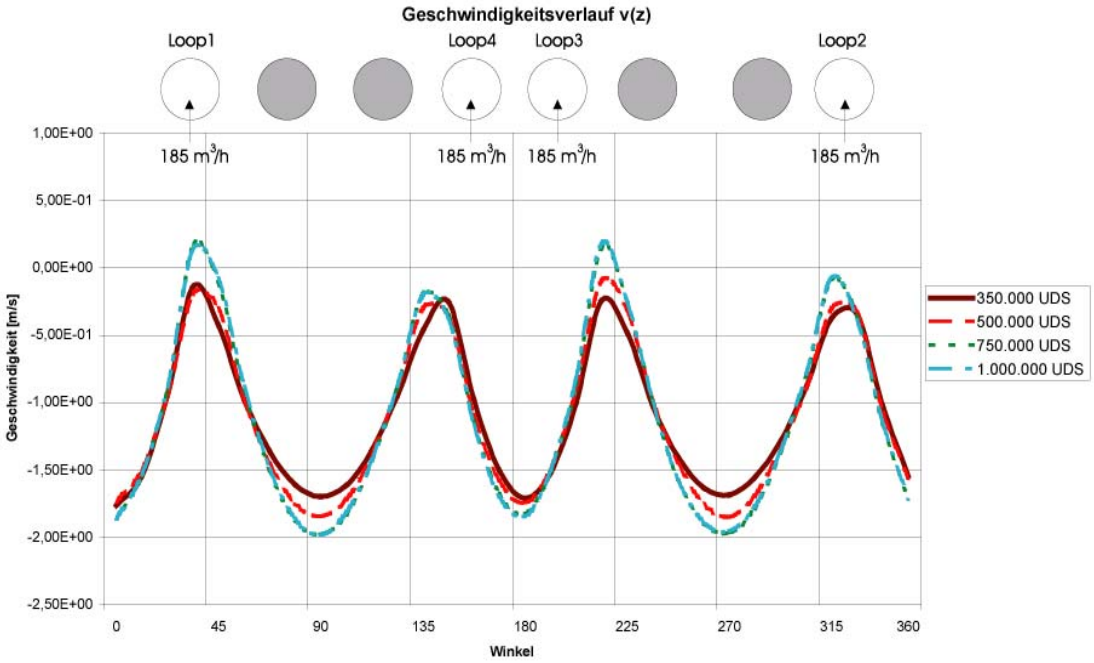

Fig. C.4.1 Convergence of calculated velocity distribution with mesh refinement

The CFD-Codes used for mixing studies at the Forschungszentrum Rossendorf (FZR) are CFX-4 and CFX-5. The specifics of CFX-4 are block structured discretisation grids and a porous medium model with volumetric, isotropic porosity and implementation of body forces added to the momentum equation, which can be anisotropically. In addition CFX-5 offers:

- Advanced coupled multi-grid linear solver technology
- Unmatched meshing flexibility
- Superb parallel efficiency
- Excellent pre- and post-processing capabilities

However, the porous body model of CFX-5 shows deficiencies, as it was found in simple test calculations. Therefore, first CFX-4 calculation were performed using the porous body approach, while in the CFX-5 calculations a very detailed mesh was used to confirm the CFX-4 results without additional physical models.

In CFX-4 the generated block structured grid contained ca. 450000 hexahedral elements (Fig. C.4.2 left). A finer mesh was created in the area of the inlet nozzle plane, in the area of the downcomer extension, around the perforated drum and at the core support plane. In CFX-5 the mesh contained 5 Mio. tetrahedral elements (Fig. C.4.2 right). Mesh refining was used in the area of the perforated drum and in the lower support plate. n the calculated cases, the turbulence was modelled using the standard (k, ε) approximation.

To investigate flow distribution and mixing under nominal operation conditions, experiments at the ROCOM test facility and CFD-calculations were for all main coolant pumps running. The velocity fields, visualised in fig. C.3.3, show a qualitatively good agreement between the CFX-4 and CFX-5 calculations and the experimental results gained earlier at an air operated model [Ul83] and confirmed by LDA measurements at ROCOM [Pr03] . Particularly, the calculations confirm the location of minimum flow velocities below the inlet nozzles found in earlier experiments [Ul83]. A maximum velocity exists at azimuthal positions between the two inlet resp. the two outlet nozzles. A comparison between measured and calculated velocity distribution in the lower downcomer is shown in fig. C.4.3. Please note, that in fig. C.4.3 the absolute values of the velocity are plotted.

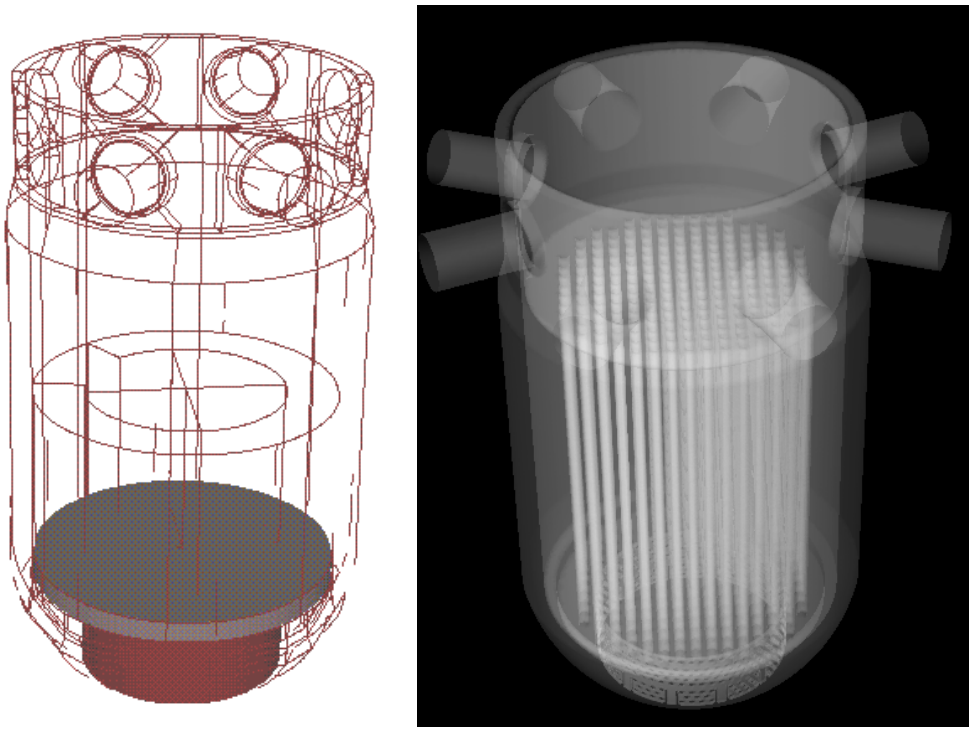

Fig. C.4.2 Computational mesh for CFX-4 (block structure, left) and CFX-5 (right)

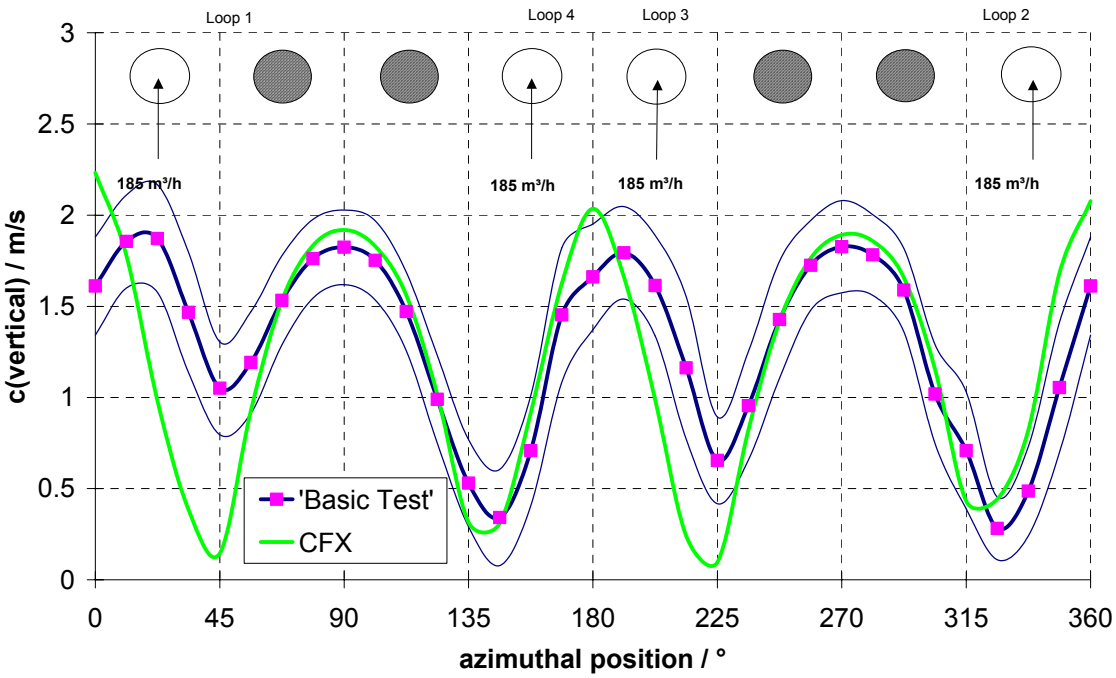

Fig. C.4.3 Velocity measurements vs. CFX-4 results at the end of the downcomer

The calculated and measured velocity distributions agree mostly within the uncertainty band of the measurements, with exception of the velocity minimum at 45 degrees (loop 1). There is obviously a deviation from the symmetry to be expected in the measured velocity field due to equal mass flow rates in all loops. A measurement error of this magnitude in the mass flow rates can be excluded. However, in loop 1 the mixing device for the tracer injection was installed. The mixer creates an additional flow resistance, which was taken into account by adjustment of the pump head in this loop. It is assumed, that the mixer affects the velocity profile, distribution of turbulence or occurrence of swirls induced by the pumps in the corresponding cold leg pipe, what may have an impact on the velocity distribution. However, this assumption could not be checked because velocity measurements near the RPV inlet were not possible.

Fig. C.4.4 shows comparisons between the calculated and measured mixing scalar (normalized, dimensionless boron concentration or temperature perturbation). At the inlet nozzle (fig. C4.4a) the same conditions as in the experiments (mixing scalar per time step, velocities in all loops) were set as inlet boundary conditions for the CFD calculations. In fig. C.4.4b, the instantaneous maximum of the mixing scalar at the core inlet independently of the actual fuel element position is plotted against the time. The maximum mixing scalar at the core inlet rapidly increases to the maximum. There is a good agreement between the measurement and the CFD calculations, especially in the averaged global mixing scalar at the core inlet (fig. C.4.4c). At the local position of the maximum mixing scalar the time course of the measurement and the calculations are also in good agreement (fig. C4.4d). The coolant from the loop with tracer injection almost completely arrives in the corresponding sector of

the core inlet (figures C.4.4e,f). On the other hand, some areas of the core inlet were not affected at all.

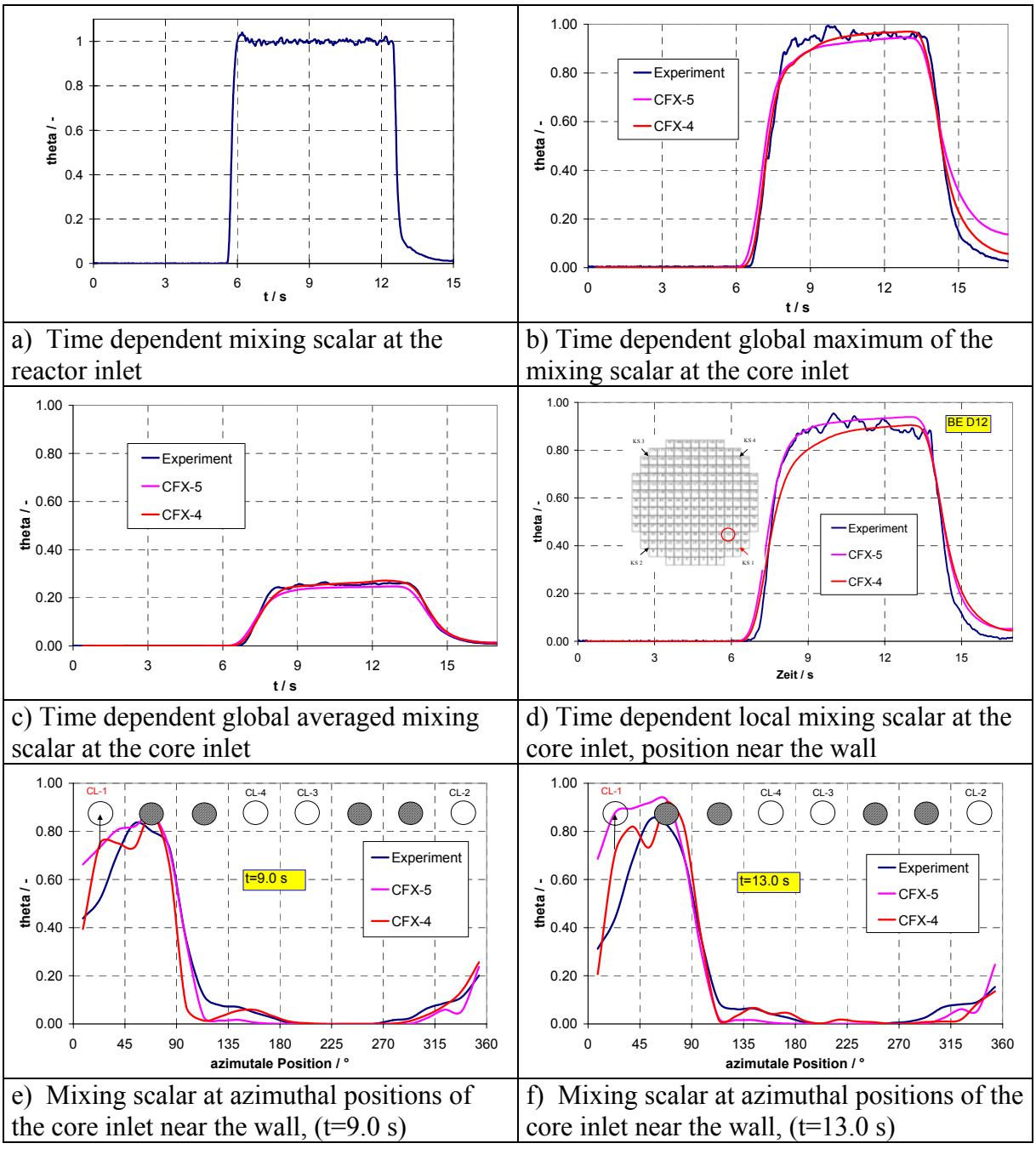

a) Time dependent mixing scalar at the reactor inlet

b) Time dependent global maximum of the mixing scalar at the core inlet

c) Time dependent global averaged mixing scalar at the core inlet

d) Time dependent local mixing scalar at the core inlet, position near the wall

e) Mixing scalar at azimuthal positions of the core inlet near the wall, (t=9.0 s)

f) Mixing scalar at azimuthal positions of the core inlet near the wall, (t=13.0 s)

Fig. C.4.4

Comparison of the measured and calculated mixing scalar (steady state flow field, 185 m³/h)

Despite of the flow deflection in the lower plenum and the partial penetration of the perforated barrel, the maximum disturbance observed at the core inlet is 91 % (CFX-4), 94% (CFX-5) and 95% (measurement) in comparison to a 100 % concentration change at the inlet nozzle. These results can only be obtained, if a sufficiently large slug of tracer has been

injected to create a quasi steady-state tracer concentration plateau shown in Figure C.4.4c, on which all data were time averaged. If smaller slugs are injected, steady state conditions at the core inlet are not achieved.

There are some local differences between the results of the CFX-4 and CFX-5 calculations seen at the sector of the maximum mixing scalar (figures C.4.4e and C.4.4f). Nevertheless, the comparison shows, that the use of the porous body approach with additional body forces gives reasonable results. However, there are local differences of both calculations to the experimental values, which are probably a result of unknown unsteady inlet boundary conditions (changing velocity profiles, turbulent fluctuations etc.).

Figure C.4.5 in section C.4.3.2 shows the plateau averaged mixing scalar distribution at the core inlet of the experiments and two CFX-5 calculations. One CFX calculation was done with the steady state flow field and the transient slug behavior was modeled. The other calculation was done in a steady state mode. For the transient calculation case the maximum value (94%) and the shape of distribution of the mixing scalar is in better accordance with the experimental value than for the steady state calculation. The sector formation of the mixing scalar below the injection loop is clearly to be seen in all pictures.

C.4.3.2 FLUENT results

The CFD code FLUENT has been used for performing second code calculations for the basic steady state mixing test ROCOM-stat01 and for calculating additional steady state tests with asymmetric operation of loops. The tests ROCOM-stat01 and ROCOM-stat04 (see table C.3.1) have been calculated by VUJE. AEKI calculated ROCOM-stat01 and –stat09. Second code calculations are an important contribution with respect to different mesh structures, specific turbulence models and particularly for modelling of internal structures.

Studies were performed to optimise meshing, set-up of boundary conditions and choice of turbulence models. Two turbulence models were used in the VUJE's calculations with the aim to find the impact of different turbulence models on results (standard K-ε model and RNG K-ε model). The calculations have shown, that RNG K-ε standard turbulence model and non-equilibrium wall function did not have noticeable beneficiary effect on the results. Therefore, in the "production calculations" the K-ε model was used. Second order upwind discretisation schemes was applied. K-ε model and Reynolds stress model (RSM) was used in AEKI's calculations.

For the description of the perforated drum in lower plenum, two models were tested: porous media and reduced number of holes. In the final calculation of VUJE, adapted hybrid mesh with perforated drum modelled as solid structure with reduced number of holes was used. Outlet boundary position was located at half of the core, which was modelled applying porous body approach. The finer mesh with 1.504.881 cells was used. However, no completely grid independent solutions were obtained. AEKI used the porous body approach for the sieve

drum. The mesh consisted of about 640.000 elements. The ROCOM tests were calculated as steady-state problems, no time step was defined in the calculations.

A comparison of the different FLUENT and CFX-5 results with measurement data (plateau averaged mixing scalar distribution at core inlet) for ROCOM-stat01 is shown on fig. C.4.5.

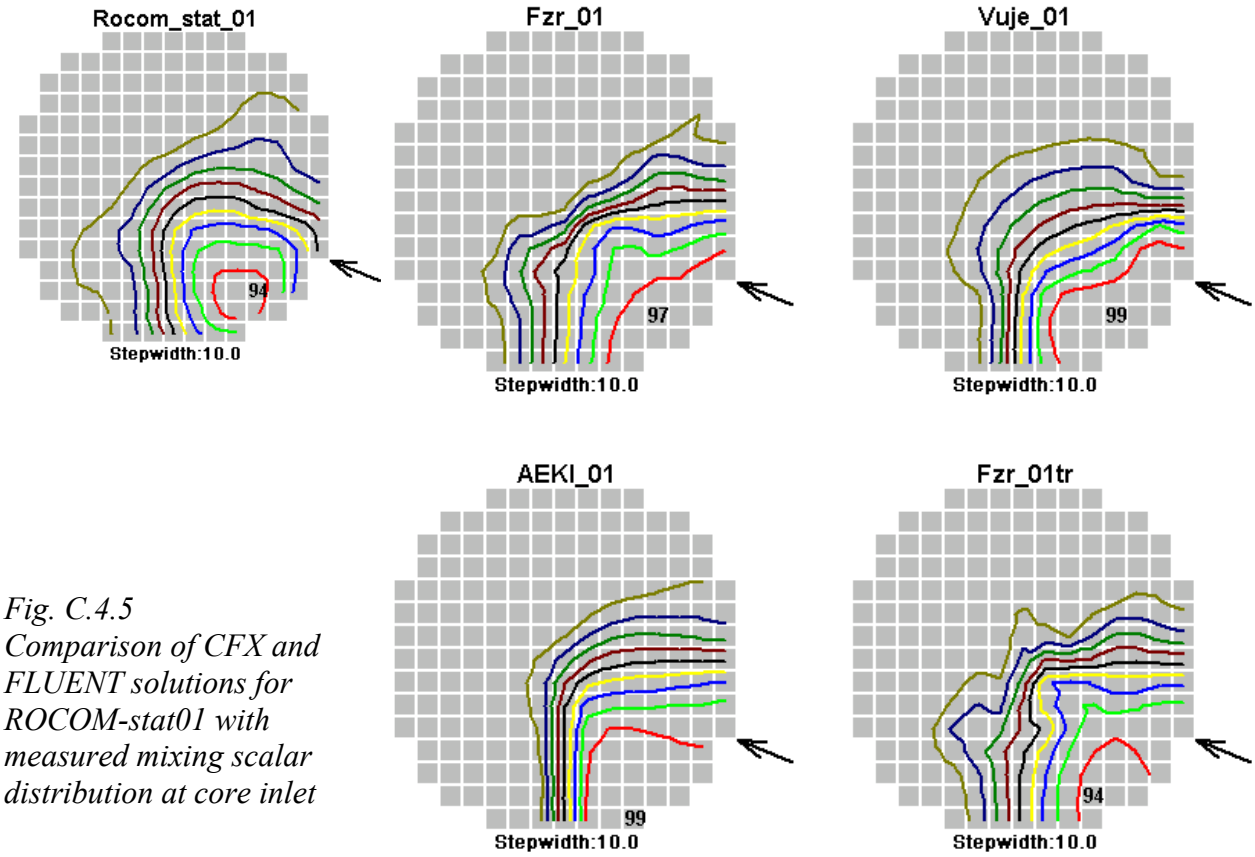

Fig. C.4.5
Comparison of CFX and FLUENT solutions for ROCOM-stat01 with measured mixing scalar distribution at core inlet

Fig. C.4.5 shows, that better agreement between measurement and calculation is achieved, when a transient calculation is performed, although the flow field is in principle steady state. However, macroscopic turbulent fluctuations occur even under steady state flow conditions, which are better reproduced as averaged in the transient solution. In all steady state calculations with CFX and FLUENT, the mixing is underestimated in comparison with the experiment.

By VUJE resp. AEKI, additionally the tests ROCOM-stat04 and ROCOM-stat09 have been calculated. The same options as in the "production" calculation for ROCOM-stat01 were used in the VUJE's calculations for ROCOM-stat04. The comparison for the mixing scalar at core inlet are shown on fig. C.4.6.

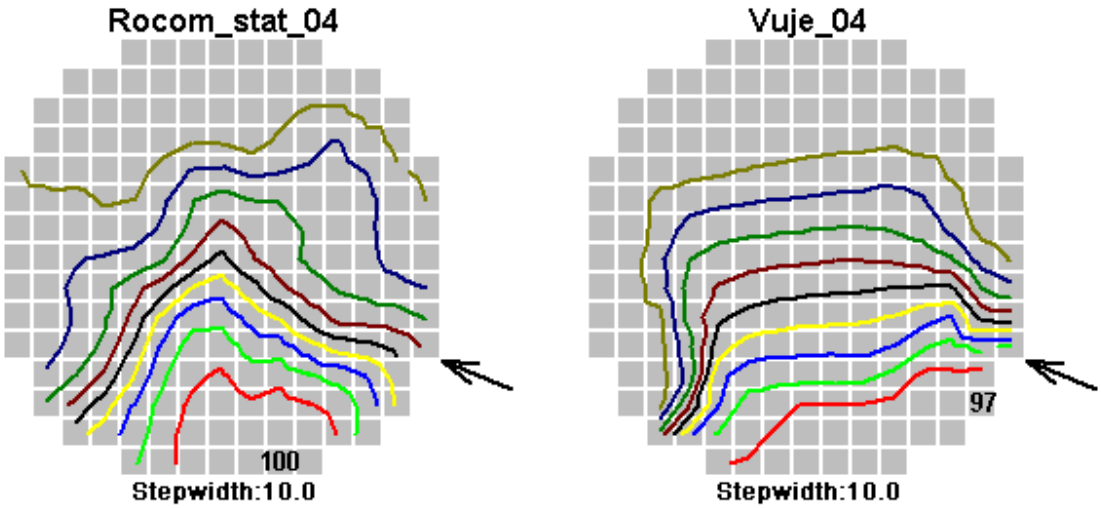

Fig. C.4.6 Comparison of mixing scalar distribution at core inlet for ROCOM-stat04

Calculated vertical velocities in the downcommer (Fig. C.4.7) have, in general, similar character as measured velocities with exception of the region below the nozzle of loop 1.

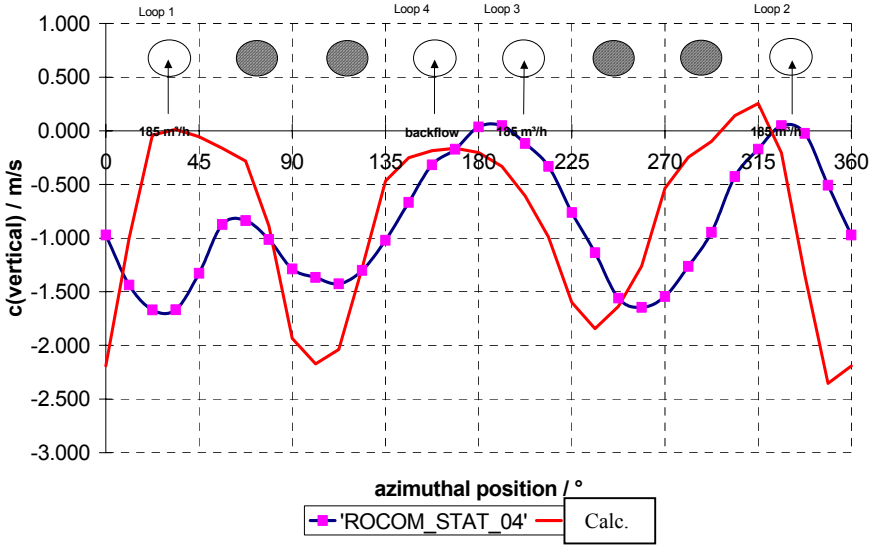

Fig. C.4.7: Measured and calculated downcomer vertical velocities in ROCOM-stat04 test

Mixing scalars at the upper and lower downcomer are shown in fig. C.4.8. Again, the underestimation of mixing in the downcomer in the calculation is seen .

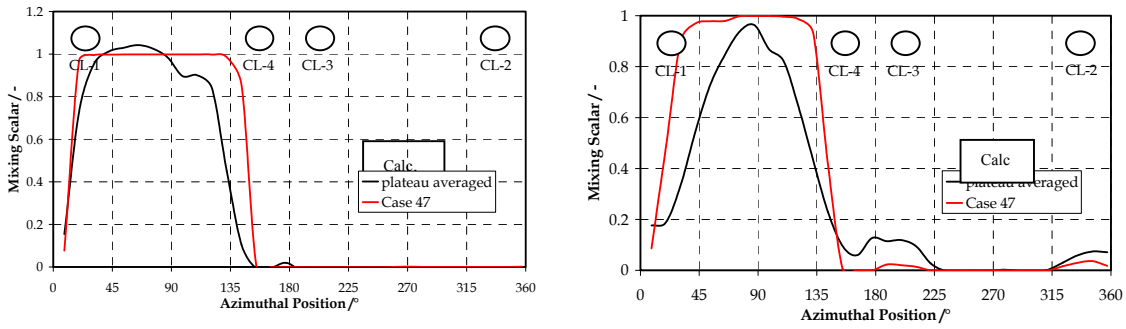

Fig. C.4.8: Mixing scalar at upper (left) and lower (right) downcomer

Fig. C.4.9. shows the comparison between calculation and measurement for the test ROCOM-stat09 calculated by AEKI.

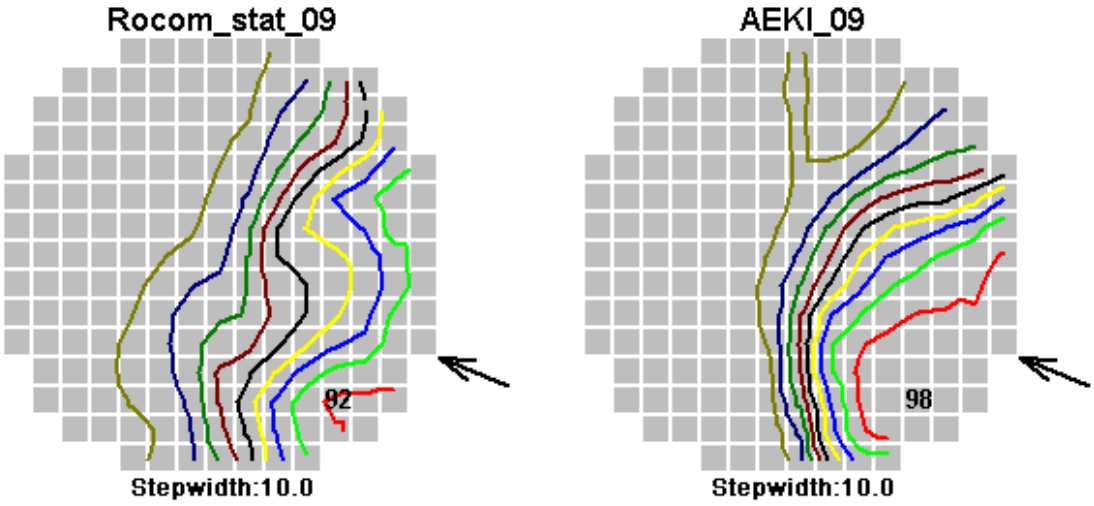

Fig. C.4.9
Comparison of mixing scalar distribution between calculation and measurement for the test ROCOM-stat09

C.4.3.3 Conclusions on CFD calculations of ROCOM steady state mixing tests

In general, the flow pattern, velocity distribution in the downcomer and mixing scalar distributions at the core inlet are qualitatively well predicted in the CFD calculations. The velocity field in the downcomer has inhomogeneous character with maximum downwards flow components in the regions in-between the inlet nozzles. A clear sector formation of the flow in the downcomer is seen. This leads to maximum mixing scalar values at the core inlet

of 92 – 99 %. That means, a part of the fluid remains almost unmixed. The re-distribution of the velocity field and mixing scalar distribution in the case of asymmetric flow conditions is also qualitatively well reproduced in the calculations.

Finer grids in the CFD simulation tend to give better results. Also modelling of perforated sheets (such as the drum in the lower plenum) as real structure rather than porous medium improves quality of results. Influence of porous medium as a substitute of a perforated sheet can be, in some extent, controlled by proper definition of direction-dependent resistance of the porous medium. Other investigated effects (turbulence model, wall function, position of outlet boundary) do not have an unambiguous influence on results. In general, the mixing along the flow path in the downcomer is under-predicted in all calculations. Disturbance in the inlet boundary conditions has significant impact on the flow pattern. This can be seen in experiment ROCOM-stat01, where a disturbance in turbulence or swirl intensity caused by the mixer is assumed to be responsible for an observed perturbation in the velocity distribution.

C.4.4 CFD calculations for the ROCOM slug mixing tests

The CFD calculations for ROCOM slug mixing tests were carried out with the CFD codes CFX-4, CFX-5 and FLUENT. The transient slug mixing cases ROCOM-01, ROCOM-02, ROCOM-03 and ROCOM-08 were calculated. Focus was put onto the benchmark case ROCOM-02. A second code calculation was performed for this case with FLUENT. In this report, only the calculations for the ROCOM-02 case will be summarized. A detailed description of all the calculations and their results is given in [D11].

The specific situation concerning CFX was, that during the duration of the project the code was undergoing an enormous development. The code versions CFX-4 and CFX-5 are practically completely different codes, concerning the code philosophy, the physical models, the numerics, pre- and post-processors. CFX-4 uses a block-structured mesh. The meshing philosophy for CFX-5 was initially based on un-structured, tetrahedral meshes. With the development of a new, CAD based pre-processor ICEM-CFD, hybrid meshes can be used with all kinds of unstructured elements, like prisms, tetrahedrals, hexahedrals, wedges etc..
Due to the specific situation with CFX, a broad variety of calculations was performed using CFX-4 and CFX-5.

C.4.4.1 CFX-4 calculations

In the CFX-4 calculations, internals were modeled using the porous media approach and additional body forces. Sensitivity studies showed, that the k-ε turbulence model together with the standard logarithmic wall functions give the best results. The block-structured grid contained 450.000 elements.

Higher order HYBRID discretization scheme was used. The temporal discretization was fully implicit 1st order backward Euler. A time step of 0.01 s was found to be an optimum between convergence and computational efforts.

Figure C.4.10 shows streamlines representing the velocity field in the downcomer and lower plenum (including the perforated drum and lower support plates as porous media) at the pump start-up scenario calculated with CFX-4. In loop 1 the MCP starts linearly from 0 to 185 m³/h in 14 s, after 14 s the mass flow rate is constant at 185 m³/h (Fig. C.4.11b), counter flows are developing at the other 3 loops.

Due to a strongly momentum driven flow at the inlet nozzle the horizontal part of the flow dominates in the downcomer (Fig. C.4.10). The injection is distributed into two main jets, the so-called butterfly distribution. In addition, several secondary flows are to be seen in various parts of the downcomer. Especially strong vortices occur in the areas below the non-operating loop nozzles and also below the injection loop. Here a strong re-circulation area occurs, which is controlling the size of other small swirls.

The initial space-averaged value of the mixing scalar at the inlet nozzle of Loop 1 was used as the inlet boundary condition (Fig. C.4.11a). The transient course of the maximum value at the core inlet is shown in Fig. C.4.11c. That maximum value or the minimum boron concentration is an indicator for possible reactivity insertion during a transient. In the experiment as well as in the calculation, the maximum value is determined at each time step over all fuel element positions. Therefore the position can vary, which has also an influence on the width of the confidence-interval of the experimental data. In the calculation, the maximum concentration at the core inlet is very close to the experimental data. The absolute value of the calculation and the experiment reaches 58% of the loop value (Fig. C.4.12).

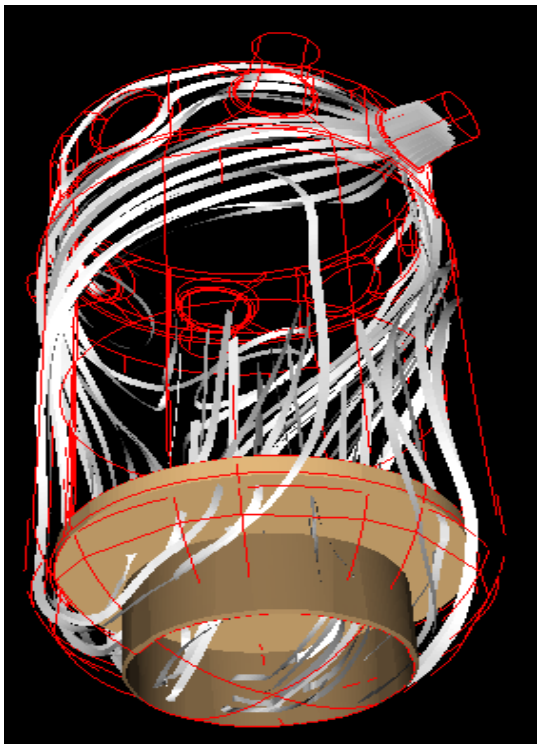

Fig. C.4.10 Flow picture at 15 s after the start-up

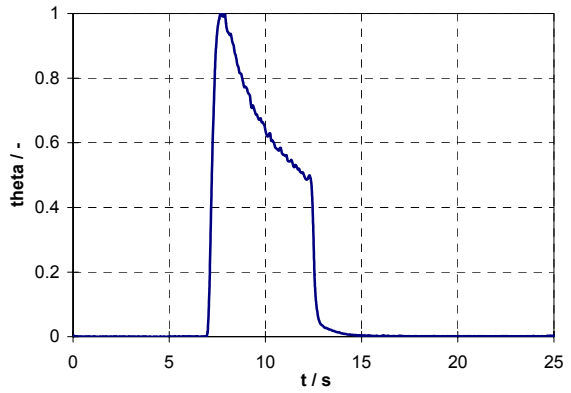

a) Time dependent mixing scalar at the reactor inlet

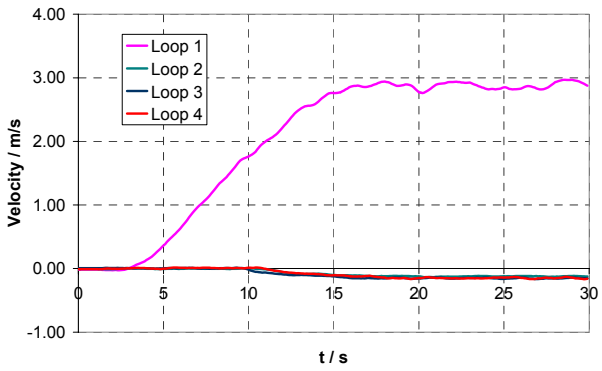

b) Inlet velocity loops 1-4, ramp and backflow in the idle loops

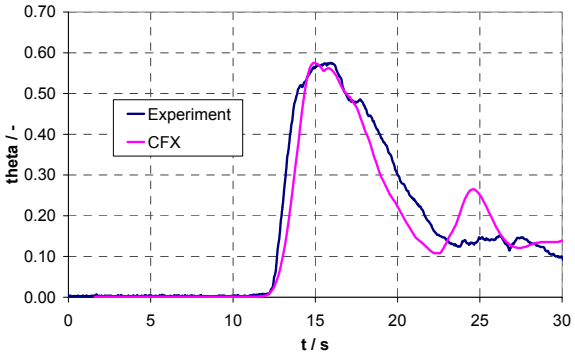

c) Time dependent global maximum of the mixing scalar at the core inlet

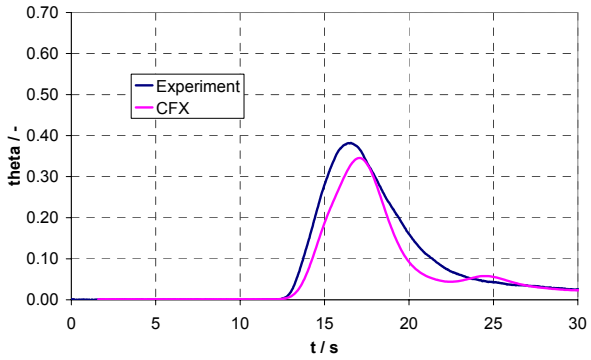

d) Time dependent global averaged mixing scalar at the core inlet

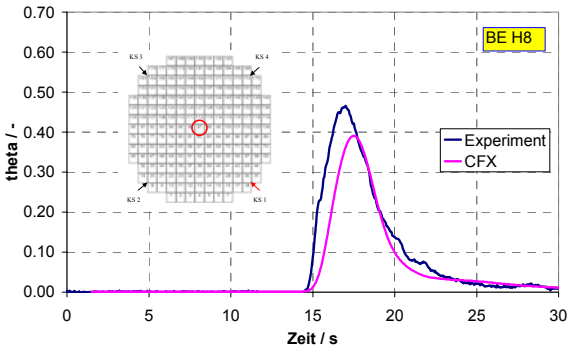

e) Time dependent local mixing scalar at the core inlet, center position

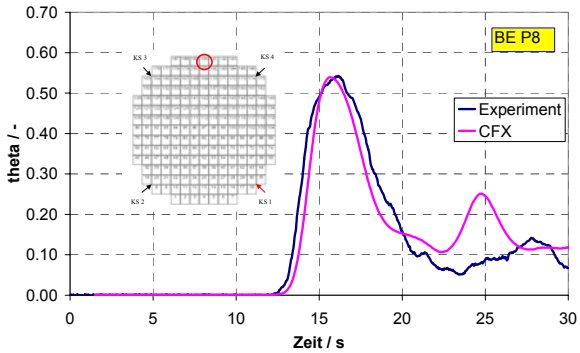

f) Time dependent local mixing scalar at the core inlet, position near the wall

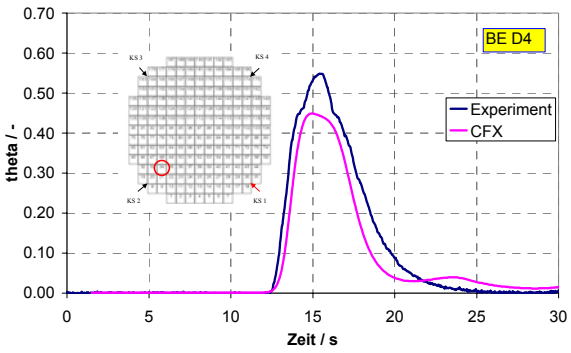

g) Time dependent local mixing scalar at the core inlet, position near the wall

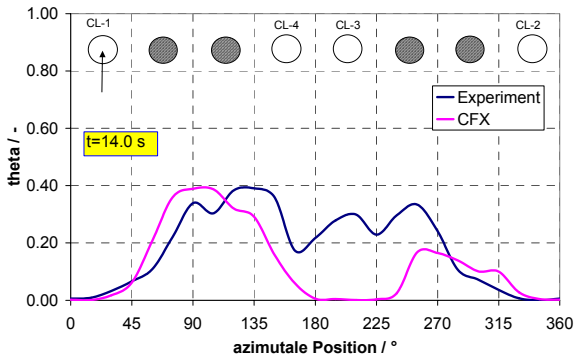

h) Mixing scalar at azimuthal positions of the core inlet near the wall, (t=14.0 s)

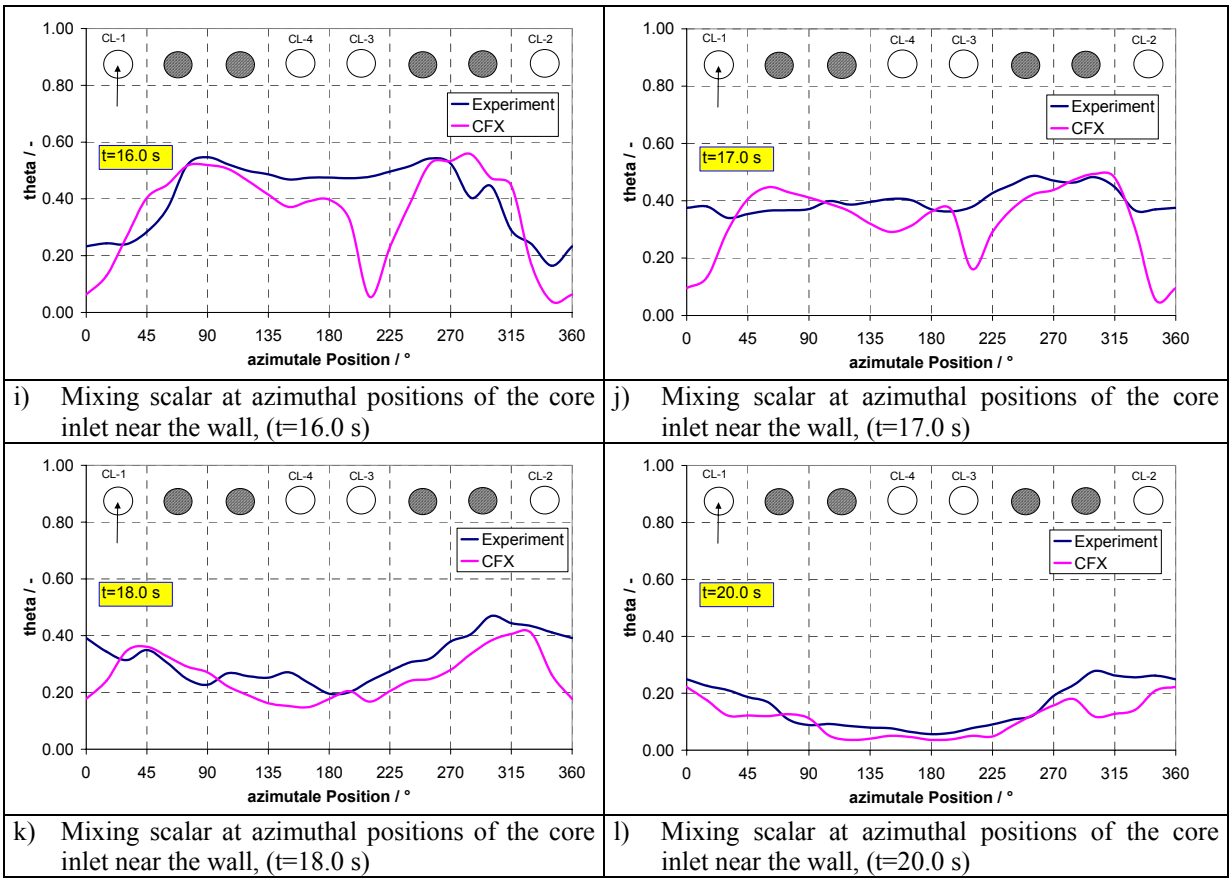

i) Mixing scalar at azimuthal positions of the core inlet near the wall, (t=16.0 s)

j) Mixing scalar at azimuthal positions of the core inlet near the wall, (t=17.0 s)

k) Mixing scalar at azimuthal positions of the core inlet near the wall, (t=18.0 s)

l) Mixing scalar at azimuthal positions of the core inlet near the wall, (t=20.0 s)

Fig. C.4.11 Comparison of the measured and calculated mixing scalar at the core inlet (ROCOM-02, start-up of the 1st coolant pump, 20m³ slug)

Local time dependent mixing scalars at fuel element positions in the center and near the wall of the core inlet are shown in the Figures C.4.11e-g. The turbulent fluctuations are significant only in the later part of the transient, when the maximum of the deboration front already passed the corresponding fuel element position. As can be seen, the fluctuations are higher in the outer part of the core. In addition, the mixing scalars at azimuthal positions near the wall of the core inlet are shown in Figure C.4.11h-l. About 15 s after switching-on the RCP, the deboration front reaches the core inlet at two positions in the periphery of the core about 90° shifted from the azimuthal position of the inlet nozzle of the loop with the starting pump. In the CFX-calculation the deboration front reaches the core at the same positions but earlier. The maximum of the deboration front moves over the center of the core to the side of the injecting loop (see also Figure C.4.11h-l).

The maximum mixing scalar value and the time point of its occurrence are well met in the CFX-4 calculation. Deviations between experiment and calculation occur at local positions. The mixing scalar distribution at the core inlet is qualitatively similar in experiment and calculation (two maxima). Results of calculations for the experiments ROCOM-01 are similar and are described in [D11].

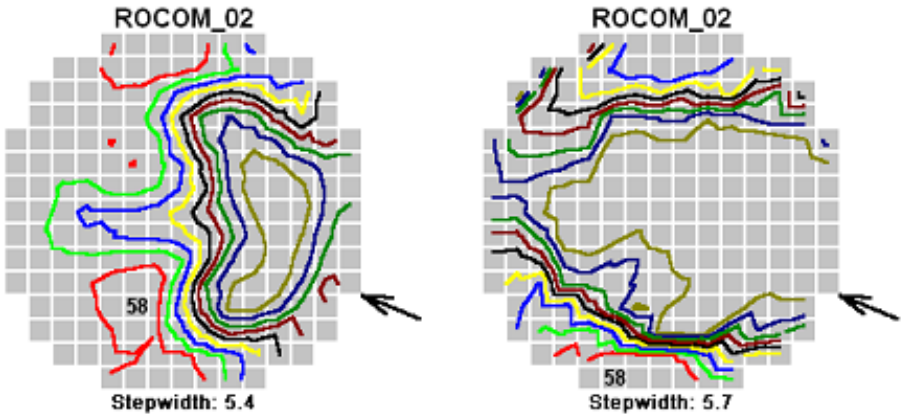

Fig. C.4.12 Core inlet plane, mixing scalar distribution at the time of the global maximum, experiment (left) vs. CFX-4 (right)

C.4.4.2 CFX-5 calculations

Grid

11 different grid types were generated, and the calculation results were compared with the experiment (Table C.4.1). Different mesh generators and features and also different mesh structures were used. Sensitivity tests using different grid sizes were made using variations of Grid 1. Only small differences were observed in the mixing scalar distribution between 650000 and 1.08 Mio. elements (using inflations near the wall). However, it was noticed, that the grid generation consumes most of the work and a totally grid independent solution was not yet achieved.

Based on the meshing studies, finally two grid types were used for the basic calculations. They were called production meshes, because on the one hand, they allow to get the maximum correct results with minimum meshing efforts: the tetrahedral production mesh (grid 5, Fig. C.4.13) and the hybrid production mesh (grid 9). The production mesh is an optimum between maximum possible refined grid on the one hand, but with omitting parts of the flow domain, which were found to be of small impact on the results, e.g. the cold leg loops. The production mesh is not yet a mesh, for which grid-independent solution was reached. This could not be fully achieved. In general, the choice of the production mesh is dependent from the process to be simulated. The production mesh for momentum driven mixing calculations might be different from that one for the analysis of buoyancy controlled mixing.

Modifications of these grid types were used for further investigations (Table C.4.1). On average the y^+-values are in the downcomer $y^+ = 65$ for the tetrahedral mesh (grid 5) and $y^+ = 29$ for the hybrid mesh (grid 9). Both grid types are suitable for the post test calculation of basically all ROCOM experiments, with slightly preferences of the tetrahedral production mesh for the steady state mixing experiments and the hybrid production mesh for the slug mixing and density driven experiments. Because no full grid independence was achieved,

there are differences in the results obtained with different mesh types like tetrahedral mesh and hybrid mesh.

Table C.4.1 Comparison of different grid types

Grid	Type	Size	Mesh generator	Remarks
1	Tetrahedra	1.03 Mio. elements	Build	• Perforated drum as porous body • outlet at half core
2	Tetrahedra	808000 elements	Build	• Perforated drum as porous body • outlet at core inlet
3	Tetrahedra	1.17 Mio. elements	Build	• Perforated drum as porous body • outlet at outlet nozzles
4	Tetrahedra	5 Mio elements, 1.08 Mio. nodes	Build	• Perforated drum with reduced number of holes • outlet at half of core
5	Tetrahedra	7 Mio elements, 1.33 Mio. nodes	Build	• Perforated drum with original number of holes • outlet at half of core • tetrahedral production mesh
6	Tetrahedra	5 Mio elements, 1.01 Mio. nodes	Build	• Perforated drum with original number of holes • outlet at outlet nozzles
7	Tetrahedra	5 Mio elements, 1.01 Mio. nodes	Build, ICEM-CFD	• Perforated drum with original number of holes • outlet at outlet nozzles • four loops modeled
8	Tetrahedra	1.8 Mio. elements, 360000 nodes	ICEM-CFD	• Perforated drum as porous medium • outlet at core inlet, • 2nd code calculation grid
9	HYBRID	4 Mio elements, 2 Mio. nodes •Tetrahedra: 2277307 • Pyramids: 26404 • Hexahedra: 1221476	ICEM-CFD	• Perforated drum with original number of holes • outlet at outlet nozzles • hybrid production mesh
10	HYBRID	4172248 elements, 2024206 nodes	ICEM-CFD	• Perforated drum with original number of holes, • outlet at outlet nozzles • cold leg 1 incl. ECC injection line
11	HYBRID	Number of Nodes: 2210536 Number of Elements: 5110397	ICEM-CFD	• Perforated drum with original number of holes, • outlet at outlet nozzles, • all 4 loops are modeled

Analyzing the number of nodes of the mesh, it was found, that there is an influence on the flow field and mixing in the downcomer. In fact, with modelling all internals (core support plate, detailed model of the perforated drum) and in accordance with the quality check performed by the meshing tool, there was no possible variation below 1 Mio. nodes. It was found, that the meshing tool provide good tools for mesh quality check (aspect ratio, min. and max. angle), which is recommended to be used.

The tetrahedral production mesh is shown on Fig. C.4.13.

Internal geometry

In the CFX-5 calculations, all internals were modeled in detail. No porous body approach was applied. All the 194 orifices in the core support plate were modeled.

The perforated drum in the lower plenum contains 410 orifices of 15 mm diameter. A model with a reduced number of holes (90 holes) and a complex model using all 410 holes was used as a result of extensive sensitivity tests analyzing the influence of the perforated drum of the flow field and mixing in the lower plenum.

The core contains 193 fuel element dummies with a diameter of d=30 mm. The fluid flows through the hydraulic core simulator inside the tubes. The core can be modeled as porous body or as free flow field it is not expected to affect significantly the mixing in the lower plenum. This was done in the production mesh (Grid 5). However, the core was modeled in detail in Grid 6 and Grid 9 (Table C.4.1).

Inlet boundary conditions

Inlet boundary conditions are located at the inlet nozzle sensor plane. In cold leg with injection , the mixing scalar is set to unity uniformly over the cross section. In a sensitivity study, the local values at all positions of the measurement plane at the inlet nozzle sensor were used as an inlet boundary of the mixing scalar. They can differ from one, when the tracer solution is not homogeneously distributed by the injection device. Using the measured mixing scalar distribution in all 216 positions at the inlet nozzle plane instead of the planar distribution improves the agreement of the CFX-5 calculation with the experiments at least in the upper downcomer sensor plane.

Modeling all four loops with bends in the mixing test facility could affect the velocity field in the downcomer. However, the influence is rather small. The variation of the turbulent kinetic energy and dissipation rate shows that there is no influence on the velocity field at the end of the downcomer. Of major influence on the flow field in the downcomer could for instance be the impinging jet from the loop into the downcomer and the downcomer extension below the inlet nozzles, so that the given turbulence values at the inlet nozzles do not play an important role for the flow field and mixing in the downcomer.

Outlet boundary conditions

The influence of the outlet boundary position on the flow field and mixing in the downcomer and lower plenum is negligible. However, the outlet just above the core inlet should not been

used because backflow from the outlet could influence the results at the core inlet plane. The effect was investigated on Grids 1 – 3.

Turbulence models and wall boundary conditions

Turbulence model	**Wall treatment**
k-ε-Standard Turbulence Model	adiabatic with scalable logarithmic wall functions
Shear Stress Transport Turbulence Model	adiabatic with automatic Menter modified wall functions
Reynolds Stress Turbulence Model	adiabatic with scalable logarithmic wall functions

It was shown, that in the case of a highly turbulent flow the used turbulence models gave almost the same results in the velocity and mixing scalar profile in the downcomer. However, the SST model was preferred as it is more accurate than the k-ε model near the wall.

Discretization schemes

All transient calculations were done with the higher order scheme “High Resolution” in space and “Fully implicit 2nd order backward Euler” in time. For both discretization schemes the target variable does not change any more for convergence criteria below 1.E-04. Therefore this convergence criterion is used for all calculations. The round-off error was quantified by comparing the results obtained with single and double precision. No difference was observed.

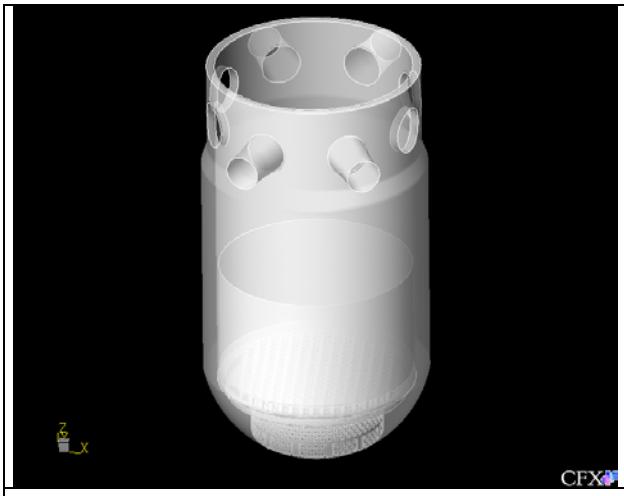

RPV

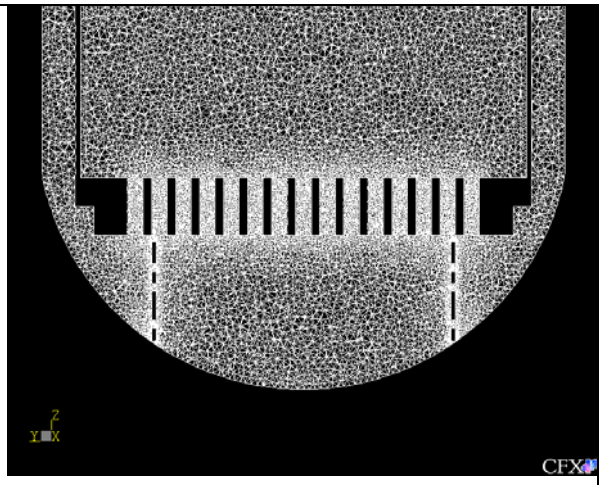

Vertical cut: Lower plenum with perforated drum

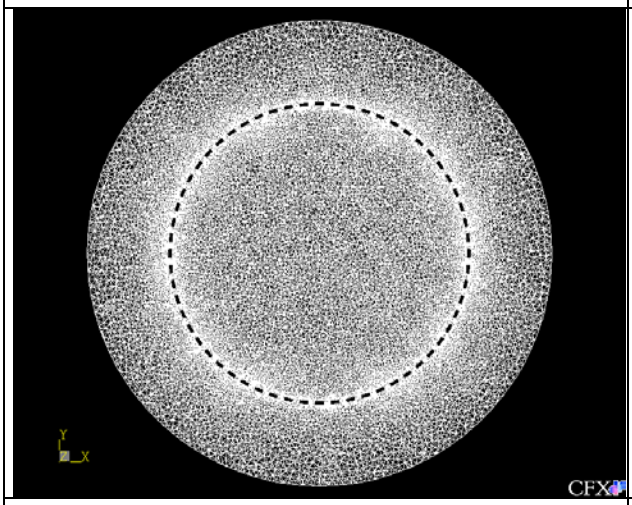

Horizontal cut: Lower plenum with perforated drum

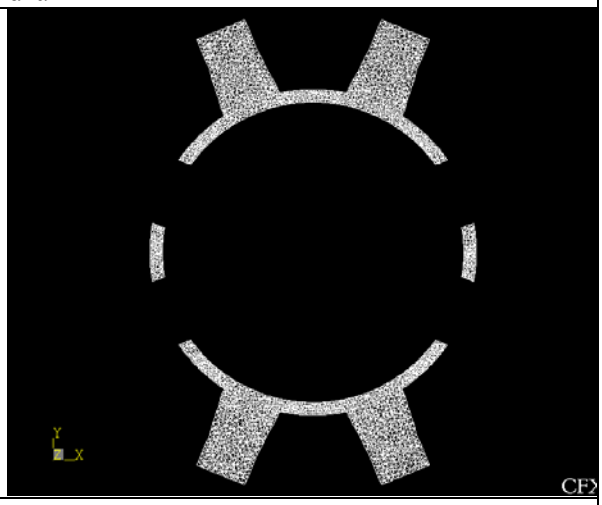

Horizontal cut: Inlet nozzle plane

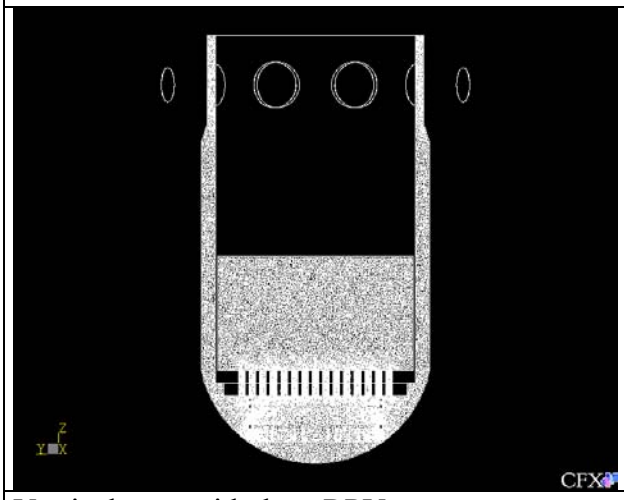

Vertical cut: mid plane RPV

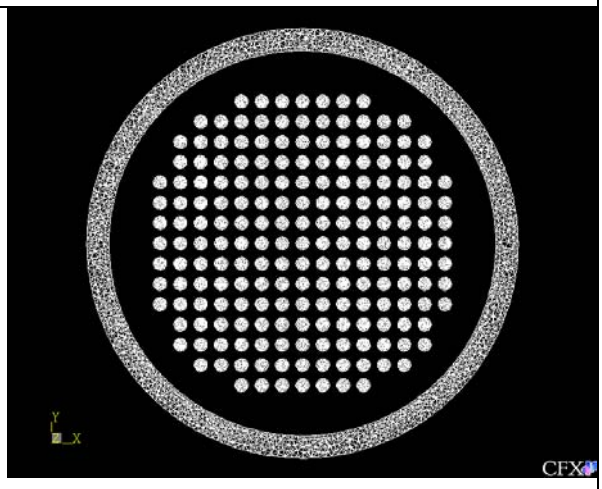

Horizontal cut: Core inlet plane

Fig. C.4.13 Production mesh based on tetrahedral elements

Mixing during start-up of coolant circulation, ROCOM-02

In this report, only results of the calculation of the benchmark case ROCOM-02 are shown. A more detailed presentation of CFX-5 results for the ROCOM slug mixing tests is given in [D11].

Figure C.4.14 shows streamlines representing the velocity field in the downcomer at the pump start-up scenario calculated with CFX-5. In loop 1 the MCP starts linearly from 0 to 185 m³/h in 14 s, after 14 s the mass flow rate is constant at 185 m³/h (Fig. C.4.15b), counter flows are developing at the other 3 loops. The initial space-averaged value of the mixing scalar at the inlet nozzle of Loop 1 was used as the inlet boundary condition (Fig. C.4.15a). Due to a strong impulse driven flow at the inlet nozzle the horizontal part of the flow dominates in the downcomer (Fig. C.4.14). The injection is distributed into two main jets, the so-called butterfly distribution. In addition several secondary flows are seen in various parts of the downcomer. Especially strong vortices occur in the areas below the non-operating loop nozzles and also below the injection loop. Here a strong re-circulation area occurs, which is controlling the size of other small swirls.

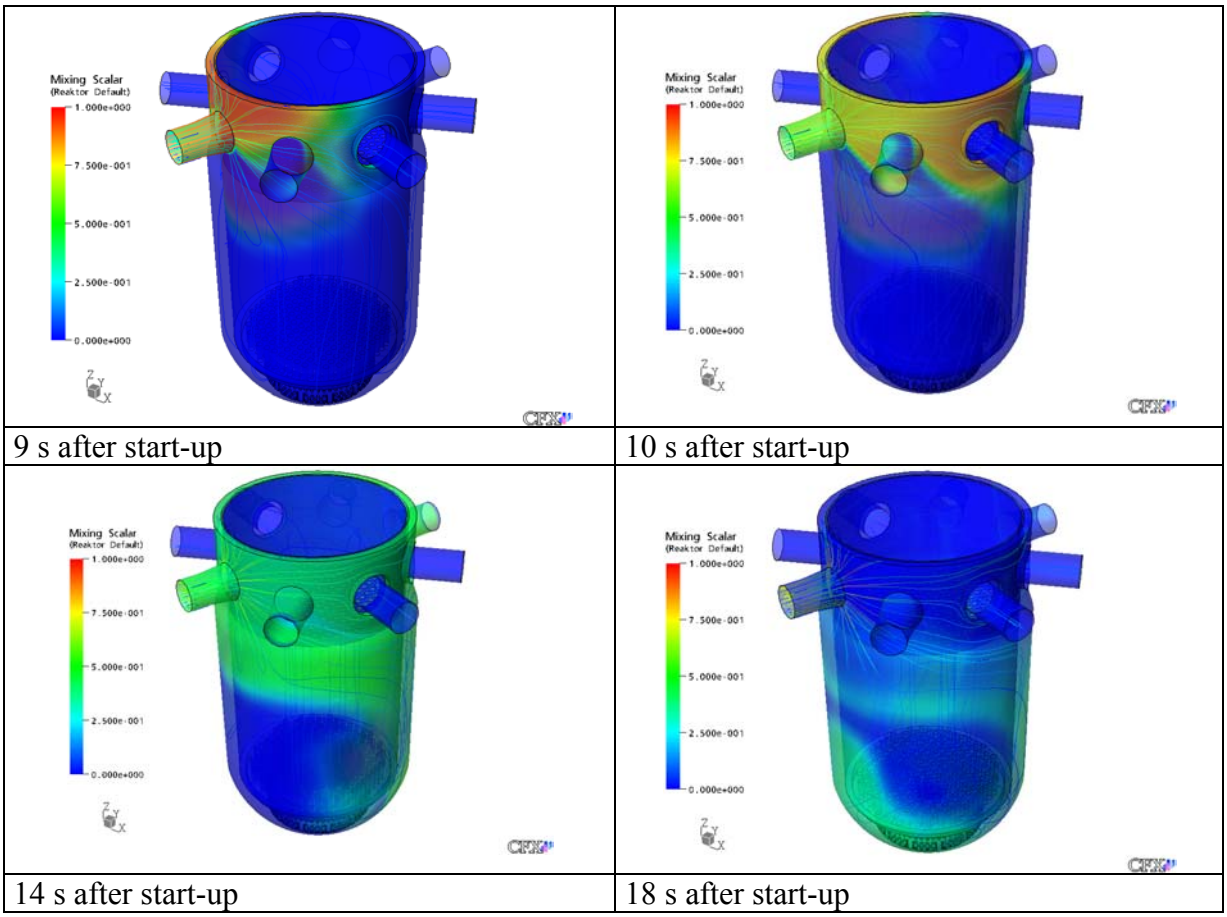

Fig. C.4.14 Time dependent mixing scalar distribution in the downcomer, CFX-5

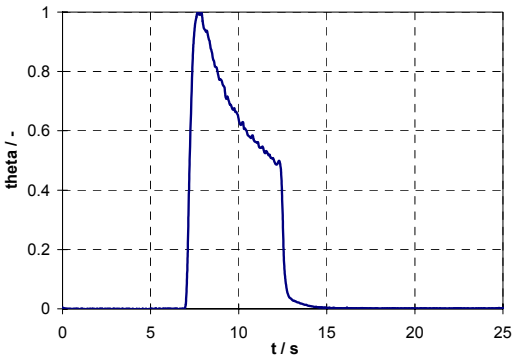

a) Time dependent mixing scalar at the reactor inlet

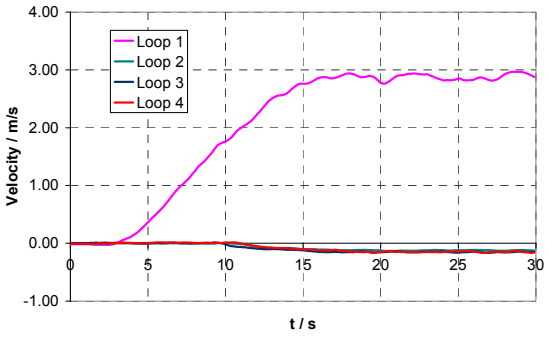

b) Inlet velocity loops 1-4, ramp and backflow in the idle loops

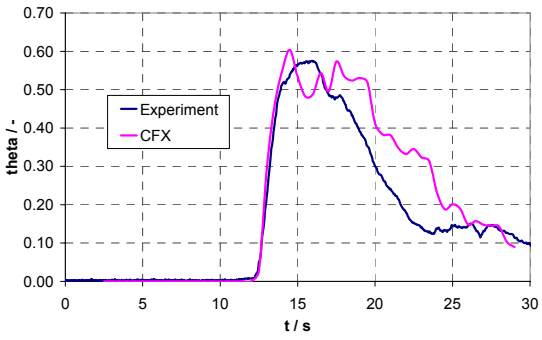

c) Time dependent global maximum of the mixing scalar at the core inlet

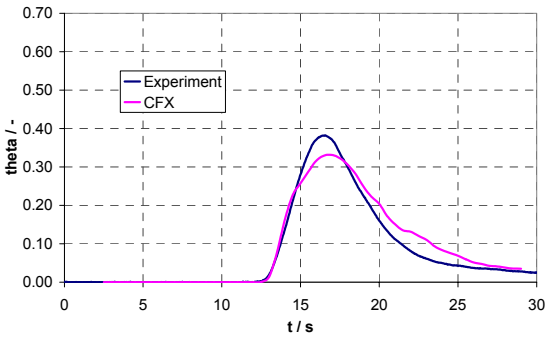

d) Time dependent global averaged mixing scalar at the core inlet

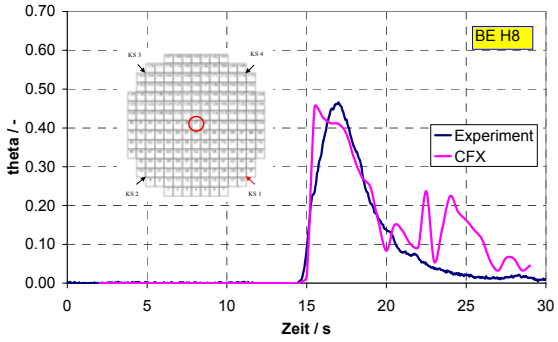

e) Time dependent local mixing scalar at the core inlet, center position

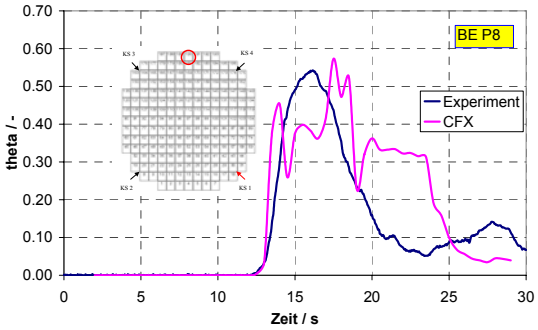

f) Time dependent local mixing scalar at the core inlet, position near the wall

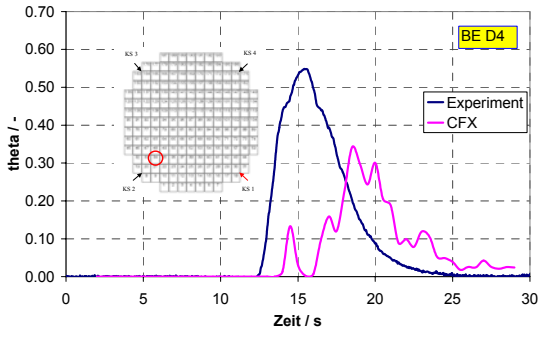

g) Time dependent local mixing scalar at the core inlet, position near the wall

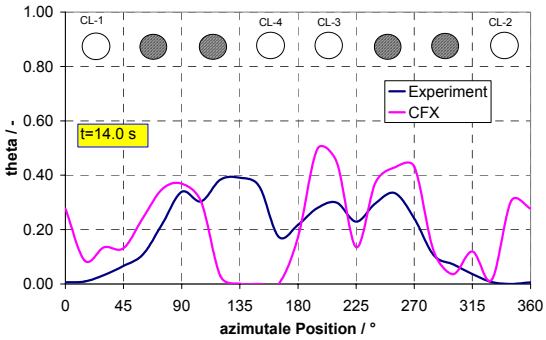

h) Mixing scalar at azimuthal positions along the core perimeter (at t=15.0 s)

Fig. C.4.15 *Comparison of the time dependent mixing scalar at the core inlet sensor position (experiment, CFX-5 calculation)*

The transient course of the maximum value at the core inlet is shown in Fig. C.4.15c. That maximum value or the minimum boron concentration is an indicator for possible reactivity insertion during a transient. In the experiment as well as in the calculation, the maximum value is determined at each time step over all fuel element positions. Therefore the position can vary, which has also an influence on the width of the confidence-interval of the experimental data. In the calculation, the maximum concentration at the core inlet is very close to the experimental data. The absolute value of the calculation reaches 60% compared to the experiment with 58% of the loop value (100%). Local time dependant mixing scalars at fuel element positions in the center and near the wall of the core inlet are shown in the Figures C.4.15e-g. The turbulent fluctuations are significant only in the later part of the transient, when the maximum of the deboration front already passed the corresponding fuel element position. As can be seen, the fluctuations are higher in the outer part of the core. In addition, the mixing scalar at azimuthal positions along the core perimeter is shown in Figure C.4.15h. About 15 s after switching on the RCP, the deboration front reaches the core inlet at two positions in the periphery of the core about 120° shifted from the azimuthal position of the inlet nozzle of the loop with the starting pump. In the CFX-5 calculation the deboration front reaches the core at the same positions but earlier.

Conclusions

The CFD calculations were carried out with the CFD-code CFX-5. All internals of the RPV of ROCOM were modeled in detail. A production mesh with 7 Million elements was generated. Detailed and extensive grid studies were made. It was shown, that a detailed model of the perforated drum in CFX-5 gives the best agreement with the experiments. However, no full grid independence of the CFD solutions was achieved.

Sensitivity studies have shown, that the SST turbulence model and the automatic wall functions together with higher order discretization schemes should be used if possible.

The qualitative and quantitative agreement of the CFX-5 calculations with the corresponding experiments is very good for steady state flow case ROCOM-stat01 and acceptable for the pump-start-up case ROCOM-02.

C.4.4.3 FLUENT counterpart calculations

A transient calculation of the ROCOM slug mixing experiment ROCOM-02 was performed by FORTUM. Similar settings were, if possible, used in both codes. Table C.4.2 shows the settings:

Table C.4.2: Input deck for CFX-5 and FLUENT 6

	CFX-5	**FLUENT 6**
Target variables:	Scalar (Loop 1) concentration at measurement points: core inlet, two levels at downcomer	Scalar (Loop 1) concentration at measurement points: core inlet, two levels at downcomer
Inlet and Outlet Boundary Conditions, Turbulent kinetic energy and dissipation at inlet	time-dependent values from experiments; Inlet: Inlet nozzle sensor plate, Outlet: above core support plate. Turbulence intensity = 2%, turbulence length scale 5 mm	time-dependent piecewise-linear values from exp.; Inlet: Inlet nozzle sensor plate, Outlet: above core support plate. Turbulence = 2 %, turbulence length scale 5 mm
Grid	Grid 8 from Table C.4.1	Grid 8 from Table C.4.1
Internals	Core support plate modeled in detail, perforated drum modeled as porous body: quadratic pressure loss coefficient 321 m^{-1}	Core support plate modeled in detail, perforated drum modeled as porous body: quadratic pressure loss coefficient: 321 m^{-1} for radial direction, 32100 m^{-1} for axial and circumferential directions
Physical models:	Scalable wall functions, k- eps turbulence model	Standard logarithmic wall functions, smooth walls. Standard k-eps turbulence model, Sc_{turb} = 0.7 for scalar mixing
Numerical models:	- implicit pressure based formulation - high resolution scheme in space, - fully implicit 2^{nd} order backward Euler in time, - dt = 0.1 s	SIMPLE pressure-velocity coupling method, - 2nd order upwind discretization, - 2nd order implicit temporal discretization method. - dt = 0.1 s
Solver	Finite element based finite volume method for hybrid unstructured meshes, coupled solver for momentum and mass, implicit pressure based formulation, co-located variables, algebraic multi-grid method	FLUENT's segregated solver: linearized equation system is solved using a point implicit (Gauss-Seidel) linear equation solver in conjunction with an algebraic multigrid (AMG) method
Convergence criteria:	all RMS residuals below 10^{-4}	pre-specified number of iterations/time-step: 20

Due to limits in computational resources the mesh of the 2nd code calculation was coarse, internals were simplified and the core region was not modeled at all. The mesh had therefore accuracy limitations. The grid was generated with IC4C (ICEM-CFD). The perforated drum was modeled as porous media with resistance coefficients. The core support plate was modeled in detail (193 holes), the outlet boundary was placed on the top of core support plate. The unstructured mesh contains 363106 nodes and 1846679 elements. The output mesh was generated for the FLUENT 6 and the CFX-5 solver.

Results of the Code Comparison

One can observe discrepancies in the mixing behavior between the two codes at the upper and lower downcomer and core inlet for local but also for the averaged values of the mixing scalar in Figure C.4.16.

The difference of the averaged values compared to the loop value between the two CFD codes of the mixing scalar at the time dependent maximum of each value in the upper downcomer is 10% (Fig. C.4.16a-b), in the lower downcomer 3% (Fig. C.4.16c-d) and at the core inlet 13% (Fig. C.4.16e-f). Nevertheless, the time dependent mixing behavior of the slug at the core inlet is quite similar. The slug arrives at the core inlet at the outer region of the opposite side of the starting loop, distributes more ore less homogenously over the core inlet plane and leaves the plane in the outer side area left and right of the starting loop. The CFX-5 calculation of the production mesh (grid 5 from Table C.4.1) showed a mixing pattern that is closer to the experiment.

Conclusions

As a result of the second code comparison, the following conclusions were drawn:

- A grid independent solution of the pump start-up slug mixing experiment with the "2nd code calculation mesh" was not achieved.
- Differences in the mixing behavior of the slug occur, which are in a range of max. 13% of the averaged values at the time of the maximum compared to the loop value, differences at selected local positions appear to be larger than the averaged values.
- Nevertheless, the global qualitative mixing pattern of the experiment in the downcomer and core inlet could be observed in the two CFD codes.
- Although similar setting were used, the solutions still strongly depend on the used solver algorithms.
- As a result of this analysis a production mesh for each code according to the Best Practice Guidelines should be generated and calculations on these meshes should be compared.

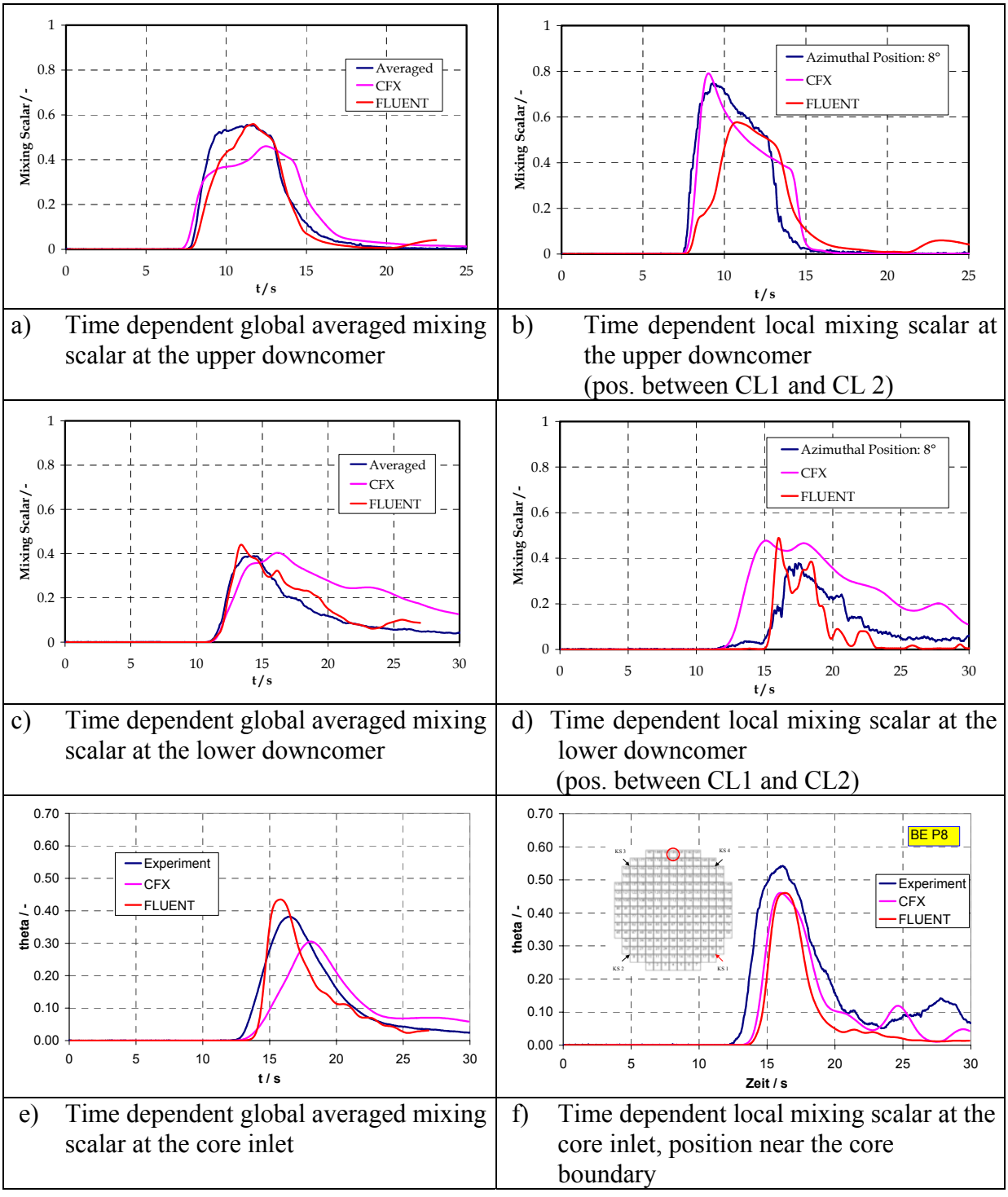

a) Time dependent global averaged mixing scalar at the upper downcomer

b) Time dependent local mixing scalar at the upper downcomer (pos. between CL1 and CL 2)

c) Time dependent global averaged mixing scalar at the lower downcomer

d) Time dependent local mixing scalar at the lower downcomer (pos. between CL1 and CL2)

e) Time dependent global averaged mixing scalar at the core inlet

f) Time dependent local mixing scalar at the core inlet, position near the core boundary

Fig. C.4.16 *Comparison of the experiment, FLUENT and CFX-5 results at the core inlet*

C.4.5 Quantitative Comparison of CFD results with measurement data for the ROCOM non-buoyant experiments

C.4.5.1 Methodology of quantitative comparison

For the assessment of agreement between calculation and measurement, not only visual and qualitative comparisons have to be performed, but also a quantitative estimation of the deviations. Deviations between calculation and measurement occur due to model errors, e.g. in turbulence modeling, but also due to uncertainties in conditions of the experiment, e.g. uncertainties in geometry, boundary conditions or measurement error.

Comparison between calculation and experiment should be performed after minimizing numerical errors according to Best Practice Guidelines [Men02]. So called "best practice solutions" were included into the comparison, where numerical errors are reduced to maximum possible extend. Target values and comparison criteria have been evaluated by B. Hemström (Appendix 11of [D11]). This methodology is applied in the following for quantitative assessment of deviations between calculation and experiment.

To investigate the coolant mixing in the ROCOM test facility, a tracer solution (salt) is injected into the cold leg of one loop. The time dependent distribution of the tracer concentration C(x,y,z,t) is measured at different positions on the way through the model of the reactor pressure vessel. The main results of the experiments are time dependent dimensionless mixing scalars $\theta(x,y,z,t)$, being calculated by relating the tracer concentration to a lower and an upper reference value. They represent the share of the initial perturbation in the cold leg at the corresponding measurement position. Details about the procedures to obtain the dimensionless mixing scalars under quasi steady-state and transient conditions in different experiments can be found in [D09, D10].

For the quantitative comparison of the experimental and calculation results, three stationary experiments and one transient experiment at the ROCOM test facility were selected. The comparison will be made between the calculated and measured data of the mixing scalar in the core inlet plane of the test facility. In this plane, 193 measurement positions are installed, one at the entry into each fuel assembly. Exactly at these positions, the calculated values for the mixing scalar were extracted from the calculations.

Additionally to the mixing scalar (tracer concentration) measurement, the coolant velocity distribution was measured at the outlet of the downcomer of the ROCOM test facility by means of a laser Doppler anemometer. The measurement was made at 32 azimuthal positions in the middle of the downcomer. For the steady state experiment at nominal flow conditions, velocity distributions will be compared between experiment and calculations.

For the quantitative comparison different types of deviations were defined (see Appendix 11of [D11]).

These are

$$DEV1_{i,t} = c_{c,i,t} - c_{m,i,t} \qquad \text{(Equ. C.4.1)}$$

where c_c is the calculated and c_m the measured value of the mixing scalar or the velocity at the position i and the time t. DEV2 is an accumulated deviation at the certain position i over the important time span, i.e. when the perturbation is moving through the measurement plane. Two representations of the accumulated deviation were selected, the first is the absolute deviation.

$$DEV2_i\_ABS = \sum_{t=t_1}^{t=t_2} \left| DEV1_i \right| \qquad \text{(Equ. C.4.2)}$$

When considering the sign, also the direction of deviation reveals:

$$DEV2_i\_SIGN = \sum_{t=t_1}^{t=t_2} DEV1_i \qquad \text{(Equ.C.4.3)}$$

The averaging of the deviation DEV2 over all measurement positions leads to the average accumulated deviation:

$$DEV3\_ABS = \frac{1}{n} \sum_{i=1}^{n} DEV2\_ABS_i \qquad \text{(Equ.C.4.4)}$$

and

$$DEV3\_SIGN = \frac{1}{n} \sum_{i=1}^{n} DEV2\_SIGN_i \qquad \text{(Equ. C.4.5)}$$

where n is the number of measurement positions used for averaging, i.e. the total number of measurement positions in the core inlet plane. The time dependent average deviation is calculated using:

$$DEV4_t = \frac{1}{n} \sum_{i=1}^{n} DEV1_{i,t} \qquad \text{(Equ. C.4.6)}$$

Further, the calculated values of the mixing scalar will be compared to the confidence intervals of the experimental data, and a comparison of calculated and measured values along selected lines in the core inlet plane will be presented.

C.4.5.2 Comparison for the stationary experiment ROCOM-stat01

In the experiment ROCOM-stat01, the flow rates in all four loops correspond to the nominal values. The pumps are operated with constant frequency values. After establishing stable flow conditions, tracer is injected into loop 1 over a time period of 7.5 s, the time dependent tracer concentration is measured at the 193 measurement positions, as mentioned above. The experiment was repeated five times, the corresponding time curves at each measurement position were averaged. Fig C.4.17 shows the time evolution of the mixing scalar at the core inlet plane averaged over all measurement positions. From t = 8.5 s to t = 13.5 s, the average mixing scalar is at a quasi-stationary plateau.

All measured values at this quasi-stationary concentration plateau are used for the determination of the mixing coefficients at each measurement position. The time interval used for the experiment ROCOM-stat01 is shown on Fig.C.4.17. As already mentioned, the mixing coefficients represent the share of the initial perturbation in the cold leg at the corresponding measurement position.

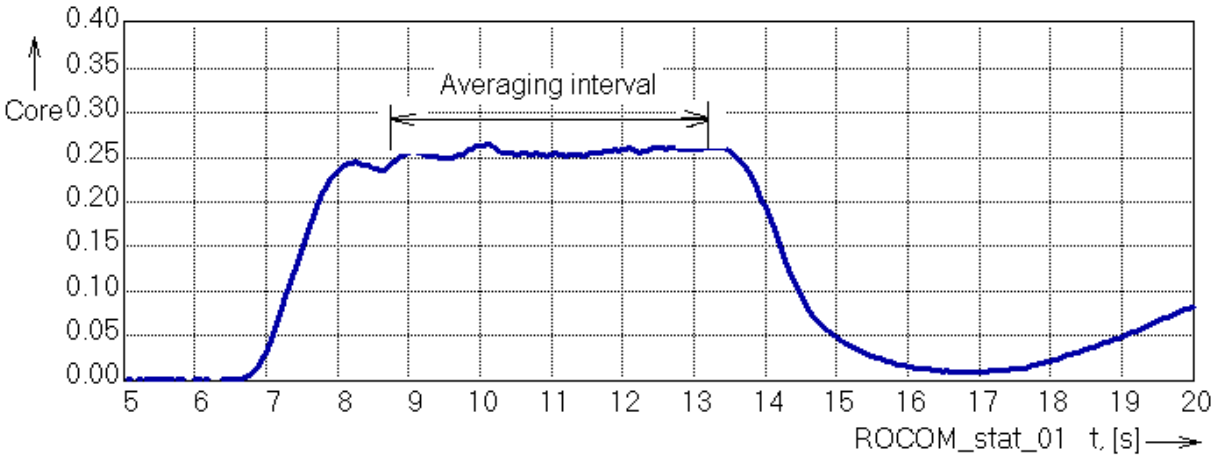

Fig. C.4.17 Time interval for determination of the mixing coefficients at the core inlet in the experiment ROCOM-stat01 (from [D10])

Four CFD solutions obtained by different project partners were included into the comparison between measurement and calculation. Tab C.4.3 contains an overview about the solutions provided for the experiment ROCOM-stat01.

Tab. C.4.3 Calculations for the experiment ROCOM-stat01

Name	Institution	Code	Calculation
FZR_01	FZR	CFX-5	Steady state
AEKI_01	AEKI	FLUENT	Steady state
VUJE_01	VUJE	FLUENT	Steady state
FZR_01_{tr}	FZR	CFX-5	Transient + plateau averaging

Each project partner provided the solution calculated using the production mesh. The production mesh is the result of the application of the Best Practice Guidelines to the creation and qualification of the computation grid and the solutions. The details are included in [D11].
Besides the three steady state calculations, one transient calculation was included into the comparison (FZR_01_{tr}). This calculation was performed with constant velocity boundary conditions at the inlet into the reactor pressure vessel. The calculated mixing scalar at the core inlet was averaged at the quasi-stationary concentration level in the same way as in the experiment. The results of the four calculations are shown on Fig. C.4.4 in section C.4.3.2.
In case of stationary experiments and calculations the introduced types of deviations reduce somewhat due to the absence of the time dependence. Tab. C.4.4 shows the averaged deviation DEV3 according to equ. C.4.4 and C.4.5. The values are absolute ones and are in same units as the mixing scalar [%]. The relative deviations $DEV3_{rel}$ are calculated relating the absolute deviation DEV3 to the integral perturbation introduced in the experiment into the core inlet plane. This perturbation should be close to 25 % in the case of 100 % perturbation in one of the four loops. However, the exact value of the perturbation depends on the velocity profile at the core inlet, which is unknown, but should be close to homogeneous in our case. Therefore, this value, shown in the second column, is a measure for the average deboration determined over all positions.

$$PERT = \frac{1}{n}\sum_{i=1}^{n}\Theta_i \qquad \text{(Equ.C.4.5)}$$

$$DEV3\_ABS_{rel} = DEV3\_ABS / PERT_{EXP} \qquad \text{(Equ.C.4.6)}$$

$$DEV3\_SIGN_{rel} = DEV3\_SIGN / PERT_{EXP} \qquad \text{(Equ.C.4.7)}$$

Tab. C.4.4 Values for different types of deviations

	Averaged perturbation PERT [%]	**DEV3_SIGN Equ. C.4.5**	**DEV3_ABS Equ. C.4.4**	**$DEV3\_SIGN_{rel}$ Equ. C.4.7 [%]**	**$DEV3\_ABS_{rel}$ Equ. C.4.6 [%]**
EXP	25.45	-	-	-	-
FZR	25.40	-0.0878	6.6502	-0.345	26.1
AEKI	24.95	-0.5206	7.2521	-2.046	28.5
VUJE	25.26	-0.2307	6.3778	-0.906	25.1
FZRtr	24.53	-0.9696	6.1974	-3.810	24.4

The relative deviation considering the sign is very low for all calculations in comparison to the absolute deviation shown in column 6 of the table. That indicates, that a tilt between the measured and the calculated distributions leads to a significant compensation. The relative deviation based on the absolute values is in the order of 25 % for all solutions.

The tilt between measured and calculated distributions can also be seen from Fig. C.4.18. In all calculations, the number of measurement positions at the core inlet with low mixing scalar values is lower than in the measurement, while the number of positions with high values of the mixing scalar is higher. That means, the calculated distributions are more smeared, the mixing is overestimated.

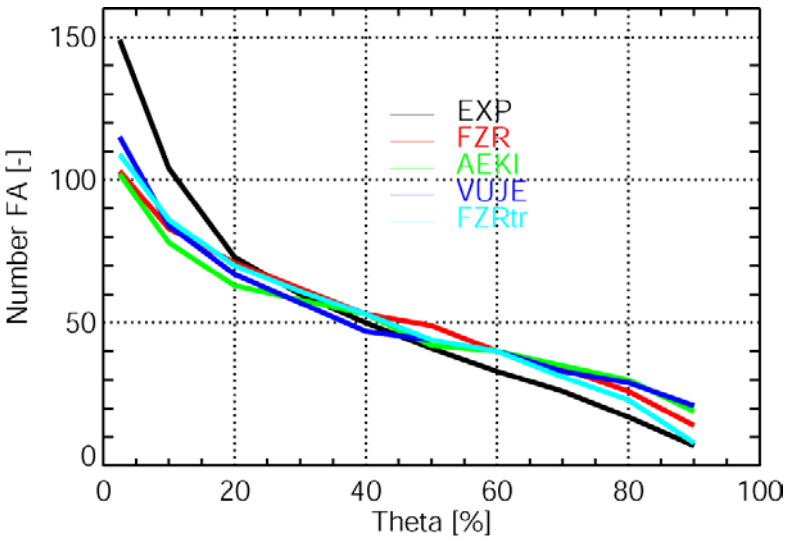

Fig. C.4.18 Number of positions with a certain value of the mixing scalar

Quantitative comparisons are also performed for the experiments ROCOM_stat04 and ROCOM_stat09. FLUENT calculations have been performed for these experiments by VUJE and AEKI. The results are presented in [D11]. The tendencies are the same as observed for ROCOM_stat01. Local deviations are compensating each other, so that the errors with sign (DEV3_SIGN) are small. The average absolute deviation between calculation and measurement, relative to the integral perturbation (DEV3_ABS_{rel}) is between 24 and 33 %.

C.4.5.3 Comparison for the slug mixing experiment ROCOM-02

In the initial state of the experiment ROCOM-02, all pumps are switched off, there is no flow in the whole test facility. A slug of 20 m^3 resting in the cold leg of loop 1 at a distance of 10 m (both dimensions are reference values for the original reactor, the real values in the experiment are reduced by the geometrical scale, 1:5 in length and 1:125 in volume) is injected into the reactor pressure vessel of the test facility with the starting up first main coolant pump (Details about the experiment can be found in [D09]).
Two solutions of FZR using the codes CFX-4 and CFX-5 were included into the comparison between measurement and calculation. Both calculations are obtained with the corresponding production mesh (tetrahedral mesh for CFX-5).

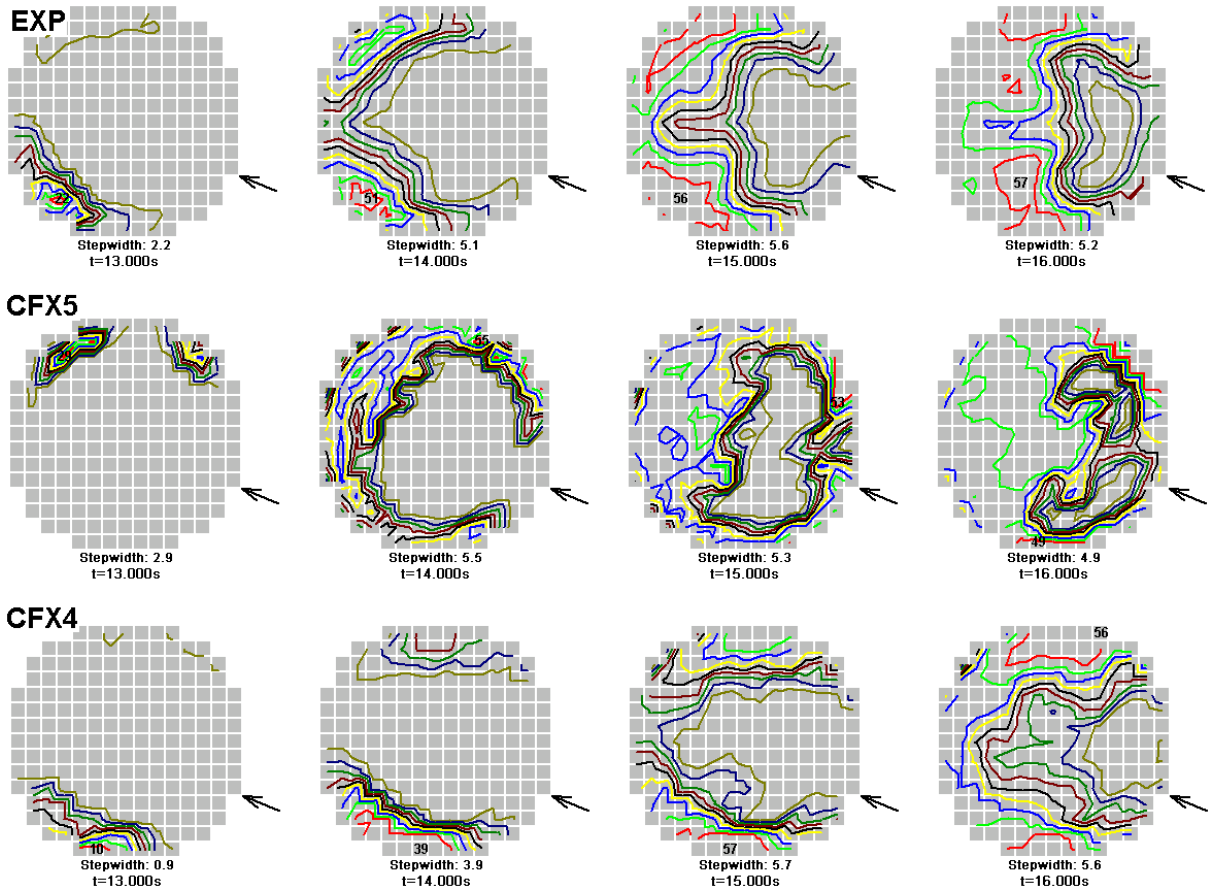

Fig. C.4.19 Distribution of the mixing scalar in the core inlet plane at different times in the experiment and both calculations
(arrow: position of the starting up loop; maximum: bold number in %, stepwidth: difference between two isolines)

Fig. C.4.19 gives an overview how the tracer moves through the measurement plane. Snapshots of the distribution of the mixing scalar at different times are shown. In the experiment, the tracer enters the plane of the sensor in the core inlet at the azimuthal position opposite to the active loop. This effect is fully reproduced by the CFX-4 calculation, in the CFX-5 calculation the first appearance of tracer is shifted clockwise by about 90°. The tracer is detected at the opposite site in that calculation shortly later. With growing time, the part of the core inlet plane, directly below the position of the loop with the starting pump is covered by tracer. That is observed in the experiment and in the calculations. The last tracer leaves the core inlet plane from that region, again in the experiment as well as in the calculations. The shape of the tracer distribution differs between experiment and calculations more than in the stationary cases, but one should consider that these are only snapshots at certain time points. The time dependent mixing pattern is, in general, well met in the calculations.

In Tab. C.4.5, the maximum values and the time point of maximum are compiled for the experiment and the two calculations. Both calculations predict the maximum of the mixing scalar slightly too early, 1 or 0.5 s respectively. The value calculated by CFX-4 of the maximum is in good agreement with the measured one, while being overestimated in the CFX-5 calculation.

Tab. C.4.5 Measured and calculated maximum values of the mixing scalar (including time of appearance)

	Total maximum [%]	**Time of total maximum [s]**	**Maximum of the average [%]**	**Time of maximum of the average [s]**
EXP	57.54	15.95	38.22	16.55
CFX5	60.34	14.50	33.12	17.00
CFX4	57.50	14.90	34.55	17.10

Fig. C.4.20 and C.4.21 show the time evolution of the maximum and of the average mixing scalar at the core inlet. The 2 σ confidence interval for the measured values is shown (the P2-line). It was obtained by averaging of the measured values from the repeated experiments. It can be concluded, that the maximum mixing scalar values of both calculations fit into the confidence interval of 95.4 % of the experimental data. After the maximum is over, larger deviations occur.

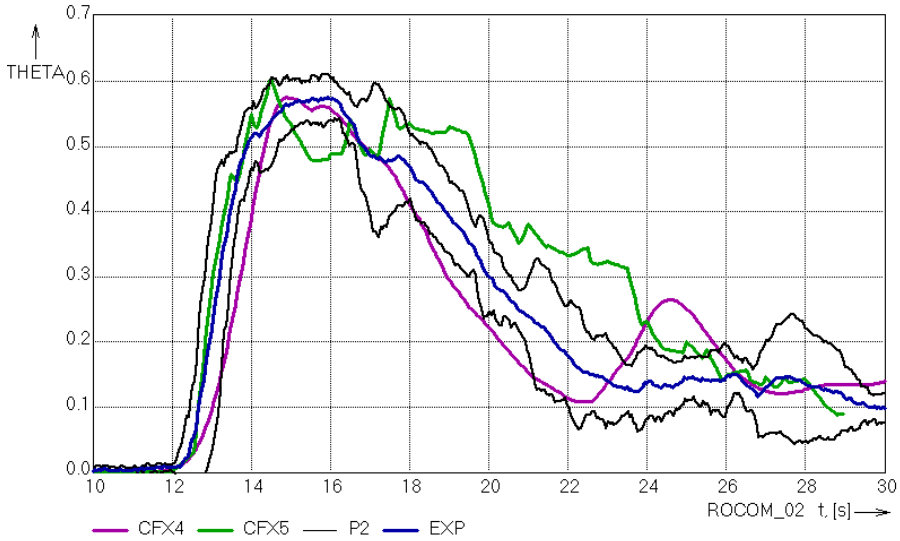

Fig. C.4.20 Time evolution of the maximum mixing scalar in the experiment and the calculations

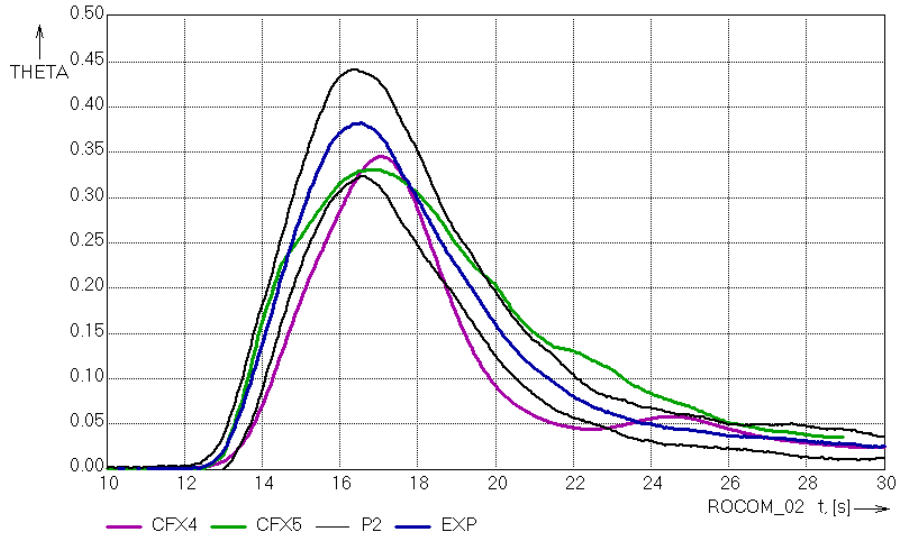

Fig. C.4.21 Time evolution of the average mixing scalar in the experiment and the calculations

In Tab. C.4.6, the values for the different types of deviations are compiled. For the determination of the integral perturbation and the deviations for the time-dependent case, the equations C.4.2 – C.4.5 and C.4.7 – C.4.9 have to be modified. Besides of the summation over all measurement positions, summation over all time steps within a given time interval, devided by the length of the time interval, has to be introduced.
The time interval used for the determination of the deviations was selected from t_1 = 10 s to t_2 = 25 s, what corresponds to the moving of the tracer through the core inlet plane. E.g. the accumulated normalized perturbation PERT0 is calculated according to:

$$PERT0 = \frac{1}{(t_2 - t_1)} \sum_{t=t_1}^{t=t_2} \frac{1}{n} \sum_{i=1}^{n} \Theta_i(t) \qquad \text{(Equ. C.4.10)}$$

The integral perturbation is normalised in this way, that a value of PERT0 = 1.0 would be reached, when the mixing scalar over the whole considered time would be unity at all measurement positions, with other words we would have a full deboration over the full considered time. The different types of the deviations are introduced for the time-dependent case in an analogous way.

Tab. C.4.6 Values for different types of deviations

	Averaged perturbation PERT0 [%]	**DEV3_SIGN0 [%]**	**DEV3_ABS0 [%]**	**DEV3_SIGN0$_{rel}$ [%]**	**DEV3_ABS0$_{rel}$ [%]**
EXP	14.6115	-	-	-	-
CFX5	15.6592	1.0477	6.3795	7.17	50.8
CFX4	11.2395	-3.3720	5.2932	-23.1	36.2

The averaged deviation over the whole time interval calculated according to equ. C.4.10 shows, that the CFX-4 calculation underestimates the introduced perturbation in comparison to the experiment, whereas the CFX-5 calculation overestimates it nearly through the whole time interval.

A local comparison is presented in Fig. C.4.22. From the experiment and both calculations, the positions were selected where the maximum of the mixing scalar was obtained during the transient. These are different positions in the core inlet plane, marked by the bold numbers in the figure.

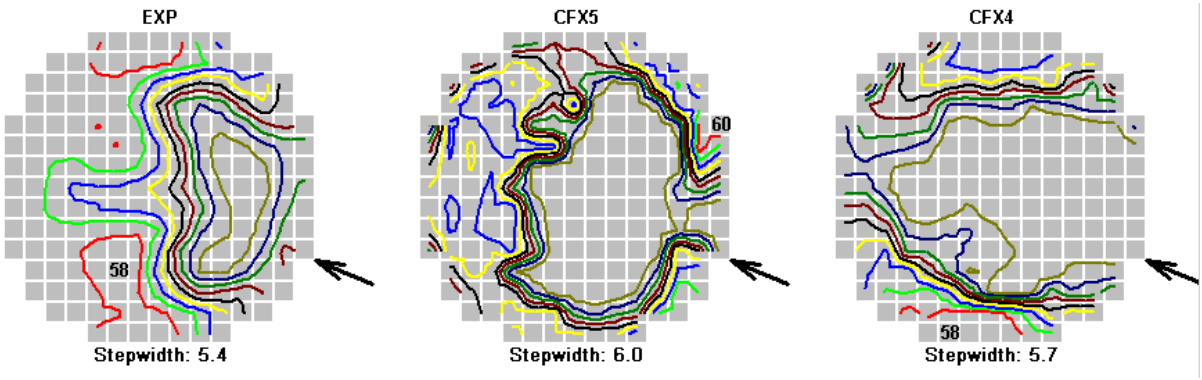

Fig. C.4.22 Distribution of the mixing scalar in the core inlet plane at the time point of maximum in the experiment and both calculations (arrow: position of the starting up loop; maximum: bold number in %, stepwidth: difference between two isolines)

Conclusions on quantitative comparison between measurement and CFD-calculations

For the first time, a detailed quantitative comparison of the results of CFD-calculations with measurements in the complex geometry of the model of a pressure vessel was performed. Different steady-state and transient experiments and calculations were considered. The comparison was mainly concentrated on the core inlet plane. Additionally, the velocity distribution in the downcomer was compared.

In the steady state experiments, the different codes show the same global tendencies. The quantitative analysis revealed, that the distribution of the tracer in radial direction is underestimated in all presented calculations. The transient calculation with constant velocity boundary conditions shows the best agreement in the shape of the distribution of the mixing scalar in the core inlet plane and in the calculated maximum value. Further, the comparison of measurement positions, for which the coolant should flow through the sieve drum or around the sieve drum revealed great differences. In the FLUENT-calculation of VUJE, water flowing through the sieve drum is more mixed, that means the role of the sieve drum in the mixing process is overestimated. The second FLUENT-calculation (AEKI) shows the opposite.

The pump start-up experiment ROCOM-02 was calculated by the codes CFX-4 und CFX-5. The time behaviour of the maximum and the average perturbation calculated by both codes is inside the confidence interval of 2 σ during the main part of the considered time interval. The analysis of the different types of deviations used for the quantitative assessment, showed the general tendency that the CFX-4 solution is in better agreement with the experimental results. This is supported by the assessment of the single measurement positions: The calculated by CFX-4 maximum value at these positions as well as the calculated time of the maximum fits into the confidence intervals of the measurement results at more positions than the CFX-5 calculation.

The introduction of such a comparison allows to quantify the deviations of different calculations form the experimental results. The use of the obtained data contributes to the assessment of the quality of the calculations and give the possibility to create a ranking of the different calculations. A detailed quantitative assessment of the correspondence between measurement and calculation can support further code development activities.

C.4.6 ROCOM buoyant mixing experiments

As described in section C.2.3, in addition to the non-buoyant slug mixing tests, experiments on buoyancy driven mixing have been performed at the ROCOM test facility (see table C.2.3). Calculations have been performed by GRS with support of FZR (test case D10M05) and by NRG (additional test case D05M00). The experiments D10M05 and D05M00 are two tests of this series of generic experiments, where water of higher density was injected with a constant injection rate into the flow of water with nominal density in one of the loops [Pr03]. These conditions are typical for an emergency core cooling (ECC) situation. The number after the "D" means the density difference in %, the number after the "M" the flow rate in % of the nominal one. The density differences between the water in the pressure vessel and the injected "cold water" are set to by using a glucose solution. The reduced flow rate in the cold leg is obtained by reducing the pump speed.

CFX-5 calculations of D10M05 were performed by GRS on a refined grid which was supplied to GRS by FZR. This grid includes detailed models of the sieve barrel, the core support plate and the rods modelling the core in the ROCOM test facility (grid number 10 from Table C.4.1). The cold leg with the ECC-injection nozzle was added in order to capture the flow stratification in the cold leg which also influences mixing in the downcomer. The injection of water with higher density was performed from 5 – 15 s. Calculations were made using second order discretisation schemes in space and time. Two constant time steps (0.1 sec and 0.05 sec) were used in combination with the SST turbulence model and scalable wall functions. Fig. C.4.23 shows the flow in the cold leg during and after the injection of the glucose solution. There is a strong stratification with a higher concentration of glucose on the bottom of the cold leg. The glucose solution flows downward directly below the inlet pipe, see Fig. C.4.24. These phenomena were also observed in the experiment.

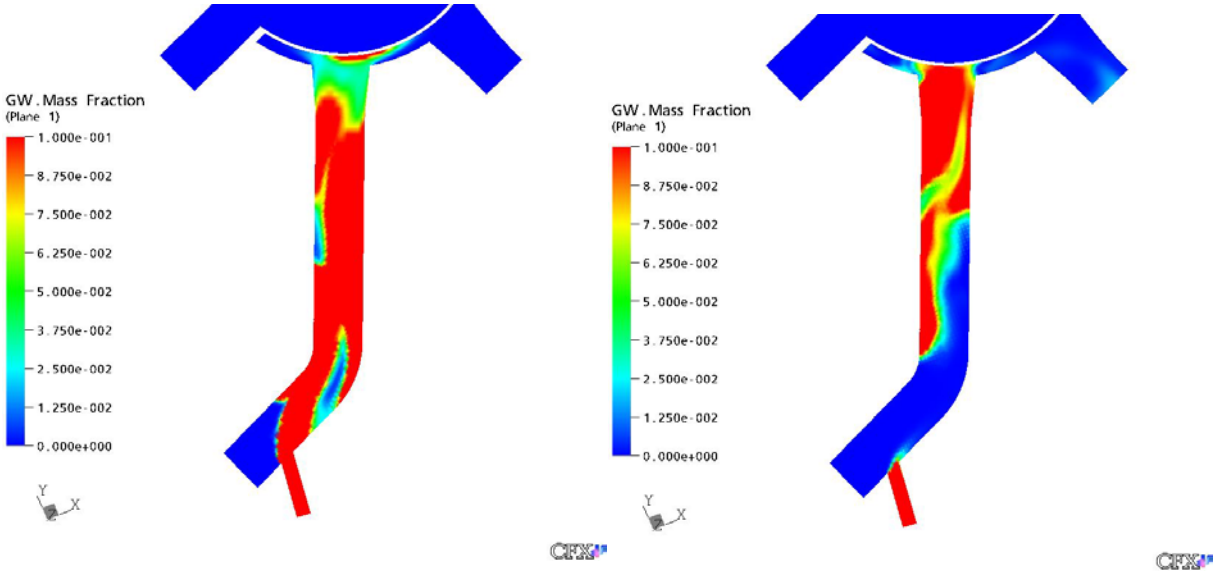

Fig. C.4.23: Glucose concentration in the cold leg, left: t = 10 s, right: t = 20 s

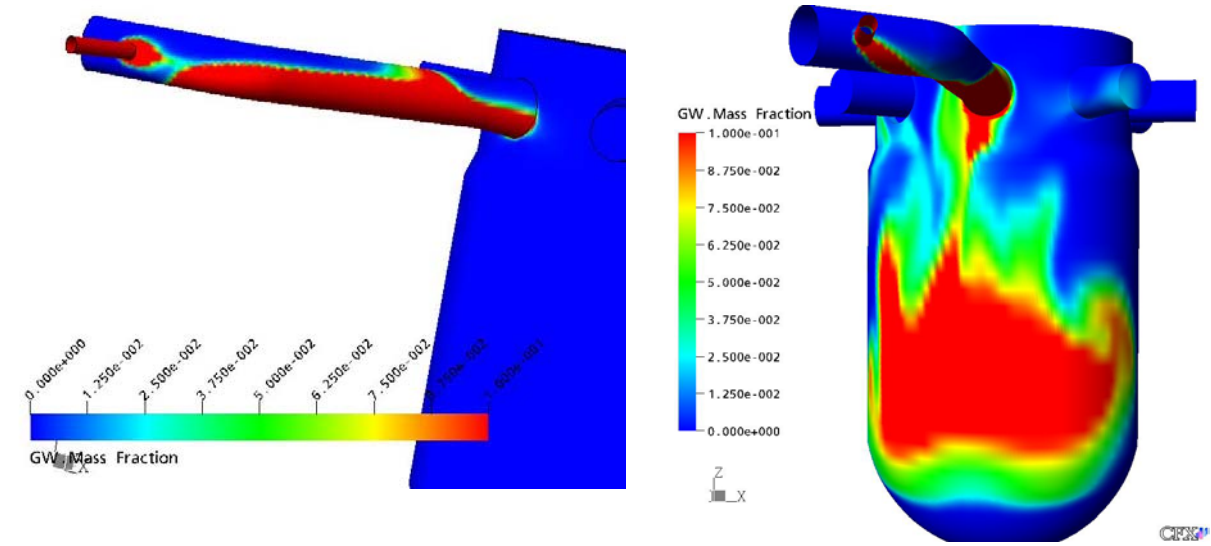

Fig. C.4.24: Glucose concentration in cold leg and downcomer, left: t= 10 s, right: t = 20 s

The glucose solution arrives at the core entrance after 30 s, see Fig. C.4.25a. After 40 s, there are higher concentrations in the core, opposite to the injection position, see Fig. C.4.25b. After 50 s, there is an even concentration distribution of the glucose solution in the core. Fig. C.4.24b also shows that in the DC the concentration "sloshes" from one side to the other.

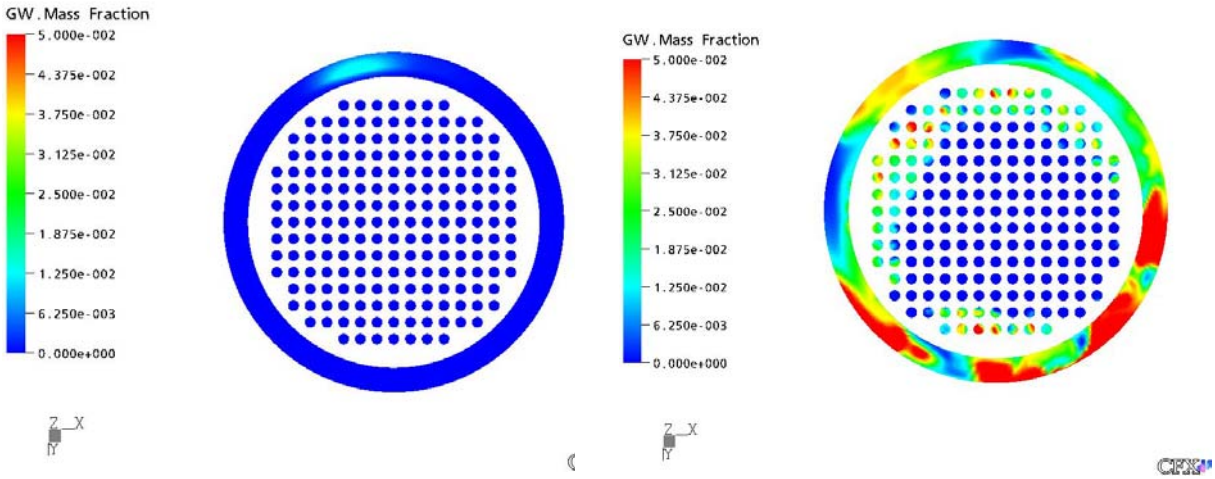

Figure C.4.25a: Glucose concentration at core entrance plane, left: t = 20 s, right: t = 30 s

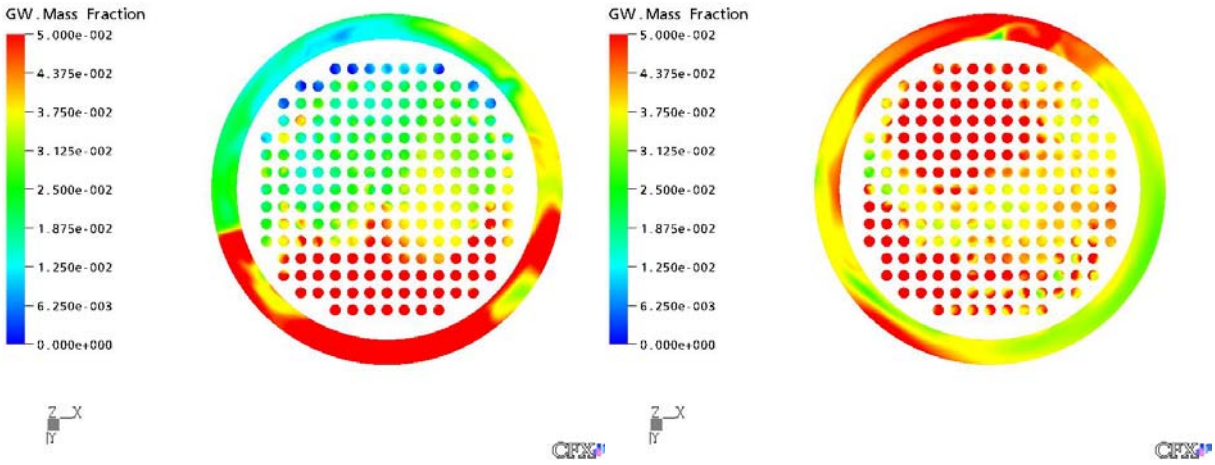

Fig. C.4.25b: Glucose concentration at core entrance plane, left: t = 40 s, right: t = 50 s

Investigations on the influence of the turbulence model were performed by using a Reynolds Stress model (RST), based on the omega equation. In Fig. C.4.26 to Fig. C.4.29, a quantitative comparison is shown between experimental data and numerical results, which were obtained with the Reynolds-Stress turbulence model at time step dt = 0.1 s, and with the SST-model at time steps of 0.1 s and 0.05 s. In Fig. C.4.26, the local glucose concentration is shown as function of time at the 42.5 degree position in the upper downcomer. In Fig. C.4.27, the concentration distribution is shown in the unwrapped upper downcomer after 20 s problem time. In both figures, there are still considerable differences between the SST calculations obtained with different time steps. The RST model, although calculated with the larger time step, shows better agreement with data. A similar trend can observed for the concentration distribution in the lower plenum, see Fig. C.4.28 and Fig. C.4.29.

The Reynolds Stress model shows an improved prediction of buoyancy effects and stratification. However, due to the large time step used for the latter calculations these results still include a fair amount of numerical error.

The D05M00 Experiment showed very complicated 3D time dependent mixing phenomena in the cold leg and the downcomer. It was not be possible to obtain full correspondence between the numerical and experimental results. However, the main phenomena are more or less well predicted. The calculation showed:

- a good prediction of stratification in the cold leg including the timing of the front,
- a reasonable good prediction of global initial mixing behavior in lower part of down comer,
- a poor prediction of the experimental mixing details in the lower part of the down comer.

There exists only a minor sensitivity of the results with respect to the sieve drum resistance and for the considered density difference increase. The modeled amount of flow of the injected water with higher density in the direction to the pump has a large effect on the computed stratification in the cold leg. However, this back flow effect was not investigated in the experiment.

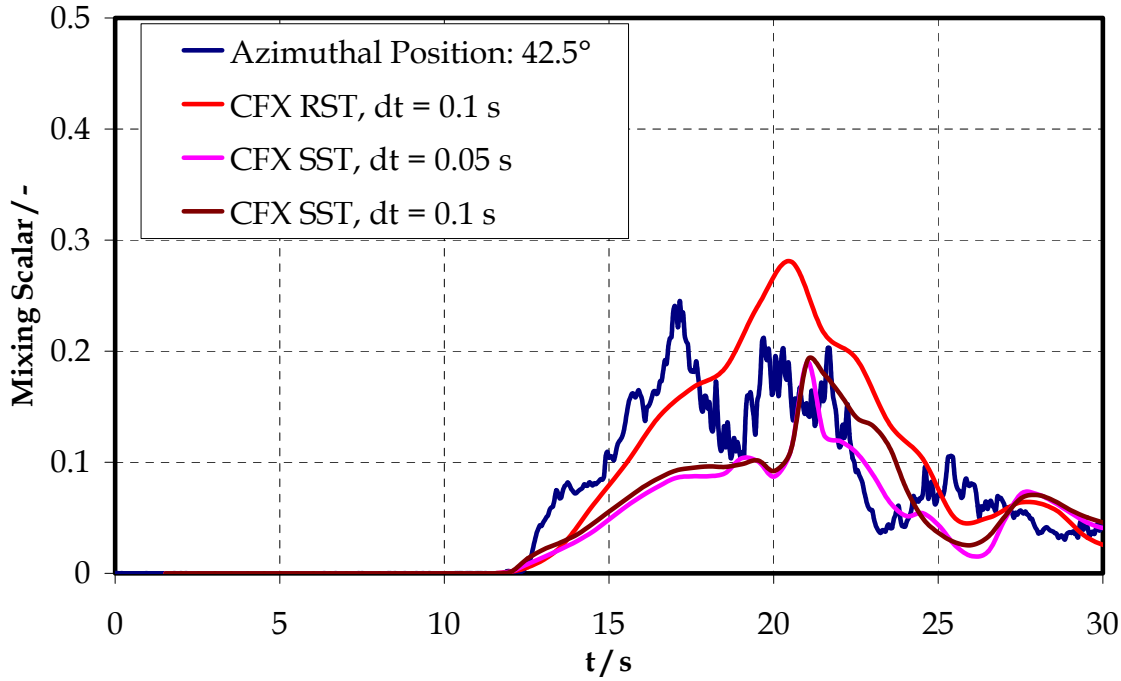

Fig. C.4.26: Upper downcomer local concentration

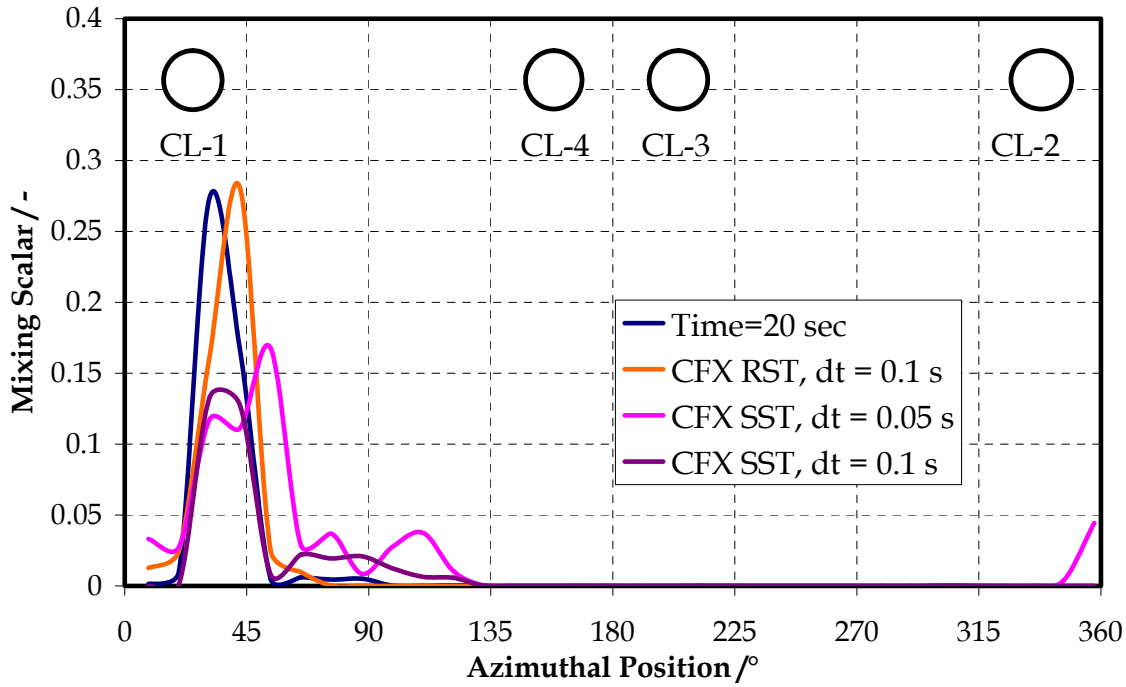

Fig. C.4.27: Upper downcomer azimuthal concentration

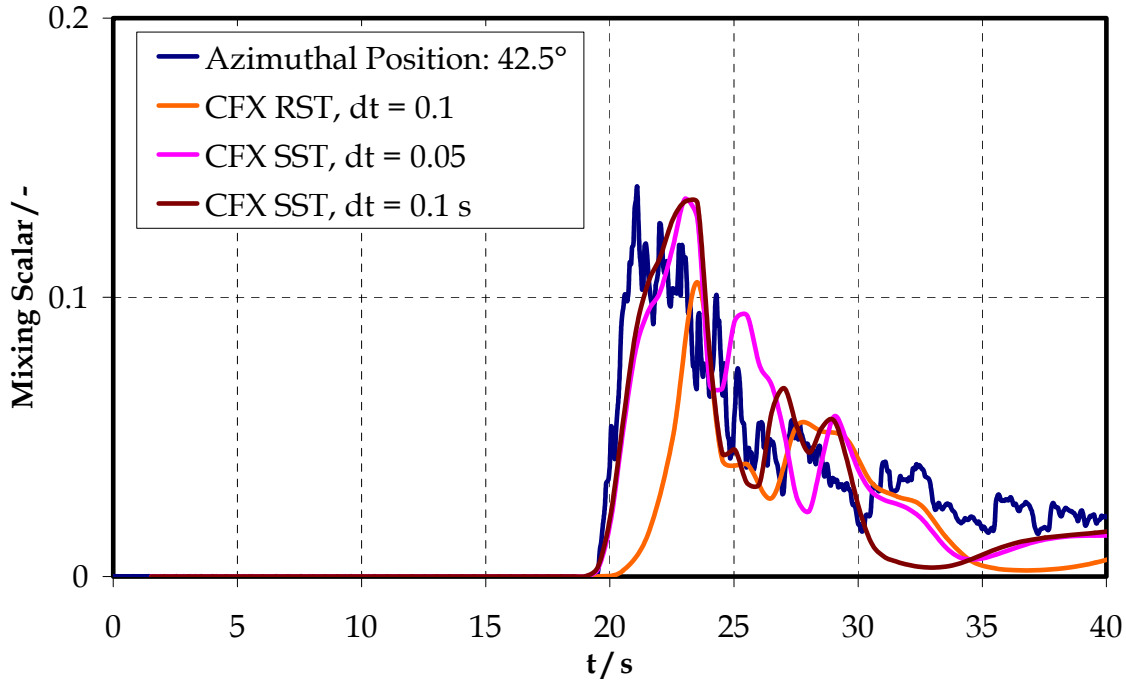

Figure C.4.28: Lower downcomer local concentration

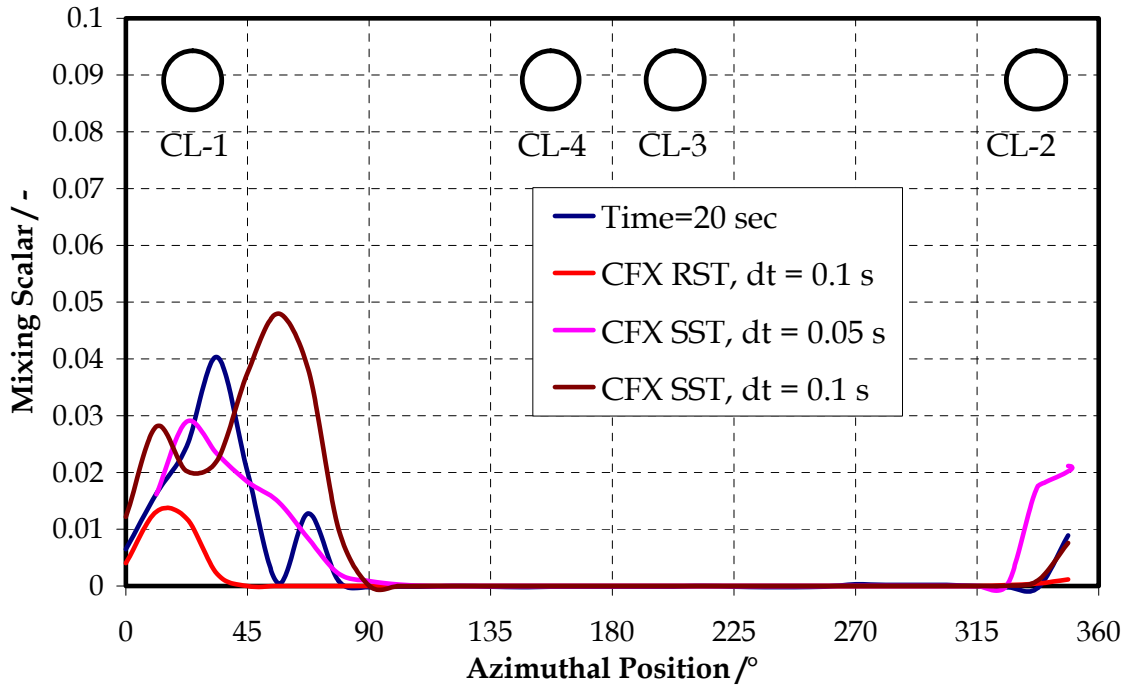

Figure C.4.29: Lower downcomer azimuthal concentration

C.4.7 CFD calculations for Vattenfall experiments

C.4.7.1 Description of CFD calculations

CFD calculations have been performed for the VATT-02 test case from the Vattenfall experiments (see Table C.2.1). It is a slug mixing transient, with a slug with low boron concentration initially present in the RCS pipe. Buoyancy forces are negligible. The Vattenfall experiments are described in detail in the report of WP2 [D09]. An outline of the CFD model is shown in Figure C.4.30. Calculations have been made by PSI (CFX-5 code), Vattenfall Utveckling and NRI (FLUENT).

The purpose of making CFD calculations of a boron dilution transient is to calculate boron concentration and vertical velocity at the inlet to the core. Target variables are therefore spatial and temporal variations of boron concentration and vertical velocity at the inlet to the core. Measurements at the core inlet are however unfortunately only available of boron concentrations. Comparisons for velocities are therefore instead made with measured vertical and tangential velocities at two levels in the downcomer, at one level close to the middle of the downcomer and at one lower level in the downcomer. Boron concentration is measured at 181 positions at the core inlet.

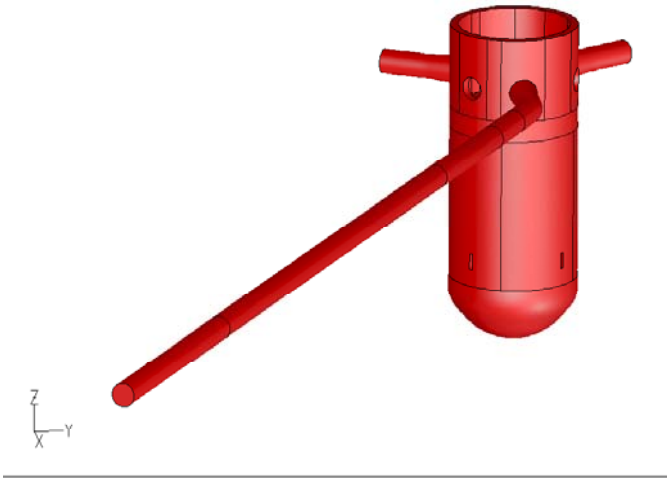

Figure C.4.30 Outline of the CFD model. Perspective view.

Of big importance for checking the quality of CFD calculations according to "the Best Practice Guidelines for CFD" is to make sensitivity test for different model assumptions. The following sensitivity tests were considered:

- Grid size
- Inlet boundary position and inlet boundary condition
- Outlet boundary position and outlet boundary condition
- Modelling of internal geometry

- Turbulence models
- Double precision
- Time step
- Height of wall adjacent cells
- Code

Transient calculations for the VATT-02 slug-mixing transient are demanding huge computer time resources. It was therefore decided to perform some sensitivity tests for the steady state flow situation instead of for the slug-mixing transient. This is done in spite of the following important differences between the steady state flow situation and the transient flow situation:

- In the slug mixing transient the flow accelerates from being laminar to being turbulent during the same period of time that the slug passes through the downcomer. The flow pattern also changes drastically during this important stage of the transient.
- The steady state situation does not include the boron concentration field.

A complete list of the calculations performed is given in [D11]. In this report, only the sensitivity analyses with respect to the BPG will be outlined and comparisons with measurements will be made for those two calculations (one for the steady state flow situation and one for the slug mixing transient) that showed best agreement with measurements.

Grid size

Calculations were made with two different grids, "Grid 1" with 200,726 cells and "Grid 2" with 1,605,808 cells. Grid 1 is a quite coarse grid and is considered to have about the minimum number of cells required to get a fair resolution of the flow field. Grid 2 is a complete refinement of Grid 1, i.e. to get Grid 2 all cells in Grid 1 are split up into 8 cells. According to "the Best Practice Guidelines for CFD" grid refinements should be made in this way. This is also the only objective way of making grid refinements, as decisions on where to make local grid refinements are always based on assumptions.

Results from calculations with these two grids showed for most cases very big differences, especially for the slug mixing transient. It can therefore be concluded that Grid 1 does not give a grid independent solution.

The calculated minimum boron concentration for the Grid 2 calculation with the RNG k-ε model is very close to the measured value (see Figure 4.2.9 below). This indicates that we are close to get a grid-independent solution. However, to be able to check this, one would have to make a calculation with a further refined grid (ideally with a grid with 8 times as many cells as Grid 2, i.e. around 13 million cells). A calculation with this grid is not possible to perform today, with the available computer resources.

Inlet boundary position and inlet boundary condition

It is well known that the choice of inlet boundary position and inlet boundary condition (turbulence level, variation in inlet velocity field in space and time) can have a big influence on the flow pattern far downstream from the inlet. In the calculations for the VATT-02 slug

mixing transient the inlet boundary was therefore put far upstream from the downcomer and the slug, in a position where the flow conditions also were relatively well known. It was consequently considered not necessary to perform sensitivity tests for inlet boundary position and inlet boundary condition.

Outlet boundary position and outlet boundary condition

Sensitivity tests for steady state conditions with the coarse grid (Grid 1) were made for three different main outlet positions; at the inlet to the core, at the middle of the core and at the outlet from the core. These three calculations gave approximately the same flow field at the inlet to the core for a steady state flow situation. Despite this conclusion the outlet from the core was used as main outlet position for the rest of the calculations.

Modelling of internal geometry

Some internal structures were omitted (the vertical cylinders and the lowest structure in the lower plenum and small structures and protrusions) and some structures were simplified (no chamfers on thermal shields and supports, no vertical extension of lower plenum structures and the core is modeled with distributed resistances and porous media).

Calculations were made with and without lower plenum structures by NRI. These calculations were made for the steady state situation and with Grid 1. This sensitivity test showed that modeling the lower plenum structures gave a better agreement with measured velocities in the downcomer.

Double precision

It was concluded from sensitivity tests that double precision in Fluent leads to lower residuals for transient calculations. All transient calculations in Fluent were therefore made with double precision. For steady state calculations, however, double precision gave no influence on residuals. For the CFX calculations single precision was used, as the required residual levels could be reached with single precision.

Time step

All slug mixing transient calculations were run with a time step of 0.01667 s. This approximately gives a CFL (Courant-Friedrichs-Lewy) number of 10 at the front or back of the slug. Due to limited computer resources no sensitivity tests were made for time step size. Priority was instead put on sensitivity tests for turbulence models.

Height of wall adjacent cells

A sensitivity test was made for the height of the wall-adjacent cells. This was made for the steady state situation. The y^+ values are very high in calculations with both Grid 1 and Grid 2. The maximum y^+ in the Fluent calculations with Grid 1 is around 2300 in the region where the jet from the main inlet pipe hits the inner wall of the downcomer. Wall-adjacent cells in

the downcomer and the lower plenum in Grid 1 were therefore refined to give values of y^+ that was closer to the optimal values of around 30-40. The maximum y^+ is around 300 in the region where the jet from the main inlet pipe hits the inner wall of the downcomer. Calculations with this grid gave worse results than for Grid 1. This is a surprising result, as better results are to be expected when the y^+ values are more optimal. One reason can perhaps be that the wall function does not work well for the wall boundary layers in the present application, especially at the flow impingement at the outlet from the inlet pipe.

Code

Fluent 6.1.18, Fluent 6.1.22, CFX5.6 and CFX5.7 were used. The differences between the results from Fluent and CFX were significant, especially for the transient calculations. However, as none of the calculations probably are grid-independent one cannot expect to get the same results from the two codes, as the numerics in the two codes are different. Another difference between the two codes is that exactly the same wall functions could not be applied. For example, in CFX wall functions are applied at nodes, not at cell centers as in Fluent.

Turbulence models

Calculations were made for 13 different turbulence models, 6 versions of the RSM included. RNG k-ε was treated as the first choice turbulence model. Most sensitivity tests for turbulence models were made only for steady state conditions. Sensitivity tests for slug mixing transient calculations were made only for two other turbulence models than the RNG k-ε model (k-ω SST and RSM (Omega (BSL)).

- Standard k-ε, Standard k-ε (Kato-Launder) and Realizable k-ε
- Standard k-ω and SST k-ω RSM, with the following versions: LRR-IP, QI, SSG, Omega, Omega (BSL), Fluent version of RSM

Steady state calculations were all made with Grid 1, the coarse grid, except for the RNG k-ε model. The differences in results between calculations with different turbulence models were quite big. The best result was achieved with the RNG k-ε model. Also for the slug mixing transient the RNG k-ε model gave the best agreement with experimental data, compared to the RSM (Omega BSL) and the k-ω SST model.

C.4.7.2 Comparisons with measurements

Comparisons with measurements are only made for the calculations that showed best agreement with measurements. These calculations have the following characteristics.

- Code: CFX5.6 (steady-state)and CFX5.7 (slug mixing)
- Grid: Grid 2 for slug mixing transient, Grid 1 for steady state (calculations with Grid 2 had convergence problems for the steady state situation, showing a periodically fluctuating velocity field with a higher frequency instability superimposed upon it)

- Turbulence model: RNG k-ε model

When drawing conclusions from these comparisons one should bear in mind that these calculations have not been shown to give grid- and time step- independent solutions. The results can be quite different for a calculation that is grid- and time step independent.

Comparisons for the steady state flow situation

Comparisons are made for vertical velocity, tangential velocity and velocity angle (flow direction) at two levels in the downcomer, one level at the middle level of the downcomer and one level closer to the bottom of the downcomer. The measurement positions are given in Figure C.4.30.

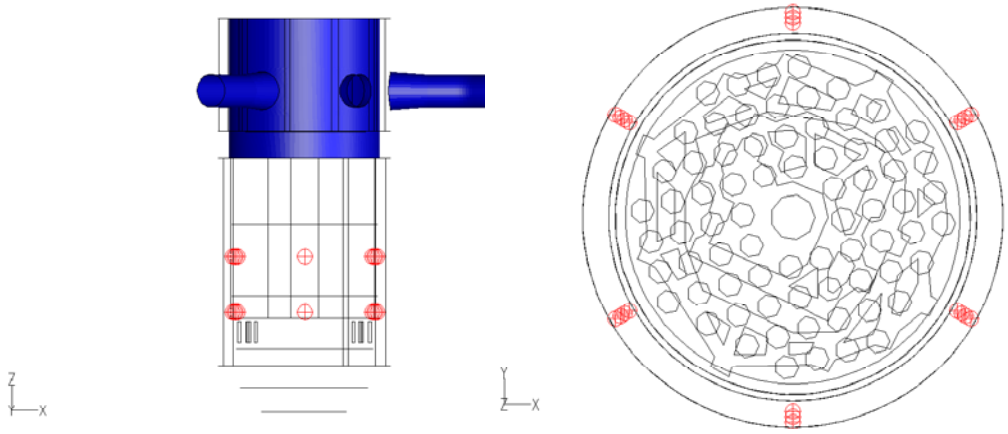

Fig. C.4.31 Positions for velocity measurements

In Figures C.4.32 comparisons of measured and calculated velocity components are presented. The angular position of angle=0° is defined as the angular position where the main inlet pipe enters the downcomer, which is to the right in the figures. Positive angles are to the right of this position, negative angles are to the left, when looking at the model from the outside standing at angle=0°. Tangential velocity is defined as being positive when the flow is directed to the right when looking from an upright position outside the model, i.e. counter-clockwise. Vertical velocity is positive when directed upwards. Only the radial averages are shown in the figures for each angular position. One can see that the qualitative agreement is good. The important non-symmetry in the flow field found in the experiments is captured quite well.

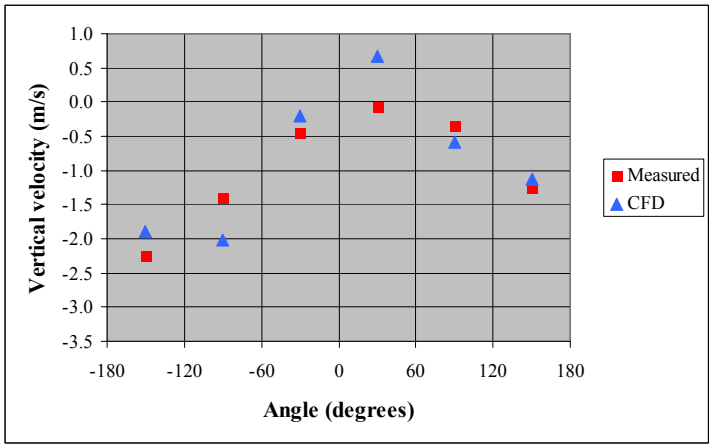

Fig. C.4.32a VATT-02 steady state. Radially averaged vertical velocity at the middle level in the downcomer as a function of tangential angle.

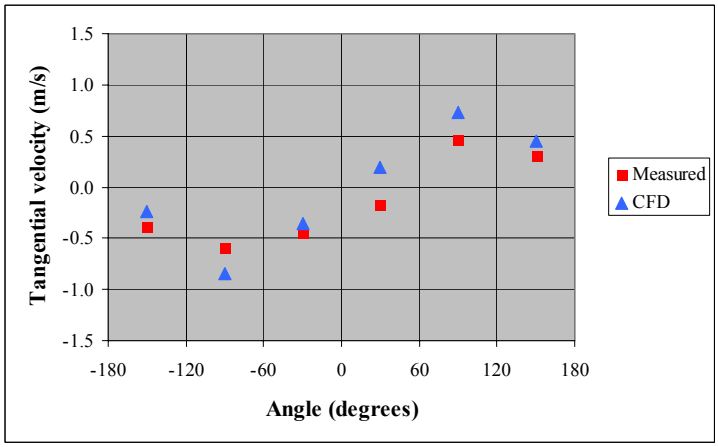

Fig. C.4.32b VATT-02 steady state. Radially averaged tangential velocity at the middle level in the downcomer as a function of tangential angle.

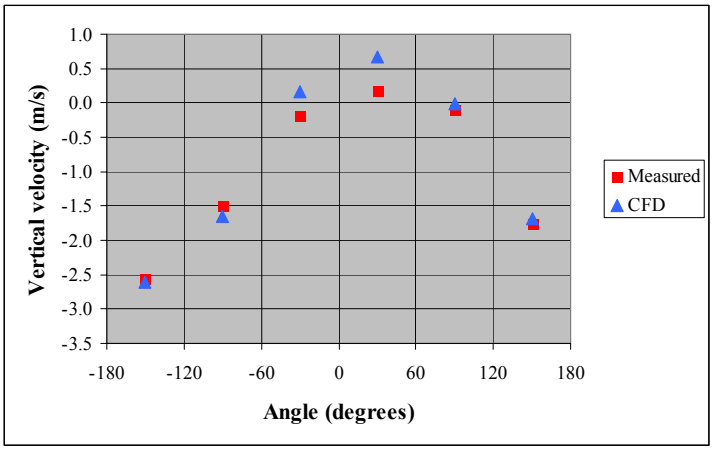

Fig. C.4.32c VATT-02 steady state. Radially averaged vertical velocity at the low level in the downcomer as a function of azimuthal angle.

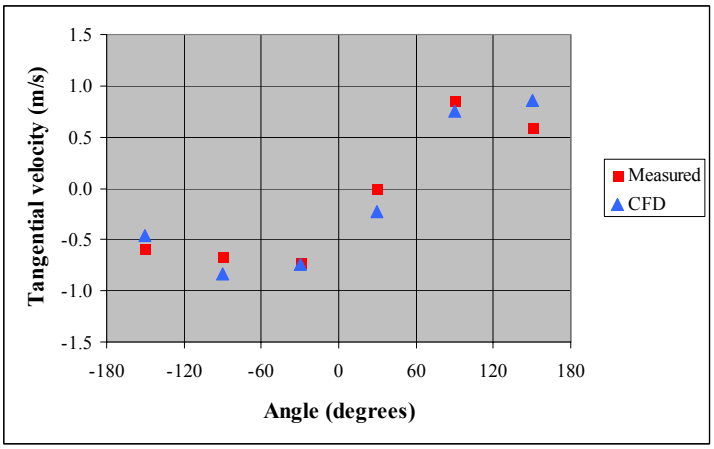

Fig. C.4.32d VATT-02 steady state. Radially averaged tangential velocity at the low level in the downcomer as a function of azimuthal angle

Comparisons for the slug mixing transient

Figure C.4.33a shows mean dimensionless boron concentration at the core inlet as a function of time. One can see that the CFD calculation gives approximately the same minimum value, around 0.8, as the experiments. The calculated concentration is, however, delayed around 0.9 second compared to the measured concentration. This can to a large extent be due to an inaccuracy in the measured flow rate [D09]. Figure C.4.33b shows the minimum boron concentration at the core inlet, independently of position, as a function of time. The calculated minimum value is quite close to the measured value. One should again point out that this is a result from a calculation that has not been verified to be grid- and time step independent.

However, not only the minimum boron concentration should be met well, but also the positions of low boron concentrations must be captured. Figure C.4.34 shows the measured and calculated minimum boron concentrations, independently of time, at the whole core inlet. The inlet pipe is positioned to the right and the view is from above. One can see that the calculated minimum is positioned far from the measured minimum, approximately 180 mm in the model scale of 1:5 (or around 0.52R, where R is the radius of the core inlet plane) from the measured minimum. The displacement of the concentration field is however mainly a rotational displacement. The difference in radial position of the minima is only about 0.15R. This could be relevant in reality, as a core is primarily different radially, as far as enrichment and reactivity are concerned. Two “islands” of low boron concentrations are present in both the measurement and in the CFD calculation. One can also notice that the calculated minimum concentration field show more variations in space, compared to the measurement. The plot from the measurement is, however, based on data for the average from five tests.

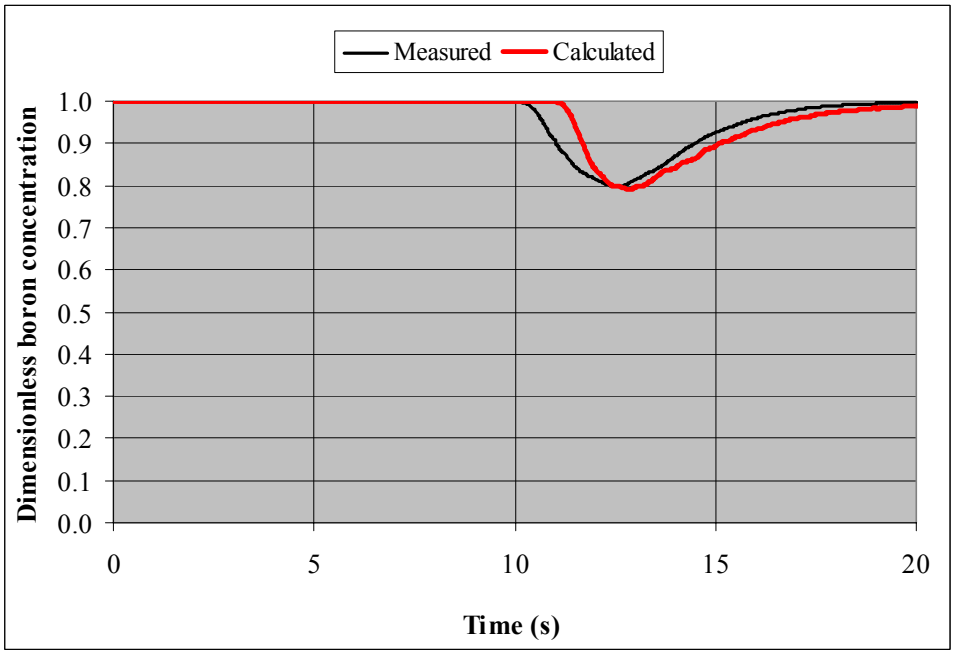

Fig. C.4.33a VATT-02 slug mixing transient. Mean dimensionless boron concentration at core inlet as a function of time.

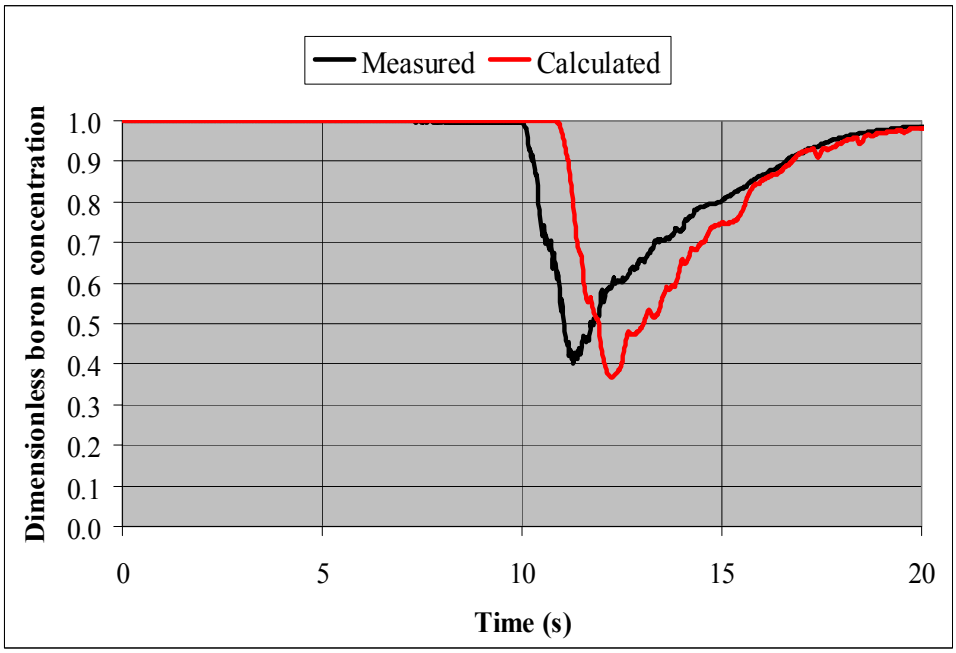

Fig. C.4.33b VATT-02 slug mixing transient. Minimum relative boron concentration at core inlet (independently of position) as a function of time.

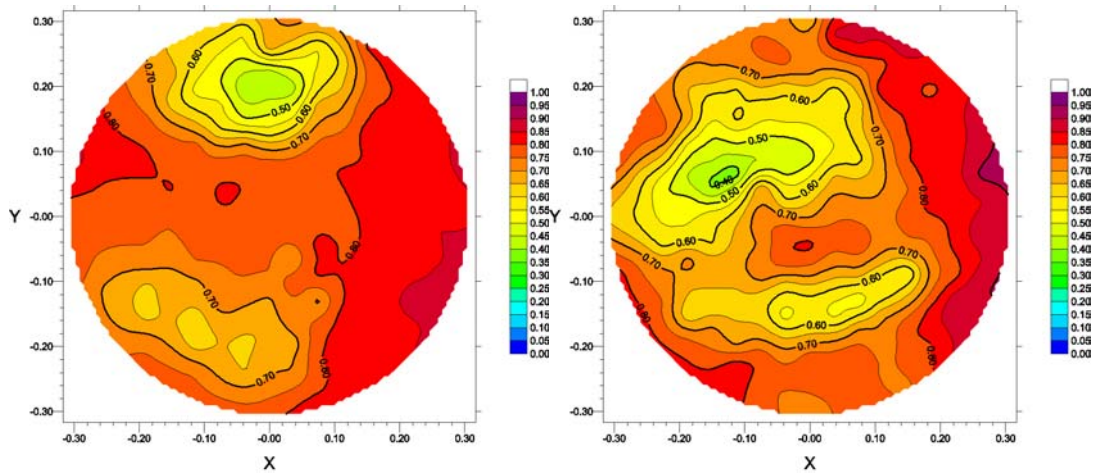

Fig. C. 4.34 VATT-02 slug mixing transient. Minimum relative boron concentration, independently of time.Measurement to the left, CFD calculation to the right.

Results from a quantification of the deviation from experimental values are made in Table C.4.7. When making these comparisons a time shift of 0.9 s of the calculated values have been made, as discussed above. Additionally, a space shift of 176 mm, corresponding to the deviation in calculated position in the minimum concentration, has been made. Comparisons are only made in the time span when the lowest concentrations are measured (from 11.0 s to 12.0 s). Comparisons are also only made in the area where the minimum concentrations occur in the measurements. This area encompasses the area for 7 probe positions. DEV3_SIGN is very small, which tells us that the average of the dimensionless boron concentration for the selected time span and area is captured very well. DEV3_ABS is higher, which means that the variations inside the area and time span have not been captured quite as good. Please notice, that the values of DEV3_SIGN and DEV3_ABS given in table C.4.7 cannot quantitatively compared to the values from tables C.4.4 or C.4.5, because hey are normalized in a different way.

Table C.4.7 *Calculated deviations for slug mixing transient CFD calculations.*

Position	**Quantity**	**DEV3_SIGN**	**DEV3_ABS**
Close to inlet to core	Dimensionless boron concentration	0.0023	0.1228

One reason for calculating incorrect boron concentrations at the core inlet can be that the calculated velocity field is wrong. Figures C.4.35 shows measured and calculated velocities as a function of time at the two levels in the downcomer where velocities were measured. The measured velocities shown in these figures are averaged over a time span of approximately one second. Most of the fluctuations in the measured signals are therefore not seen in these figures. One can see that the rather abrupt change in flow direction at around 7-10 seconds in the measurement and the following transition to the steady state fully turbulent flow pattern is

not captured quite accurately by the CFD calculation. This will have an effect on the mixing and transport of the boron concentration field.

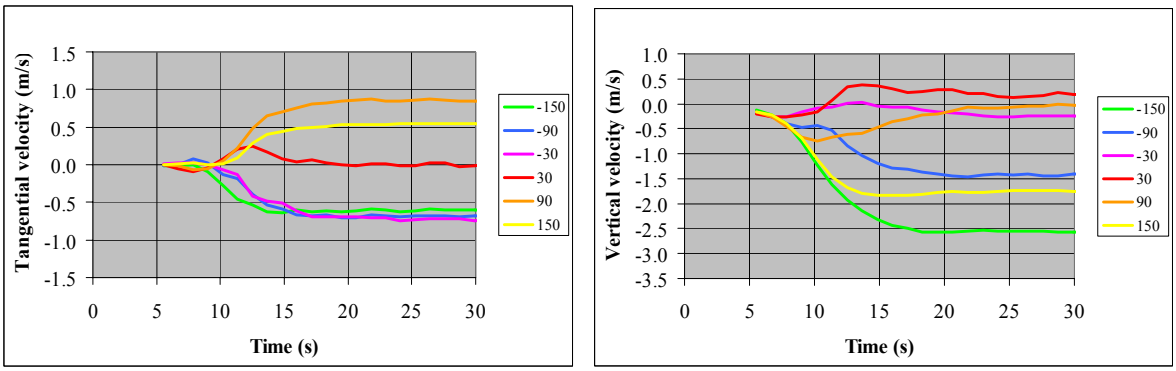

Fig. C.4.35a VATT-02 slug mixing transient. Measured radially averaged vertical (left) and tangential (right) velocity at the low level in the downcomer as a function of time.

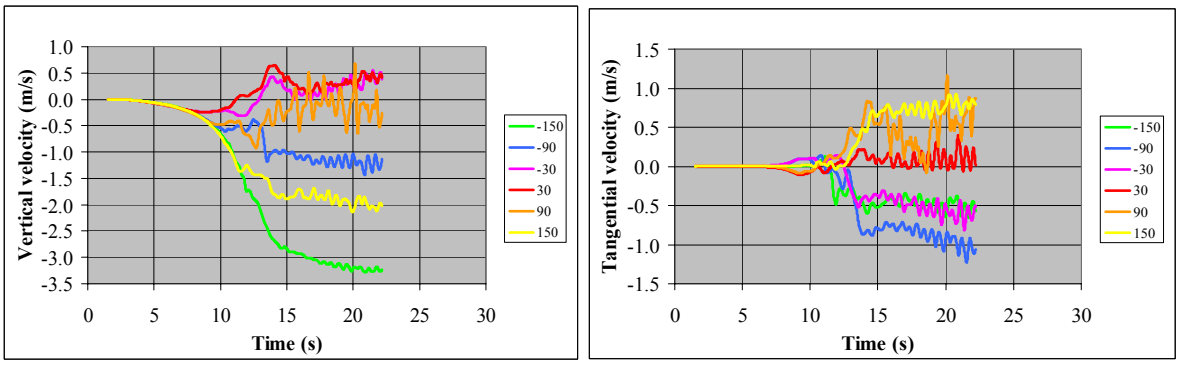

Fig. C.4.35b VATT-02 slug mixing transient. Calculated radially averaged vertical (left) and tangential (right) velocity at the low level in the downcomer as a function of time.

Conclusions

CFD calculations have been performed for the VATT-02 test case from the Vattenfall experiments. It is a slug mixing transient, with a slug volume containing low boron concentration initially present in the RCS pipe. Buoyancy forces are negligible for this case.

Comparisons with measurements show best agreement with measurements for a calculation with CFX 5.7, the RNG k-ε turbulence model and a grid of 1,605,808 cells. The minimum average boron concentration at the core inlet was captured very well by this calculation. Also the minimum boron concentration at the core inlet was quite well simulated. The distribution of low boron concentration across the core inlet plane was not, however, accurately modeled by the CFD calculation.

The reasons for not getting a better agreement with measurements can maybe be found among the following items:

- Too few computational cells. Sensitivity tests showed a big influence of number of grid cells. Due to limited computer resources it could not be shown that a grid of 1,605,808 cells gives a grid-independent solution. There are, however, indications that this grid is not far from giving a grid-independent solution in this case. Maybe a few million cells will be enough for getting a grid-independent solution.
- A too long time step might have been used. Due to limited computer resources time step sensitivity tests have not been made.
- Simplifications in geometry can be more important than expected. Chamfers, vertical cylinders and the lowest structure in the lower plenum are neglected. Even if these structures are small they can have a significant influence on the flow field and the mixing. A sensitivity test showed that it is very important to model the horizontal structures in the lower plenum.
- Poor modeling of turbulence. Sensitivity tests showed big differences in results for different turbulence models, which indicates that more advanced turbulence models will give a better agreement with measurements. In the VATT-02 slug mixing transient there are certain features that are especially problematic for turbulence modeling, which also points to the need for more advanced turbulence models than have been used here. These are:
  - transition to turbulence in accelerating flow
  - impinging jet at the entrance to the downcomer
  - flow past obstructions

Faster computers, more efficient solution methods and lower license costs for the CFD codes for parallel processing will allow users to make calculations with more cells, shorter time steps and more advanced turbulence models and thereby reaching better agreement with measurements.

C.4.8 CFD calculations for the FORTUM PTS experiments

The thermal mixing phenomena of the Loviisa VVER-440 reactor was studied by Fortum (former IVO) with an experimental program in 1983. With a 2:5-lenght-scale semi-annular model of the Loviisa VVER-440 pressure-vessel downcomer and the cold legs the thermal mixing and stratification of the cold leg safety injection was determined with varying density differences and flow conditions. A detailed description of the experiments and their resuluts are given in [D09]. An overview is given in section C.2.3 of this report. During the FLOMIX-R project these experiments were calculated with the commercial CFD code FLUENT, and by comparing experimental and calculated results conclusions are made on how well the buoyancy driven turbulent flow with stratification and mixing can be modeled. The results of the CFD calculations and the comparison with the experiments are described in detail in [D11]. In the following section, a summary and overview on the CFD simulations is given.

C.4.8.1 Description of the CFD simulations

The original experimental program consisted of about 50 tests. Selected tests performed under conditions comparable to the ROCOM buoyancy mixing tests are compiled in Table C.2.3. Three of these tests were chosen for CFD simulations. The cold leg and injection flow rates and density difference ratio of these cases are presented in Table C.4.8.

Table C.4.8 Simulated Fortum PTS mixing tests

Test #	Q_{HPI} l/s	$Q_{CL,A}$ l/s	$Q_{CL,B}$ l/s	$Q_{CL,C}$ l/s	$Fr_{CL,HPI}$	$\Delta\rho/\rho$
10	2.31	0	0	0	0.147	0.16
20	2.31	1.87	0	1.87	0.146	0.16
21	2.31	1.87	1.87	1.87	0.147	0.16

The chosen tests represent three different flow situations: in test #10 there is a stagnant cold leg flow in all three loops, in test #20 there is side loop flows and in case #21 there is a loop flow in all three loops (numebring of the tests according to table C.2.3).

The CFD simulations of Fortum and NRI were made with the CFD code FLUENT using the same meshes and models. The commercial CFD code FLUENT 6.1 was used in all simulations. The pre-processing was made using GAMBIT version 2.1. The computations were made using dual CPU 2.2 GHz Intel Xeon workstation of Fortum or eight CPU (500 MHz) SGI ORIGIN 2000 of NRI.

Case matrix

The CFD simulations performed are presented in table C.4.9.

Table C.4.9 CFD simulations

Case	Partner	Experiment	Calculation type	Grid	Turbulence model	Sc_t	dt [s]
10.1	Fortum	10	Transient	Grid 1	Re k-ε	0.9	**0.2**
10.2	Fortum	10	Transient	Grid 1	Re k-ε	0.9	1.0
10.3	NRI	10	Transient	Grid 1	**RNG k-ε**	0.9	1.0
20.1	Fortum	20	Transient	Grid 1	Re k-ε	0.9	**0.2**
20.2	Fortum	20	Transient	Grid 1	Re k-ε	0.9	1.0
20.3	Fortum	20	Transient	Grid 1	Re k-ε	0.9	**10.0**
20.4	Fortum	20	Transient	Grid 1	Re k-ε	0.9	**4.0**
20.5	Fortum	20	Transient	Grid 1	Re k-ε	**0.5**	1.0
20.6	Fortum	20	Transient	Grid 1	Re k-ε	0.9	**0.02**
21.1	Fortum	21	Transient	Grid 1	Re k-ε	0.9	1.0
20.s1	Fortum	20	Steady	Grid 1	Re k-ε	0.9	**-**
20.s2	Fortum	20	Steady	**Grid 3**	Re k-ε	0.9	**-**
20.s3	NRI	20	Steady	**Grid 2**	Re k-ε	0.9	**-**

Grid

Three grids were made for simulations:

Grid 1: Hexahedral cells, total of 326910 cells. The main grid for the simulations.

Grid 2: Hexahedral cells, total of 807794 cells. The main valve added to the geometry, also more cells in the downcomer and in the main cold leg.

Grid 3: Hexahedral cells, total of 2615280 cells, adapted from the grid 1.

In all simulations the y^+ values were less than 300 in about 98 % of cells. The modeled geometry included downcomer, cold legs, part of the HPI injection pipe, parts of cold leg flow injection pipes with last flow elbows, outflow chamber and the outflow pipe. The valve model in the main loop was omitted in the first geometry version and added to the geometry version 2. The elliptic perforated bottom plate was modeled using a porous media model with a pressure loss proportional to the square of the velocity.

Grid sensitivity studies were made with steady state simulations 20.s1, 20.s2 and 20.s3. The comparison of results with grids having three different grid number and two different geometries indicated that no fully converged results were achieved, probably due to the time-dependent nature of flow field. The conclusion was that the grid study should be made with a time-dependent simulation. However computation resources did not allowed that during the FLOMIX-R project.

Boundary conditions

The inlet boundaries were at the injection pipes of the cold leg loops so far upstream from the downcomer and the mixing regions that the effect of uncertainties with boundary conditions were assumed to be small. At the inlet boundaries the constant velocity, the turbulence intensity and the turbulence length scale were specified.

The outlet boundary was put so far from the vessel to the drain pipe that boundary condition uncertainties should not affect the results. A constant static pressure was specified at the outlet boundary.

For wall boundary conditions the logarithmic wall function for the velocity profile was specified. The non-equilibrium wall function of FLUENT was used as it should be an improvement compared to the standard wall function.

Numerical methods

The segregated solver of FLUENT was used in all simulations. The temporal discretization was made using the 2nd order implicit method and the spatial discretization was made using the QUICK scheme. For pressure discretization the FLUENT's standard scheme was used. The pressure-velocity coupling was made using the SIMPLE scheme.

Time step

The effect of the time step size was tested with simulations 20.1-20.4 and 20.6 (Table C.4.9) with the following time step sizes: 0.02, 0.2, 1.0, 4.0 and 10.0 s. Also some preliminary tests were made with the time step size 0.1 s. Based on the Courant number in the cold leg the time step of about 0.01 s would be ideal, however, comparison of result with different time step sizes show that 0.02, 0.2 and 1.0 s produced basically similar behaviour of the target variables whereas 4.0 s and 10.0 s were too long giving unphysical results.

The numerical convergence was achieved with all time step sizes with 2nd order implicit temporal discretization.

Physical models

The material properties for the mixture of the injection and the main water were mass-weighted averages for density and volume-weighted averages for viscosity. The material properties for single fluids were constants taken from standard tables based on the fluid temperature. The mass diffusivity was defined to be negligibly small: 10^{-10} m^2/s.

The buoyancy forces in the momentum equations were modeled using the gravitational acceleration with the density difference.

The realizable *k-ε* turbulence model of Fluent was used in all simulations except one simulation of transient #10 that was made by NRI using the RNG *k-ε* turbulence model. The realizable k-ε turbulence model is a modified version of standard k-ε model that should be more accurate in case of flow separation and circulation. The turbulent Schmidt number variation was made with values of 0.9 (default value) and 0.5. No significant differences in the target variables were observed.

Additional sensitivity tests

Calculations of two Fortum PTS tests aimed at additional sensitivity tests were performed by NRI . In the test 10, RNG k-epsilon model was used instead of the Realizable one (which was used in all other calculations), so comparison of two models of turbulence is possible. In the

test 20, the effect of modelling the main gate valve (Fortum grid 2) was studied. For the transient test 10 the Fortum „standard" grid 1 was used.

C.4.8.2 CFD results and comparison with measurements

The comparison was mainly based on the temperature/concentration data from the thermocouple locations near the pressure vessel wall and in the main (middle one) cold leg. The comparison can be divided into the main cold leg area and the downcomer area, however these mixing volumes are strongly linked; the mixing in the loop affects to the plume entering the downcomer, and on the other hand the mixing in the upper part of the downcomer affects the possible backflow from the downcomer to the cold leg. The stratification and mixing in the main loop was studied using backflow ratio $Q^* = Q_h/Q_{HPI}$ where Q_{HPI} is the cold-water injection flow rate and Q_h is the flow rate from the downcomer to the main loop (see Fig. C.2.16).

The mixing of the cold water plume in the downcomer was studied using time-dependent maximum and average injection water concentrations at RPV wall at vertical levels z = -1.460 m and z = -0.812 m below the loop level.

The qualitative comparison of the calculated and the experimental flow field was made comparing the calculated concentration fields at the downcomer to the available experimental data.

For comparison of steady state simulations 20.s2 and 20.s3 the axial line concentrations in the downcomer at locations r = 646 mm, 668.5 mm and 691 mm and a circle line concentration and velocity profile at location r = 668.5, z = -1460 mm were also used.

Stratification and mixing in the main loop

When the backflow ratios of the simulations and the experiments are compared, the results are quite similar in case of the experiment 10. The backflow ratio decreases with time as expected, and is similar except during the period between 100 - 200 s, when the CFD simulation overestimates the backflow with about 30 %.

In case of experiment 20 with the side loop flows the behaviour of the backflow ratio is also qualitatively similar in the simulations and the experiment. The backflow ratio converges rapidly to a constant value, indicating a flow field where the side flows enter quite directly to the stratified main cold leg, mixes there and then the mixture forms a plume entering to the downcomer. The backflow ratio is about 0.20 - 0.25 in the experiment, and about 0.26 - 0.27 in the CFD simulation. The fluctuation of the backflow ratio is clearly larger in the experiment indicating small time-dependent behaviour not fully modeled by the CFD simulation.

In case of experiment 21 with the loop flows in all three cold legs the difference between the CFD simulation and the experiment is largest. The backflow ratio is about 1.0 in the

experiment and 0.7 in the CFD simulation. In case of flow in the main cold leg the physical meaning is not exactly backflow, but the value describes how the main cold leg flow and the backflow together mixes with the injection. If that backflow ratio is converted to the real backflow ratio the value in the experiment is about 0.3 and in the CFD simulation about zero. The reason to the lower value in the CFD simulation can be for example the turbulence modelling; in case of experiments 10 and 20, the main mixing region is closer to the injection jet where there is more clear turbulence, but in case of experiment 21 the mixing region is more downstream, where the turbulence level is lower, and the ability to model the turbulence in case of stratification and buoyancy effects is more important.

Stratification and mixing in the downcomer

The qualitative behaviour of flow in the downcomer is different in experiment 10 than in experiments 20 and 21. Without loop flows the cold plume entering the downcomer tends to go to sidewards and downwards at the same time, forming then a large swirl-like flow field to the downcomer. With side flows the plume is more balanced to the middle of the downcomer, forming a clear stratification layer. This qualitative behaviour was repeated also by CFD simulations. The backflow from the side loops to the main loop in case of experiments 20 and 21 was seen also in the simulations, as well as the asymmetric stratification in the downcomer. The swirl-like flow field of the experiment 10 is also modeled by the simulation.

The behaviour of the maximum and the average injection concentrations at the thermocouples located near the pressure vessel wall at levels z = - 812 mm and z = - 1460 mm was mainly similar to the experiments, however there were also some differences:

- In the simulations of cases 20 and 21 the cold water plume tends to move from the pressure vessel wall to the core barrel wall and stay there, while in the experiments there seems to be more time-dependent movement between the walls. This effect is visible in the upper part of the downcomer before the plume mixes.
- In the simulations of cases 20 and 21 the simulated maximum values are a little lower at the level z = - 812 mm than the experimental results, probably due to the radial misplacement of the plume mentioned above.
- In the simulation of cases 20 and 21 the simulated maximum values are a little higher at the level z = - 1460 mm than the experimental values. The plume decay seems to be slightly underestimated by the CFD simulation.
- The average transient cooldown/injection concentration increasing follows the exponential decay law both in the experiment and simulations. However in simulations the cooldown seems to be faster. There is no clear reason for that effect. Simulated cooldown follows quite directly the analytical estimation based on model volume and full mixing assumption, while the experimental results indicate that there can possibly be more direct outflow of the colder plume water before full mixing.

Turbulence model

The transient simulation of experiment #10 was performed with Realizable *k-ε* (case 10.2) and RNG *k-ε* (case 10.3) turbulence models. Based on the comparison of target variables the results of models were quite similar. With both models the calculated backflow ratio and molar fractions were slightly higher than the measured values, Realizable model giving values slightly nearer to the measured. The simulated and experimental backflow ratio and maximum molar fractions at PV wall at level z = -1460 are presented in figures below.

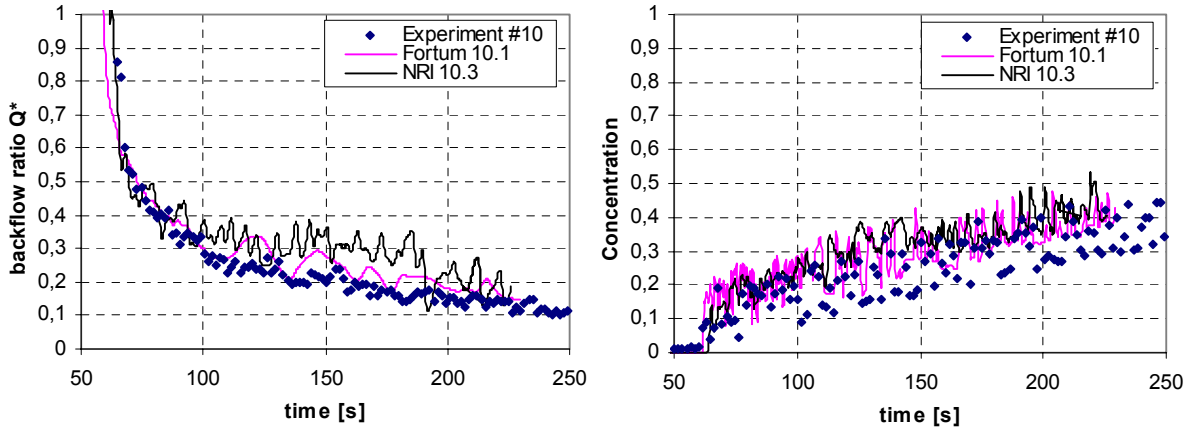

Fig. C.4.36 Turbulence model tests: backflow ratio (left) and maximum molar fraction at PV wall at level z = -1460 (right) during simulations of experiment #10.

Numerical convergence was better with Realizable *k-ε* than with RNG *k-ε* model. Especially in the beginning of the transient the RNG model required shorted time steps for converged results.

Effect of main gate valve simulation

Results of FORTUM No.20 steady-state test are presented in Fig. C.4.37 in the form of mole fractions (concentrations) of injected higher-density water at different positions. The values from the NRI calculation are compared with calculated results of Fortum using the standard grid 1 and the grid FORTUM_adapted (grid 3). In the NRI calculations, the Fortum grid 1 was used.

However, the performed steady state analyses were not well converged which is caused by unsteadiness of the flow. Therefore, well based conclusions on the impact of the main gate valve modeling could not be drawn.

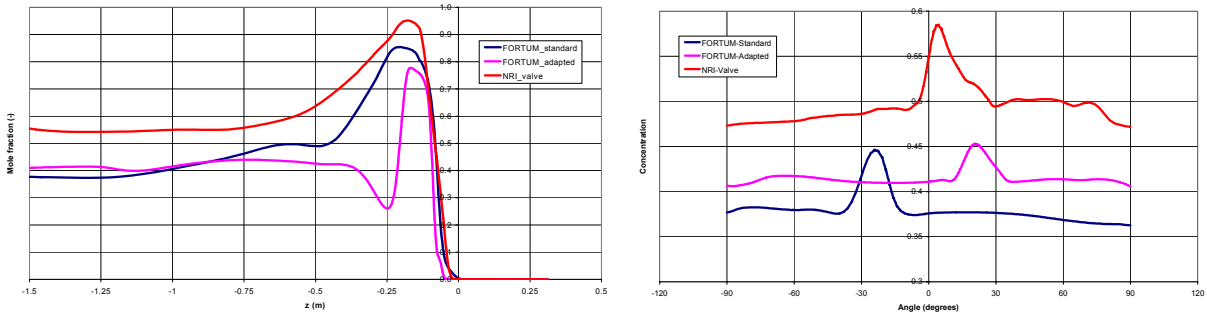

Fig. C.4.37 Mole fraction of injection on vertical line at r = 0.6685 m (left) and along azimuthal direction at r = 0.6685 m and z = -1.460 m (right)

Summary

The buoyancy driven turbulent flow with stratification and mixing in selected Fortum mixing tests was modeled with the commercial CFD code FLUENT. The main goal was to start the validation of CFD methods for PTS simulations of real PWRs.

The main features of flow and mixing were quite well simulated; stratification in the main cold leg and the downcomer, backflow from the downcomer and side loops to the main loops and the flow field in the downcomer. A more detailed comparison with main loop backflow rate and the average and maximum injection concentration / minimum temperatures near the pressure vessel wall showed also mainly good equivalence. However there were some differences. The mixing in the main loop was not correctly calculated in case of experiment 21, the CFD simulation underestimated mixing a little. Also the mixing of the cold water plume was not as effective in simulations as in real experiments, and there was also small difference in average cooldown rate without any clear reason.

The geometry and mesh as well as the physical and numerical models used here were chosen so that those can be applied also to the real plant scale analysis with current computation capacity having approximately the same accuracy as here. More grid size tests with transient simulations are needed to test the grid-independency of simulations, the steady state tests made in this work are not good enough due to the poor convergence.

Preliminary turbulence models tests with Realizable k-ε and RNG k-ε models did not bring out any significant differences between models.

C.4.9 CFD calculations for the GIDROPRESS experiments

NRI simulated two from three slug-mixing experiments provided by EDO Gidropress (see section C.2.2). The experiments simulated slug mixing in the reactor vessel of a VVER-1000 reactor. In the tests, the experimental facility was filled with hot water (temperature of 71 °C in test 1, 73.3 °C in tests 2) and slug of cold water (temperature of 25.8 °C in test 1, 27.4 °C in tests 2) was situated in the loop seal. The loop flow rate was then increased up to 175 m^3/hr (test 1) and 470 m^3/hr (test 2).

C.4.9.1 Description of the CFD calculations

Pre-processor GAMBIT 2.1 and solver FLUENT 6.1.22 were used in the simulations. A more detailed description of these calculations is presented in [D11].

Geometrical Simplifications, Local Details

In both tests the perforated walls of supporting tubes were modeled by porous jump „membrane".Pump simulator was included into the computational domain. Cold leg valves were not modeled. In test No.1 the elliptical perforated bottom with original 1324 holes (diameter of 8 mm) was modeled as porous media zone in the first version of the grid (variant 1A), and the number of holes was decreased to 312 holes with diameter of 16 mm in the second grid (variant 1B). In test No.2 the elliptical perforated bottom was modeled with the reduced number of holes.

Grid generation

In test 1, where the elliptical perforated bottom was modeled as porous medium, 970 000 cells were used (variant 1A). In variant 1B and test 2, when the elliptical perforated bottom was modeled with lower number of bigger holes, 1 100 000 cells were employed. Even this grid probably did not produce grid-independent solution. View of the grid and calculation domain used in test 1 is shown on Fig. C.4.38.

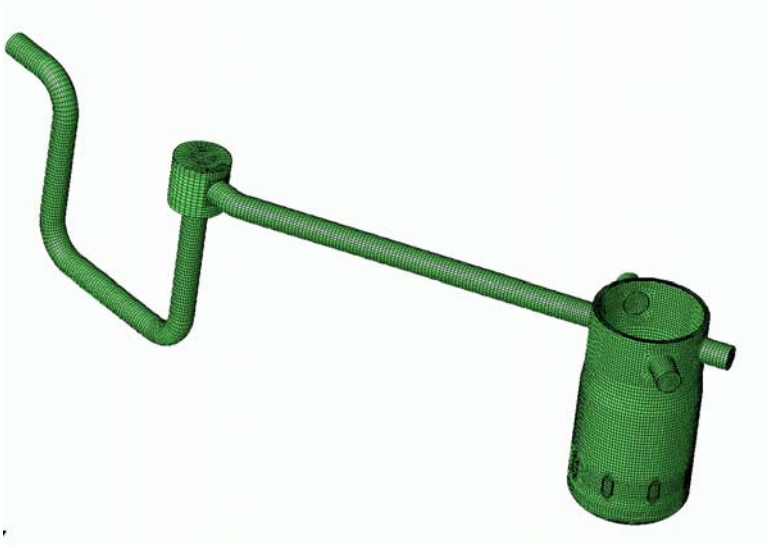

Fig. C.4.38 Computational domain with grid used in Gidropress test No.1– overall view

Boundary Conditions

Inlet boundary with “velocity inlet” type of boundary condition was placed in the horizontal part of the loop upstream of the loop seal (see Fig. C.4.38). Outlet boundary with “outlet vent” boundary condition was placed at the reactor core inlet where thermocouples are located. At walls, adiabatic (Neumann) boundary condition was used for the energy equation. For test 2, also adiabatic and constant temperature boundary conditions were tested (variant 2A and 2B).

Turbulence modelling

Realizable k-ε model was used with differential viscosity option and standard wall functions (y^+ lower than 250). Full buoyancy effects including the effect of buoyancy on ε were considered. Turbulent Prandtl number was set to 0.72.

Discretisation schemes and time step

Second-order upwind scheme for convection terms and second order implicit scheme for temporal discretization were used. Time step size was 0.025 s in the test 1 calculation and 0.020 s for the test 2.

C.4.9.2 Results of Gidropress slug mixing test calculations

Fig. C.4.39 shows the velocity contours at symmetry plane of the RCP simulator for various options of turbulence model from the test 1 calculation. It becomes clear from this figure, that there is a relevant pre-mixing in the pump simulator what is not very well modeled. Therefore, this pre-mixing is one reason for uncertainties in the calculated results.

Fig. C.4.40 shows the dimensionless averaged temperature at the core inlet. Calculated minimum of average core inlet temperature is lower than the experimental one. The calculated average values are almost independent from the grid option (porous body or reduced number of holes). Fig. C.4.41 shows the temperature distribution at the core inlet calculated with both grid options. Grid with perforated bottom (variant 1B) provides better mixing than grid with porous zone (variant 1A).

The underestimation of the minimum value in the calculation is an indication, that heat exchange between cold slug and walls cannot be neglected.

Calculated cold slug lags behind the experimental one. The reason for this time shift could not be clarified finally.

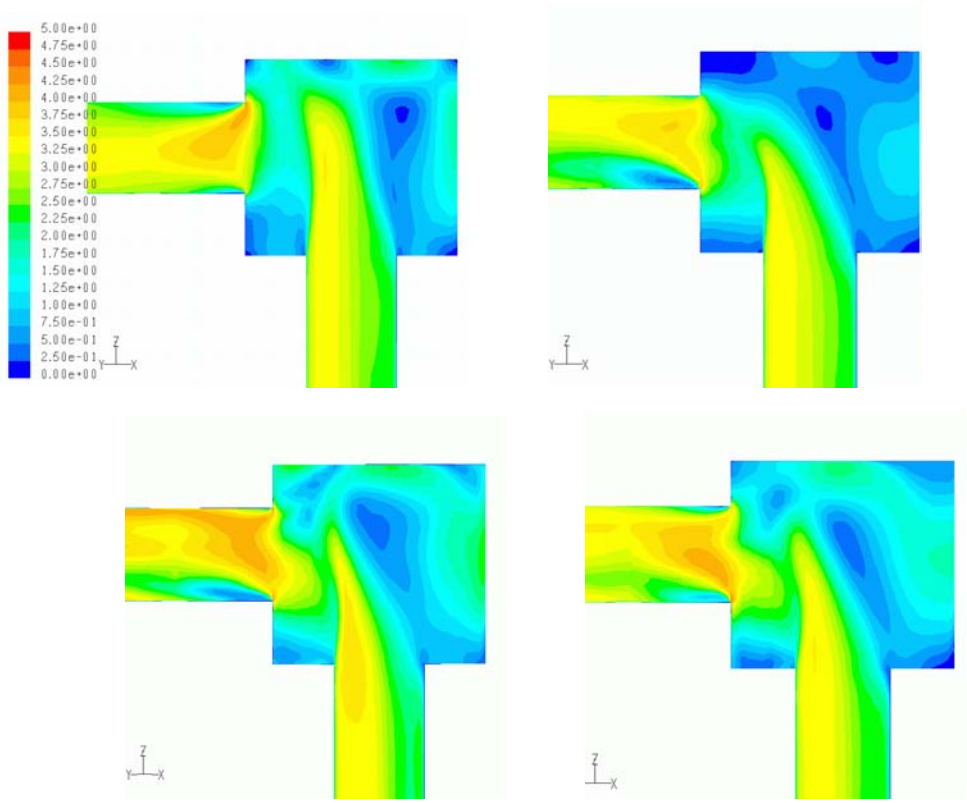

Fig. C.4.39 Velocity contours at symmetry plane of the RCP simulator for: Standard k-ε model (upper left), Realizable k-ε model (upper right), RNG k-ε model (lower left), and k – ω model of turbulence (lower right)

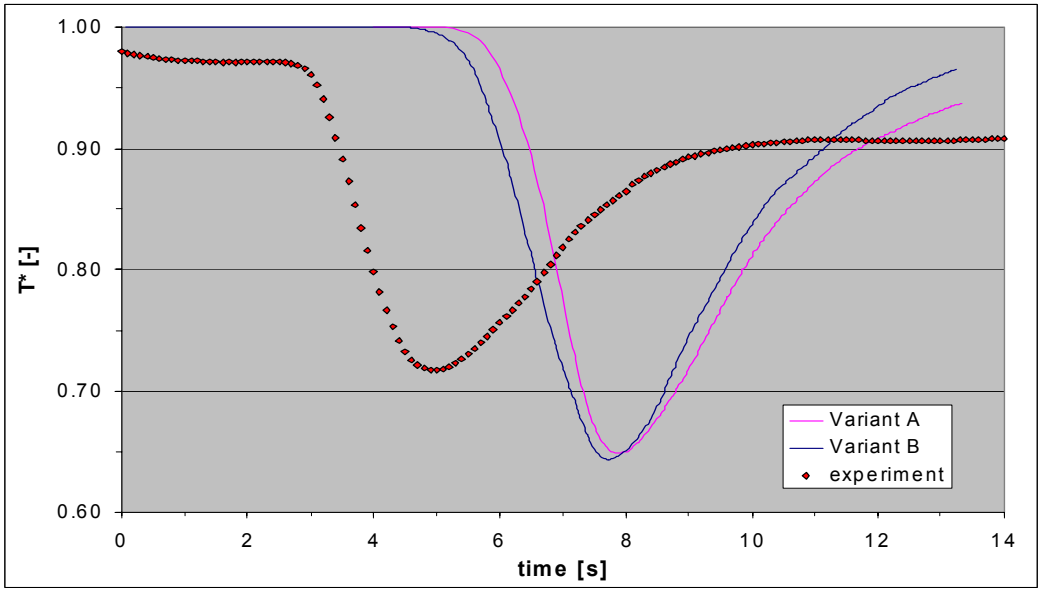

Fig. C.4.40 Test 1 - Average dimensionless temperature at the core inlet vs. time

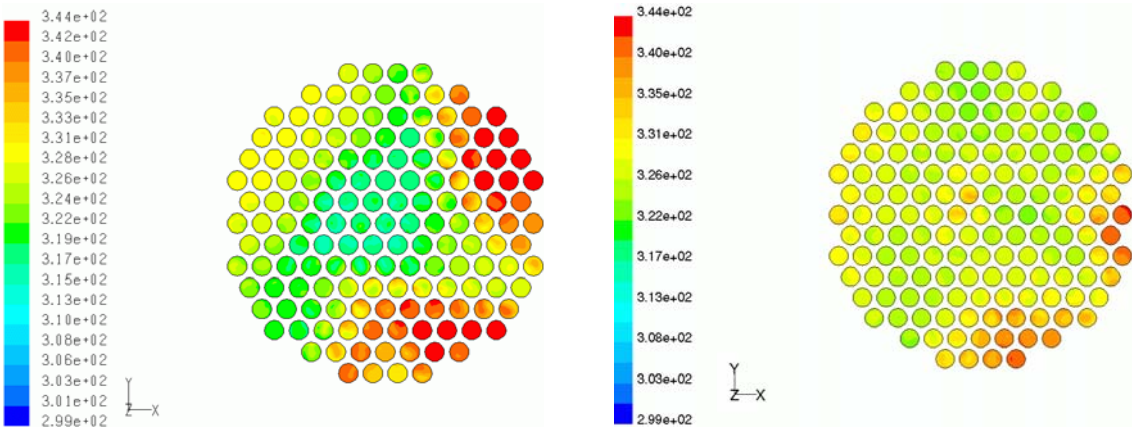

Fig. C.4.41 Calculated temperature distribution at the core inlet plane: Variant 1A (porous medium - left) and 1B (reduced number of holes - right)

The transient of the average dimensionless temperature at the core inlet for the test 2 is shown on Fig. C.4.42. In variant 2A zero wall heat fluxes are assumed as in the simulations of tests 1. In variant 2B, constant wall temperature, equal to temperature of the hot water outside the cold slug, is assumed. In both cases, detailed model of the perforated bottom and realizable k-epsilon model are used. In case 2A, no heat release from the wall to the fluid is considered. The minimum temperature is underestimated in the calculation. In the case of constant wall temperature, the heat release is overestimated, because in reality, the wall will be cooled down somewhat, which leads to a reduction of the heat flux. Consequently, the minimum temperature is overestimated in the calculation. In the case of realistic heat transfer modeling (solution of the coupled fluid dynamics – heat conduction problem), a good agreement between measurement and calculation can be expected. However, this coupled calculation could not be performed within the FLOMIX-R project.

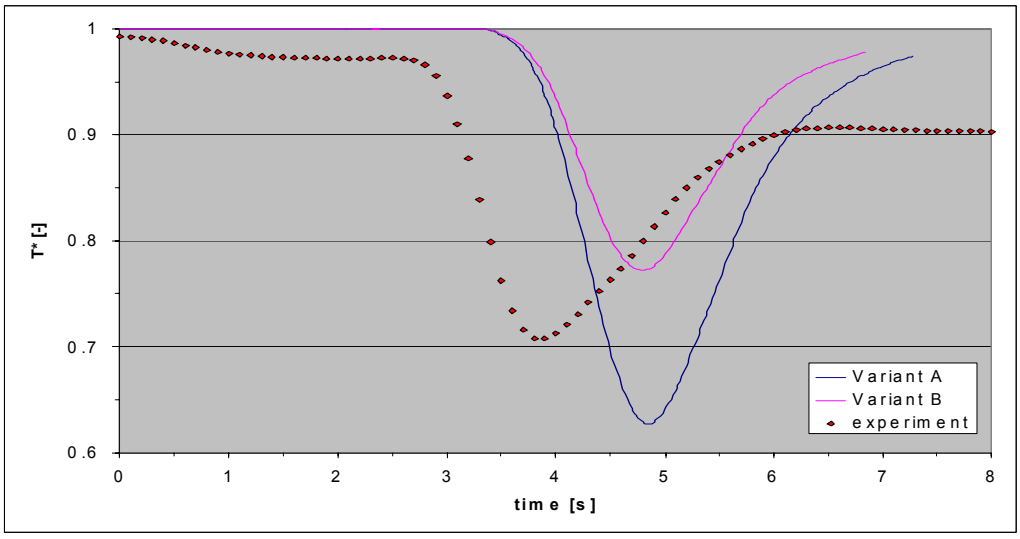

Fig. C.4.42 Dimensionless avregae core inlet temperature for variant 2A with zero wall heat fluxes and variant 2B with constant wall temperature

Summary and conclusions

NRI calculated two slug-mixing experiments provided by EDO Gidropress, which simulated the slug mixing in the reactor vessel of VVER-1000 reactor. The transient behaviour of average temperature at the core inlet was studied with two variants - with the elliptical perforated plate modeled as porous medium and with the elliptical perforated plate modeled as solid structure with reduced number of holes. Based on these simulations it was found that grid with perforated bottom provided better mixing than grid with porous zone. However, the calculated minimum of the average core inlet temperature was lower than the experimental one with both grids. Conclusion was made that the heat exchange between the cold slug and the walls probably cannot be neglected.

C.4.10 CFD simulation mixing tests at Paks NPP (VVER-440 reactor)

Additional test data were made available by Paks NPP and AEKI for the FLOMIX-R project. The data come from the commissioning tests of Paks NPP performed in years 1987-1989. The tests addressed mixing among coolant loop flows in the downcomer and up to the core inlet in forced flow conditions. The goal of the tests was investigation of potential loop temperature asymmetry that might occur and significantly affect power distribution in the core. An overview on the results is given in Section C.3.3. Detailed description of the tests can be found in reference [Elt02].

Paks mixing experiments were calculated by VUJE (FLUENT), AEKI (FLUENT) and TU Budapest (CFX5). These calculations are described in section C.4.10.1. Results from the calculations are presented in section C.4.10.2. More detailed Descriptions of the CFD analyses is given in [D11].

C.4.10.1 Description of the CFD calculations

CFD codes

CFD code FLUENT 6.1.18 was used in these analyses by VUJE. The code version FLUENT 6.1.22 was used by AEKI. TU Budapest used the code CFX5.5.1.

Geometrical Simplifications, Local Details

Comprehensive computer models of VVER 440 reactor vessel were developed. They include all 6 loops with inlet nozzles and three baffles, whose purpose is to deflect the coolant injected into the reactor vessel from the safety injection tanks. Eight support consoles for the core barrel alignment were modeled as well. An overview on the different geometrical models is given in Table C.4.10.

Table C.4.10 Overview on geometrical modeling of the NPP Paks VVER-440

	VUJE	**AEKI**	**TU Budapest**
Loops	6	6	6
Baffles	simplified geometry	simplified geometry	Detailed geometry with gap between baffles and inner wall of downcomer
Alignment drifts	simplified geometry	h simplified geometry	Detailed geometry
Elliptical perforated plate	Porous medium/ structure with reduced number of holes	Porous medium with direction dependent resistance (varied)	Momentum sources determined from calculations with reduced number of holes
Planar perforated plate	Porous medium	Porous medium	Lower plenum as porous medium with directed momentum source
Lower guide tubes	Simplified geometry of perforation/ omitted	omitted	
Core support plate	Porous jump/omitted	Porous medium	
Core	Porous medium/ omitted	Porous medium	Momentum sources/ omitted
Not modelled	ECC inlet nozzles; small structures, protrusions and chamfers	Lower guide tubes; ECC inlet nozzles; small structures, protrusions and chamfers	Lower guide tubes; ECC inlet nozzles; small structures, protrusions and chamfers

Grid generation

The following four grids were used in Paks mixing tests calculated by VUJE:

- **Grid 1**: 1.752.069 cells (structured hexahedral mesh)
  In grid 1, the internals were modeled as porous media. The inlet position is situatedapproximately 4 diameters from the downcomer inlet.
- **Grid 2**: 1.609.231 cells (hybrid mesh)
  Grid 2 is a hybrid mesh based on grid 1, to which models of the lower guide tubes and the core support plate were added. Model of the lower guide tubes includes also a simple model of perforation. The elliptical perforated plate was changed to the solid structure with reduced number of holes.
- **Grid 3**: 1.698.319 cells (hybrid mesh)
  The model of the inlet pipe including bends was added to reactor inlet nozzles.
- **Grid 4**: 1.6431.99 cells (hybrid mesh)
  The model of the core was removed.

Hybrid mesh with 1172618 cells was used for AEKI calculations. In one variant the grid was refined by adaptation.

Three different grids have been built for TUB calculations:
Grid 1 (1 559 363 cells) is a coarse unstructured mesh, containing the detailed model of the downcomer (including the inlet nozzles, the hydro-accumulator baffles and the alignment drifts), and the lower plenum with the momentum source model of the elliptical perforated plate, without the modeling of the lower guide tubes.
Grid 2 (2 780 395 cells) covers the same geometry as grid1 but with finer mesh. Test calculations have shown that there are differences between the calculated flow fields with the two grids, which means that no grid-independent solution was achieved.
Grid 3 (1 838 991 cells) covers the same geometry as grid1, but it also includes the momentum source model of the lower guide tubes (in order to avoid back-flow at the core inlet). The resolution of the mesh in grid 3 is between the mesh of grid 1 and grid 2.

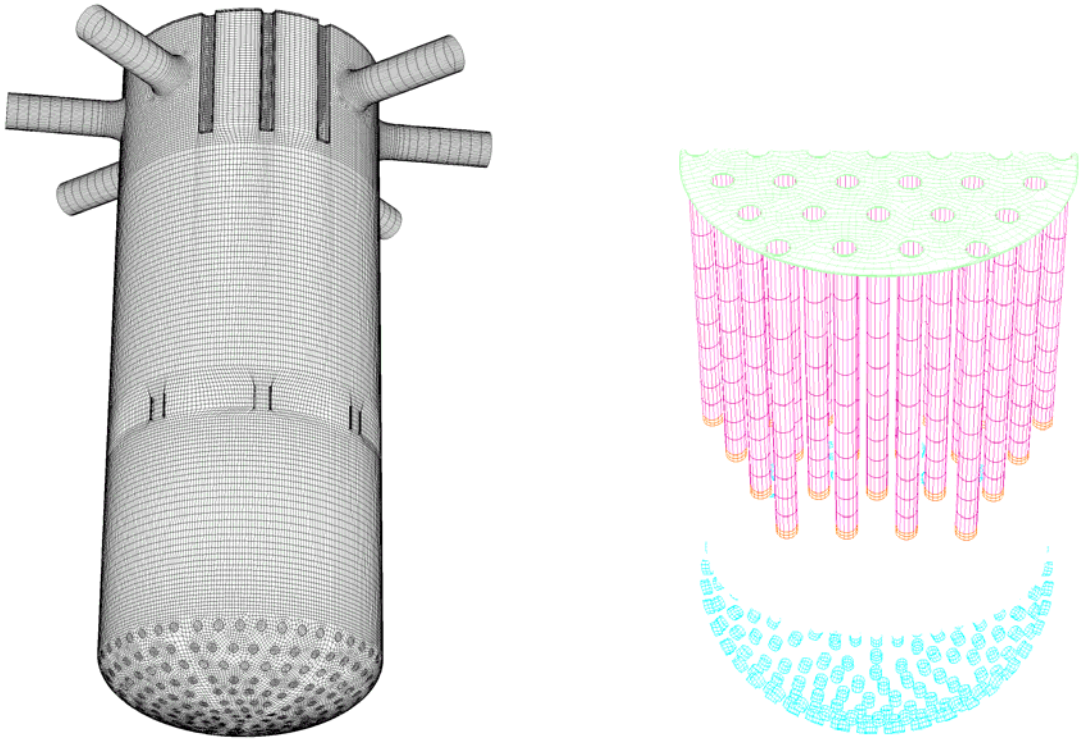

Fig. C.4.43 VUJE model of VVER 440 V-213 reactor (left) and reactor internals (right)

With the aim to include the influence of bends in the cold leg, the model was modified and inlet nozzles were extended (Fig. C.4.44). The effect of reactor coolant pump was calculated as well, but it turned out that the effect of loop bend was dominant.

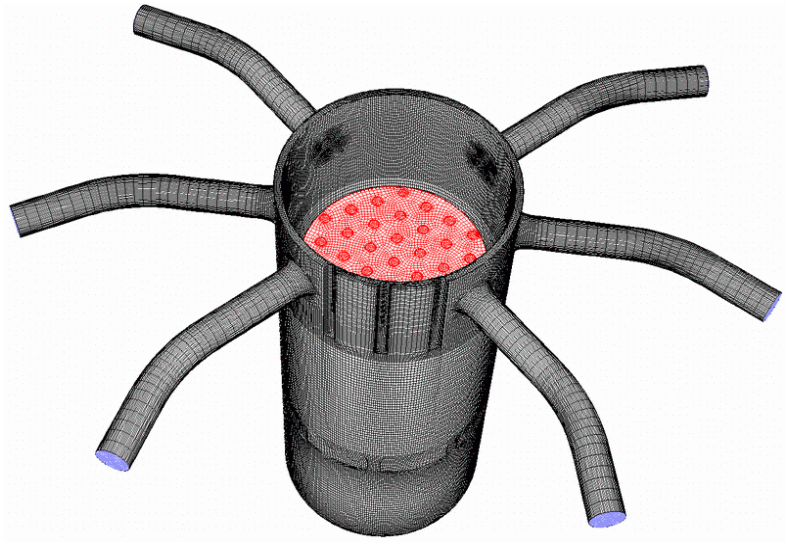

Fig. C.4.44: Model of reactor vessel with extended cold legs (Grid 4)

Boundary Conditions

The following boundary positions were defined in the test calculations:

- Inlet boundary positions were located at the inlet nozzles of all 6 loops so that geometry of inlet nozzles was included. In sensitivity calculations of VUJE the inlet legs of all loops were extended beyond the bends in the legs.
- Outlet boundary position was located either at the outlet of the core or in the core inlet. Boundary condition for the outlet was given pressure.
- Boundary conditions for the inlets were:
  - Mass flow inlet – the same value (1460 kg/s) in all 6 loops (1500 kg/s in the TU calculation);
  - The same constant temperature in 5 loops (270°C), and lower temperature in one loop (265°C). Six mixing scalar components (one for each loop) were used in the TU calculations instead of temperature.
  - Turbulence intensity at the inlet was 5%.

Numerical schemes and time step size

First order and second order upwind schemes were applied to assess their influence on results. SIMPLE pressure-velocity coupling was used. Second order ("High resolution") advection scheme was used in the TU calculation with CFX.
All calculations were performed as steady-state.

Turbulence modeling

Different turbulence models were used with the aim to find their impact on the results: Standard k-ε model and RNG k-ε model were applied by VUJE, Standard k-ε, k-ω SST and RSM turbulence models with standard and non-equilibrium wall functions were used by AEKI. By AEKI, mixing was modeled by user-defined scalars with increased diffusivity

coefficient and by using species transport model with turbulent Schmidt number 0.7. In the CFX calculations of TU Budapest, Standard k-ε model was used with "Scalable" option for the turbulent wall function. The flow is non-buoyant. Therefore, no buoyancy terms in the turbulence models were applied.

C.4.10.2 Results of the CFD analyses

The performed calculations showed that the coolant flows in sectors downwards in the downcomer, and the sectors remain also at the core inlet. The maximum of the mixing scalar is not located directly below the inlet nozzle, but an azimuthal shift of the maximums can be observed because of the asymmetric location of the inlet nozzles and because of the hydro-accumulator baffles. The effect of the baffles can be observed even at the core inlet.

The sensitivity tests of the meshing showed that the calculation meshes did not meet the grid-independency criteria, in spite of the large node number. It was concluded that hybrid tetrahedral-hexahedral mesh seems to be more suitable for the meshing of the pressure vessel geometry because of the lower mesh element number (in the new versions of the CFX hybrid meshes are available.)

Comparison of the calculation results with the measurements was done only for that simulations which gave the best agreement ("production calculations"). Summary of basic assumptions used in the production calculations of Paks mixing tests performed by AEKI, TU Budapest and VUJE is presented in Table C.4.11. The results shown in figures C.4.45 and C.4.46 in the form of temperature fields expressed in terms of mixing scalars at the core inlet and compared with experimental data. For assessment of deviations between calculated results and measurements, maps of errors are presented as well.

Table C.4.11: Basic assumptions used in the calculations of Paks mixing tests

	AEKI	**TU Budapest**	**VUJE**
CFD code used	FLUENT 6.1.22	CFX 5.5.1	FLUENT 6.1.18
Mesh	1 172 618	1 838 991	1 609 231
Elliptical perforated plate	Porous medium	Porous medium	Structure with 227 holes
Guide tubes	No	No	Yes (with perforations)
Discretisation scheme	1st order	2nd order	2nd order
Wall function	Non-equilibrium	Scalable	Standard

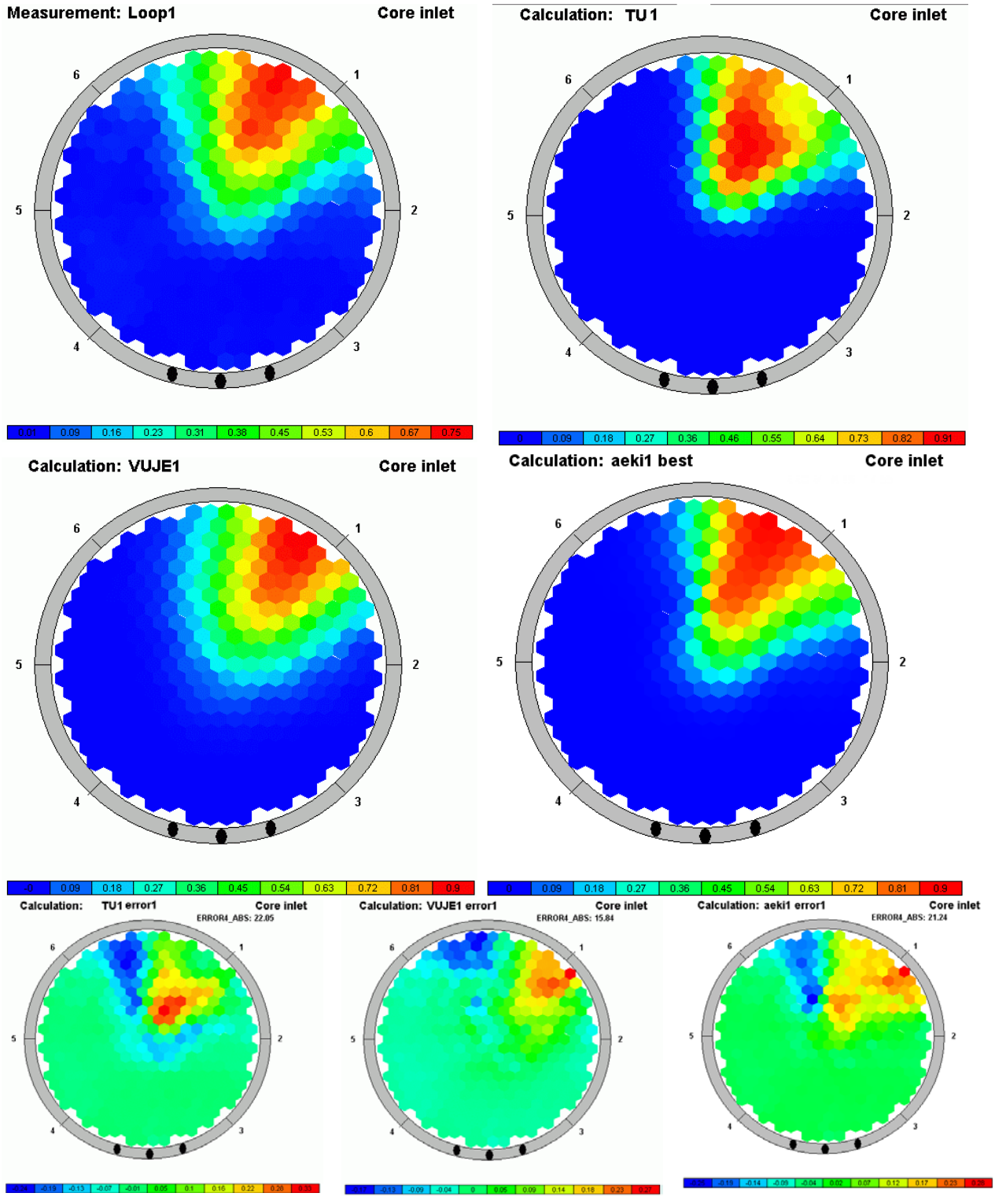

Fig. C.4.45 Comparison of calculated core inlet temperatures with measured data for loop one (upper) and deviations from measurement (lower)

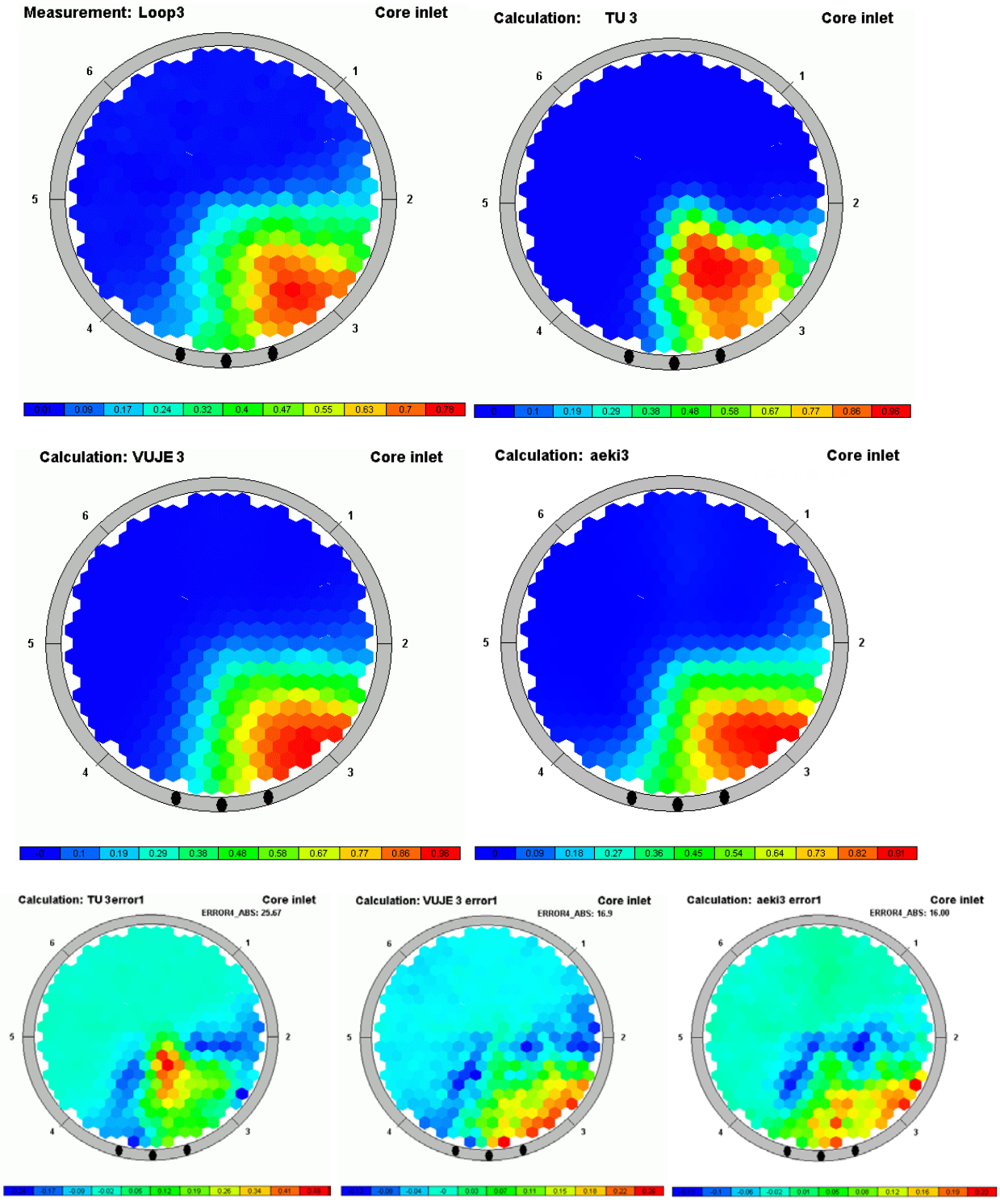

Fig. C.4.46 Comparison of calculated core inlet temperatures with measured data for loop three (upper) and deviations from measurement (lower)

Summary and conclusions from VVER mixing tests calculations

The results show qualitatively good accordance with the measured data, however numerical differences can be observed, for example the calculated maximum of the mixing scalars are larger than the measured ones.
The flows from cold legs 1,2,5 and 6 mixes only little in the downcomer and maintain own sectors. Flows from cold legs (3,4) located near to the ECC baffles are mixed a little bit more. The corresponding sectors are broader. The spreading of the temperature or concentration filed is underestimated in the calculation. For the sector corresponding to loop 1, a systematic angular shift against the measurement is observed in the calculations.

Numerical convergence:

- Good numerical convergence was achieved with basic solver and solver settings based on residuals of continuity and momentum equations (using first order upwind discretization scheme and k-ε or RSM turbulence model).
- Some numerical fluctuations of the flow field were observed below the ECC baffles in the downcomer, possibly due to some non-stationarity of the flow field.

Geometry modelling:

- Modelling of detailed internal geometry (e.g. flow baffles) may have a noticeable influence on results.
- ECC water baffles guide the main flow and generate turbulence effects in the downcomer.
- The alignment drifts have only local effect.
- Accurate model of the perforated elliptical bottom (modeling the elliptical perforated bottom as solid structure rather than using a porous medium) provides more realistic flow pattern and improves the accuracy of the calculation.
- Too much simplifications or too coarse grids can cause unphysical phenomena (e.g. mixing), which are a consequence of numerics.
- More accurate geometry modeling of perforated elliptical bottom and structures below the core is required.
- The models should include the upper plenum and the outlet nozzles.

Boundary conditions:

- Using pressure outlet boundary condition gives better numerical convergence than outflow boundary.

Grid and discretisation schemes:

- Boundary layer at the walls of downcomer should be less then 3mm, to keep y^+ parameter less then 1000.
- High order methods decrease the stability of the solution.

Turbulence modeling:

- From the tested turbulence models the standard k-ε with non-equilibrium wall function and RSM with standard wall function models give similar results and best agreement with experimental data. RSM model with non-equilibrium wall function and k-ω sst model overestimate the turbulent effects.

In general, obtained results proved the applicability of CFD codes for reactor calculations, however there are still items requiring further investigation.

C.4.11 Summary and conclusions from CFD code validation

The purpose of FLOMIX-R WP4 was to obtain indications on how well boron dilution transients and steady state mixing in Pressurized Water Reactors (PWR) can be modeled by CFD codes and to give recommendations for use of CFD for these purposes. CFD calculations have been validated against measurements from four different test facilities. In this section, a summary of the conclusions and recommendations made from these calculations are given and also discuss what needs to be done to strengthen the CFD tool for turbulent mixing applications are discussed.

C.4.11.1 Conclusions from sensitivity tests according to the BPG

The most important conclusions from the sensitivity tests made in WP4 and WP3 are presented below. Sensitivity tests are an important part of applying the Best Practice Guidelines for CFD in terms of quality assurance. Sensitivity tests will tell if you have a grid- and timestep-independent solution, or if results are sensitive to inlet and outlet boundary conditions, modeling of geometry and turbulence model etc.

As the test facilities for which the validations were made are quite different, it is in some cases difficult to draw general conclusions. The conclusions are also based on calculations that have not been shown to be grid independent.

<u>Grid size</u>

The aim is to make CFD calculations that give grid-independent solutions, i.e. results that do not change when the grid is refined further. A grid-independent solution can be defined as a solution that has a solution error that is within a range that can be accepted by the end-user, in view of the purpose of the calculations. According to the BPG, calculations must be made with at least three different grids in order to be able to quantify the grid-dependence of the calculations. The two finer grids also have to be made using a complete refinement of the nearest coarser grid, to get an objective measure of the grid-dependency. For example, if a calculation is made with 200,000 cells, calculations also have to be made with 1,600,000 cells

and 12,800,000 cells. Due to limited computer resources, this procedure has not been possible to follow for any of the slug mixing test cases in FLOMIX-R WP4. A transient calculation for a coarse grid of around 200,000 cells takes in the order of one week to perform. The solution errors have therefore not been quantified. Developments in computer technology will make these quantifications of solution errors possible within a few years. The number of cells required for grid-independency can only be guessed. Several million cells are probably needed for most of the transient test cases in FLOMIX-R.

In spite of fully grid-independent solutions, solutions on so-called production meshes were used to assess the agreement between measurement and calculations. The production meshes were an optimum in mesh refinement what could be reached.

Inlet boundary position and inlet boundary condition

It is well known that the choice of inlet boundary position and inlet boundary condition (turbulence level, variation in inlet velocity field in space and time) can have a big influence on the flow pattern far downstream from the inlet. Some partners therefore made sensitivity tests; others put the inlet far upstream from the downcomer at a position where the flow conditions were well known.

For the ROCOM steady state mixing case, results were not sensitive to different turbulence intensities at an inlet positioned close to the downcomer. Slightly different results were achieved if the concentration profile was changed at the same inlet position. Modeling of the four cold legs, bends included, gave only slightly different results compared to having an inlet close to the downcomer.

Outlet boundary position and outlet boundary condition

For the Vattenfall steady state flow situation the results were only slightly sensitive to whether the main outlet was put at the core inlet or at the core outlet. For the ROCOM cases it was found that the main outlet should be put above the core inlet.

Modeling of internal geometry

Internal structures can have a big influence on flow and mixing. These structures can either be omitted, be simplified or be modeled in detail. One type of simplifying model is a porous media model, with distributed resistances.

Especially how the structures in the lower plenum are modeled can have a big influence on flow and mixing. There were different experiences concerning the importance of modeling the lower plenum structures. These are listed below. For most applications, a detailed model gave results that were in best agreement with measurements. A general recommendation should be that internal structures should be modeled in detail. One should be very careful with decisions to omit these structures or to use simple forms of the porous media approach.

For the ROCOM steady state calculations using CFX4, a porous body model of the steel plate and sieve barrel gave reasonably good results. For the calculations with CFX5, however,

detailed models of these structures gave better agreement with measurements than using a porous media model. Also for the NPP PAKS and GIDROPRESS calculations, detailed modeling of this types of structures gave better agreement with measurements.

For the Vattenfall steady state case, inclusion of the lower plenum structures has a significant positive influence on the flow field in the downcomer.

For the FORTUM PTS tests, modeling of the bottom plate only had a small influence on the flow field.

Turbulence models

For the Vattenfall slug-mixing transient the best results were achieved with the RNG k-ε model, with scalable wall functions, compared with the k-ω SST model and the RSM (Omega (BSL)), with automatic wall functions. For the ROCOM transient buoyant case, RSM (BSL) gave improved results compared to the Standard k-ε and the k-ω SST model. For the ROCOM steady state mixing and non-buoyant transient mixing, the results were not very sensitive to turbulence model (the Standard k-ε model and the k-ω SST model gave similar results). For the (buoyant) FORTUM PTS tests, the Realizable k-ε model produced better results than the RNG k-ε model. For the VVER mixing test calculations the Standard k-ε model with non-equilibrium wall functions and RSM with standard wall functions gave the best agreement. RSM with non-equilibrium wall functions and the k-ω SST model overestimated the mixing.

The conclusions presented above are in some cases contradictory. The RSM models should give better agreement with measurement, as they are more advanced than the two-equation models. This was not always the case for the calculations in FLOMIX-R. The contradictory conclusions make it hard to draw any general conclusion on which turbulence model to use. It should, however, once again be emphasized that these results are based on calculations that have not been shown to be grid-independent.

In general, standard turbulence models implemented in the codes can be used for turbulent mixing calculations.

Double precision

In general, the use of double precision arithmetic is recommended, but it requires more computer resources. Single precision arithmetic was used only if it was not shown that single precision gave identical results to using double precision for a similar case.

Time step

Especially if the CFL number (the Courant-Friedrichs-Lewy number) is larger than 1, and especially where there are strong gradients, one can expect problems with time-step dependency. For the sensitivity tests made for time-step, time-step independency was reached with time steps which were as long as up to 10 times the CFL number (FORTUM PTS) and 50 times the CFL number (ROCOM slug mixing transient). These CFL number are for positions where there are large gradients in concentration or temperature.

Height of wall-adjacent cells

One sensitivity test was made for the height of the wall-adjacent cells for the Vattenfall steady state case. The maximum y^+ values were very high with the grids used, up to around 5000. The grid was therefore refined at the wall-adjacent cells. However, calculations with these lower and more optimum y^+ at the walls gave worse results for the Vattenfall steady state case. This might indicate that the non-equilibrium wall function used does not work properly for the type of boundary layers present in the downcomer, especially those close to the flow-impingement where the jet from the inlet pipe hits the downcomer wall.

For the ROCOM production mesh the y+ value in the downcomer was 65, and therefore below the recommended value of 100.

Code

The commercial codes CFX4, CFX5 and Fluent 6 were used.

For both the Vattenfall slug mixing case and the ROCOM_02 slug mixing case the differences between the results from Fluent 6 and CFX5 were significant, in spite of the fact that the calculations were run with exactly the same grids. For the ROCOM steady state mixing case, the differences were smaller.

However, as none of the calculations are probably grid-independent, one cannot expect to obtain the same results from the codes, as the numerics in the codes are different. Another difference between the two codes is that exactly the same wall functions could not be applied.

Numerical schemes

At least second order schemes should be used, both in space and time. For some applications there were convergence problems (unstable solutions) when using 2^{nd} order schemes. This might indicate that there are also low-frequency fluctuations in the measurements, which cannot be resolved by a steady-state calculation. For these cases a time-averaged flow field might have to be calculated with a transient calculation.

C.4.11.2 Comparisons with measurements

Steady-state mixing and flow distribution

In general, the flow pattern, velocity distribution in the downcomer and mixing scalar distributions at the core inlet are well predicted in the CFD calculations. The velocity field in the downcomer has inhomogeneous character with maximum downwards flow components in the regions in-between the inlet nozzles. A clear sector formation of the flow in the downcomer is seen. This leads to maximum mixing scalar values at the core inlet of 92 – 99 %. That means, a part of the fluid remains almost unmixed. The re-distribution of the velocity field and mixing scalar distribution in the case of asymmetric flow conditions is also qualitatively well reproduced in the calculations.

Finer grids in the CFD simulation tend to give better results. Also modelling of perforated sheets (such as the drum in the downcomer) as real structure rather than porous medium improves quality of results. Influence of porous medium as a substitute of a perforated sheet can be, in some extent, controlled by proper definition of direction-dependent resistance of the porous medium. Other investigated effects (turbulence model, wall function, position of outlet boundary) do not have an unambiguous influence on results. In general, the mixing along the flow path in the downcomer is under-predicted in all calculations. Disturbance in the inlet boundary conditions has significant impact on the flow pattern. This can be seen in experiment ROCOM-stat01, where a disturbance in turbulence or swirl intensity caused by the mixer is assumed to be responsible for an observed perturbation in the velocity distribution.

Slug mixing transients

For the ROCOM slug-mixing transient the qualitative agreement with measurements is good. The position of the lowest boron concentrations was captured fairly well. Quantitative good agreement with the level of the measured lowest boron concentrations was achieved. Considering the agreement of the measured and calculated boron concentration values at local positions, the deviations are larger than for the global minimum. For the ROCOM buoyant slug mixing transient, the local concentration was over-predicted, i.e. mixing was under-predicted.

For the Vattenfall slug-mixing transient, the minimum average boron concentration at the core inlet was captured very well by the CFD calculations. Also, the minimum boron concentration at the core inlet was captured very well. The distribution of low boron concentration across the core inlet plane was not, however, accurately modeled by the CFD calculation. The calculated position of the minimum concentration was found around 0.52R from the measured position of the minimum concentration (where R is the radius of the core inlet plane). The displacement of the concentration field is however mainly a rotational displacement. The difference in radial position of the minima is only about 0.15R. This could be relevant in reality, as a core is primarily different radially, as far as enrichment and reactivity are concerned. The results with the best agreement with measurement data were obtained using CFX-5. However, comprehensive studies were performed by Vattenfall using the FLUENT code. They are reported about in Annex 6 of [D11]

The CFD calculations for the FORTUM PTS buoyant transient mixing case modeled the main features of the flow quite well. Quantitatively there was some poor agreement for mixing in the main loop and for the mixing of the cold plume in the downcomer.

In the GIDROPRESS slug mixing transient the calculated minimum of the average core inlet temperature was lower than the experimental one. This was probably a consequence of the fact that the heat exchange between the cold slug and the warm walls was neglected in the CFD calculation. Other possible reasons are the pre-mixing in the main coolant pump

simulator, which is difficult to model, and the not exactly known initial position of the slug boundary.

The conclusions from the various calculations made were not unanimous. The results are promising, however, better agreement with measurements is needed for a CFD calculation to be an equivalent competitor to model tests. The continuous developments in computer capacity and in software capabilities will allow more extensive calculations to be made, enabling a reduction in errors from all sources, and increase the accuracy of CFD calculations. A methodology of quantitative comparison between measurement and calculation was developed and applied. It provided very useful information concerning a quantified engineering error assessment which can be used e.g. in reactor physics calculations concerning the consequences of boron dilution transients as a safety surcharge.

C.4.11.3 Development needs

This chapter gives a summary of the conclusions drawn from the WP4 and WP3 calculations concerning what is needed in the future to obtain more accurate CFD calculations for boron dilution transients and mixing in Pressurized Water Reactors. As shown earlier in this report agreement with measurements is not satisfactory in most cases. In order to get results from CFD calculations that are in better agreement with measurements, the following points have to be considered:

- More computational cells. No grid-independent solutions were presented in FLOMIX-R WP3 and WP4. More detailed modeling of internal structures might also be needed, which leads to additional cells.
- Shorter time-steps might in some cases be needed
- More advanced turbulence models, especially models that can cope with the specific features of the flow fields present in these applications, such as accelerating flow, flow-impingements and buoyancy. Further-improved Reynolds Stress Models or LES models (or hybrids between the two) might be needed to get better agreement with measurements. Better models of wall boundary layers (i.e. wall functions) are also probably needed.
- Some steady state cases have to be run as transients, as low-frequency fluctuations cannot be captured by a steady-state calculation. A transient calculation takes at least an order of magnitude longer time to perform than the corresponding steady-state calculation.

The computation time needed for a grid- and time step-independent CFD calculation using an advanced turbulence model is today too long (in the order of months). To be able to perform such calculations in a shorter period of time, the following aspects are important:

- Faster computers

- Faster and more accurate solvers and numerical schemes
- Lower costs for parallel licenses of CFD codes. Today, parallel license costs are higher than costs for hardware.
- Automatic time-stepping. The CFD code should choose the optimal time-step (within specified limits) and relaxation for minimizing computation time and ensuring convergence to specified residual levels.
- Improvements of the grid generation process in order to be able to, in an easier way than today, make high-quality hexahedral grids that would produce more accurate solutions with fewer cells.
- Grid adaptation (refine & coarsen) during transient runs to get refinements where there are strong gradients of (especially) concentration will also produce more accurate solutions with fewer cells.
- Refined porosity models can reduce the need for cells.

The Best Practice Guidelines for CFD have increased the awareness for what is needed to produce high-quality CFD calculations. These guidelines should be extended with more detailed recommendations, for example which turbulence model to use for different types of flow situations. The CFD code should also help the user to apply the Best Practice Guidelines, for example concerning quality checks for grid and solution.

More general conclusions, encompassing more scenarios relevant for nuclear power safety, are presented in the reports from the ECORA Project.

In spite of the large amount of work performed in FLOMIX-R there are still questions unanswered about the capability of CFD codes to model boron dilution transients and mixing in primary system in Pressurized Water Reactors (PWR). The continuous development in computer capacity and in software capabilities will continuously increase the ability to make accurate CFD calculations.

In general, it can be concluded, that CFD codes can be applied for calculations of turbulent mixing in one-phase flow in an engineering way.

D. Conclusion

A new quality of research in flow distribution and turbulent mixing inside the RPV of nuclear reactors has been achieved in the FLOMIX-R project. Experimental data on slug mixing with enhanced resolution in space and time have been gained from various test facilities covering different geometrical and flow conditions. The basic understanding of momentum controlled mixing in highly turbulent flow and buoyancy driven mixing in the case of relevant density differences between the mixing fluids has been improved significantly. An unique data base has been created for the CFD code validation for turbulent mixing applications in nuclear reactor safety analysis.

In WP1, the key mixing and flow distribution phenomena relevant for both safety analysis, particularly in steam line break and boron dilution scenarios, and for economical operation and the structural integrity have been identified. Based on this analysis, test matrices for the experiments are elaborated, guidelines for the documentation of the measurement data and for performing validation calculations with CFD codes are provided.

In WP 2 on slug mixing tests, experiments on slug mixing at the ROCOM and Vattenfall test facilities were performed. The measurement data were made available to the project partners for CFD code validation purposes. Additional slug mixing tests at the VVER-1000 facility of EDO Gidropress were made available. Two experiments on density driven mixing (one from ROCOM, one from the Fortum PTS facility) were selected for benchmarking.

In WP 3 on flow distribution in the cold legs and pressure vessel of the primary circuit, commissioning test measurements performed at the Paks VVER-440 NPP were used for the estimation of thermal mixing of cooling loop flows in the downcomer and lower plenum of the pressure vessel. A series of quasi steady state mixing experiments was performed at the ROCOM test facility. CFD methods were used for the simulation of the flow field in the primary circuit of operating real scale reactor. Computed results were compared to available measurement data, and conclusions are drawn concerning the usability and modelling requirements of CFD methods for that kind of application.

In WP 4 on validation of CFD codes, the strategy of code validation based on the Best Practice Guidelines was defined. A matrix of CFD code validation calculations was elaborated. CFD validation calculations on selected benchmark tests were performed. The CFD validation work was shared among the partners systematically based on the validation matrix. Systematic studies have been performed concerning the sensitivity of the calculated results from meshing, time step, boundary conditions, turbulence models and their model parameters. Optimum modelling options have been indentified for the different applications. A methodology of quantitative comparison between measurement and calculation was developed and applied. It provided very useful information concerning a quantified engineering error assessment which can be used e.g. in reactor physics calculations concerning the consequences of boron dilution transients as a safety surcharge.

The experience gained in the project will increase the competitiveness of the European research and engineering support organisations as well as nuclear electricity generating industry. Research and engineering organisations involved in the project are Serco Assurance, GRS, PSI and FZR. The project partners Fortum Nuclear Services and Vattenfall Utveckling are important representatives of European nuclear industries. The participation of the European higher education establishments in the project supports the education of nuclear experts. A number of students and PhD students was involved into the work. The NAS extension of the project was focused to VVER type reactors and was performed by partners from VVER operating countries, which were newly associated to the EU and now are EU member states. It will help to harmonise safety assessment approaches and to reach comparable level of understanding the relevant phenomena. A VVER nuclear power plant (NPP Paks) as well as organisations providing technical support for NPPs and nuclear authorities (VUJE Trnava, NRI Rez, AEKI Budapest) were participating in FLOMIX-R The general designer of VVER type reactors, Experimental and Design Organisation "Gidropress", was involved. Quality assurance practice for CFD was applied based on the ERCOFTAC BPG specified in the ECORA project for reactor safety analysis applications. Serco Assurance and Vattenfall experts are active in the ERCOFTAC. Most of the FLOMIX-R project partners were participating also in ECORA aimed at an assessment of CFD methods for reactor safety analyses. FLOMIX-R is contributing to the extension of the experimental data base on mixing and CFD applications to mixing problems. Recommendations on the use of CFD codes for turbulent mixing problems gained in FLOMIX-R were fed back to the ECORA and ERCOFTAC BPG.

References

[Ala95] Alavyoon, F., Hemström, B., Andersson, N. G., Karlsson; R. I.: "Experimental and Computational Approach to Investigating Rapid Boron Dilution Transients in PWRs," CSNI Specialist Meeting on Boron Dilution Reactivity Transients, State College, PA, USA, October 18-20, (1995).

[Cas00] Casey, M. and Wintergerste T., "Best Practice Guidelines", ERCOFTAC Special Interest Group on Quality and Trust in Industrial CFD, Report, 2000.

[BPG] ERCOFTAC Best Practice Guidelines, see http://www.ercoftac.org/

[CFX4] CFX-4.4 Flow Solver User Guide, AEA Technology, 2001

[CFX5] CFX-5.6 User Documentation, ANSYS-CFX, 2003

[D02] Rohde, U., Kliem, S., Toppila, T., Hemström, B., et al., Identification of mixing and flow distribution key phenomena, EU/FP5 FLOMIX-R report, FLOMIX-R-D02, FZ Rossendorf, Germany, 2002

[D05] S. Kliem, U. Rohde, T. Höhne, Data sets of the 1/5-scale slug mixing experiments at ROCOM facility, EU/FP5 FLOMIX-R report, FLOMIX-R-D05, FZ Rossendorf (Germany), 2003, incl.CDROM

[D06] B. Hemström: Data sets of the 1/5-scale slug mixing experiments at Vattenfall facility, EU/FP5 FLOMIX-R report, FLOMIX-R-D06, Vattenfall Utveckling, Älvkarleby (Sweden), 2004, incl. CDROM

[D07] S. Kliem, U. Rohde, T. Höhne (2003), Data sets on steady state mixing experiments at ROCOM facility, EU/FP5 FLOMIX-R report, FLOMIX-R-D07, FZ Rossendorf (Germany), 2003, incl.CDROM

[D09] S. Kliem, U. Rohde, B. Hemström et al.: "Description of the slug mixing and buoyancy related experiments at the different test facilities (Final report on WP2)", EU/FP5 FLOMIX-R report, FLOMIX-R-D09, FZ Rossendorf (Germany), October 2004

[D10] Toppila, T., Hemström, B., et al., Flow distribution in the primary circuit (Final report on WP 3), FLOMIX-R-D10, Fortum Nuclear Servives, Espoo (Finland), 2004

[D11] Hemström, B., et al., Validation of CFD codes based on mixing experiments (Final report on WP4), EU/FP5 FLOMIX-R report, FLOMIX-R-D11, Vattenfall Utveckling (Sweden), 2005

[D16] Y. Bezrukov et al., Documentation of slug mixing experiments of OKB Gidropress, EU/FP5 FLOMIX-R-D16, Podolsk (Russia), 2002

[D17] Klepac, J., Remis, J., Progress Report on VUJE Contribution to the WP3, FLOMIX-R-D17, VUJE Trnava (Slovakia), 2004

[Drä87] P. Dräger, "Macroscopic Coolant Mixing in Pressurized Water Reactors," Ph.D. Dissertation (in German), TH Zittau, Germany. (1987).

[Elt02] Elter, J., Experiment summary report, experimental investigation of thermal mixing phenomena in a six loop VVER type reactor, Paks Nuclear Power Plant Ltd, Safety Assessment Group, Flomix-R project February 2002

[Eub99] Final Report EUBORA – Concerted Action on Boron Dilution Experiments, Report AMM EUBORA(99) – P002, compiled by Harri Tuomisto, CEC, December 1999

[Flu] FLUENT Inc., see http://www.fluent.com/

[Flu03] FLUENT 6.1 user's guide, FLUENT Inc., 2003

[Gan97] Gango, P., Numerical boron mixing studies for Loviisa nuclear power plant, Nuclear engineering and design 177, 239-254, 1997

[Gra03] D. Grabovac (2003), Simulation von dreidimensionalen Strömungen im Primärkreis von Druckwasserreaktoren, Diplomarbeit am Lehrstuhl für Thermodynamik, Technische Universität München

[Gru94] Grundmann, U.; Rohde, U. (1994): "Investigations on a Boron Dilution Accident for a VVER-440 Type Reactor by the Help of the Code DYN3D", Proc. ANS Topical Meeting on Advances in Reactor Physics: Reactor Physics Faces the 21st Century, Knoxville (Tennessee), 11. - 15. April 1994, Vol. 3, pp. 464 – 471

[Hem95] Hemström B., Andersson N.G.: "Physical Modelling of Rapid Boron Dilution Transient - 1. Reynolds Number Sensivity Study for the Ringhals Case", Report № US 95:5. Vattenfall Utveckling AB, 1995.

[Höh98] T. Höhne, "Comparison of Coolant Flow and Mixing in a Scaled Model of the PWR KONVOI with the Processes in the Original Reactor (in German). Report FZR-210, Rossendorf, Germany. (1998).

[Hyt98] Y. Hytönen, "Two leakages induced by thermal stratification at the Loviisa power plant", NEA/CSNI specialists' meeting on: Experiences with thermal fatigue in LWR piping caused by mixing and stratification. 7 - 12 June 1998, Paris, France.

[Kli99] Kliem, S.; Höhne, T.; Rohde, U.; Weiß, F.-P. (1999): "Main Steam Line Break Analysis of a VVER-440 Reactor Using the Coupled Thermohydraulics System/3D-Neutron Kinetics Code DYN3D/ATHLET in Combination with the CFD Code CFX-4", Ninth International Topical Meeting on Nuclear Reactor Thermal Hydraulics (NURETH-9) San Francisco, California, October 3 - 8, 1999

[Kli04] Kliem, S.; U. Rohde, F.-P. Weiß (2004): „Core response of a PWR to a slug of under-borated water", Nucl. Eng. and Design 230, 121-132

[Lau74] Launder, B. E., et al., the Numerical Computation of Turbulent Flows, Computer Methods in Applied Mechanics and Engineering, 3, 269-289, 1974

[Log00] Logvinov S.A., Ulyanovsky V.N., Bezrukov Yu.A., Kozlov A.N.: " Mixing of coolant with different boron concentration at the VVER-1000 core inlet during RCP start-up", Proceedings of ANNUAL MEETING ON NUCLEAR TECHNOLOGY 2000, Bonn, 22-24 May 2000.

[Men02] Menter F. et al. "CFD Best Practice Guidelines for CFD Code Validation for Reactor Safety Applications". Deliverable D01 of the EC project ECORA, 2002.

[Nou86] H. P. Nourbakhsh, T. G. Theofanus, "A Criterion for Predicting Thermal Stratification Due to High-Pressure Injection in a Circulating Reactor Loop," *Nucl. Science and Engineering*, **94**, 77-79 (1986)

[Pra98] H.-M. Prasser, A. Böttger, J. Zschau, "A New Electrode-Mesh Tomograph for Gas Liquid Flows," *Flow Measurement and Instrumentation*, **9**, 111-119 (1998).

[Pra02] Prasser, H.-M.; Zschau, J.; Peters, D. et al.:" Fast wire-mesh sensors for gas-liquid flows - visualisation with up to 10 000 frames per second", Int. Congress on Advanced Nuclear Power Plants (ICAPP), June 9-13, 2002 - Hollywood Florida, USA, Proc. CD-ROM, paper #1055

[Pra03] H.-M. Prasser, G. Grunwald, T. Höhne, S. Kliem, U. Rohde, F.-P. Weiss, Coolant mixing in a Pressurized Water Reactor: Deboration Transients, Steam-Line Breaks, and Emergency Core Cooling Injection, Nuclear Technology 143 (1), p.37, 2003

[Roh97] Rohde, U.; Elkin, I.; Kalinenko, V. (1997): "Analysis of a boron dilution accident for WWER-440 combining the use of the codes DYN3D and SiTAP", Nuclear Eng. and Design 170, pp. 95 – 99

[Roh05] Rohde, U. et al. : "Fluid mixing and flow distribution in the reactor circuit – measurement data base", Nuclear Engineering and Design 235 (2005) 421-443

[Shi95] Shih, T.-H., et al., A New-Eddy-Viscosity Model for High Reynolds Number Turbulent Flows-Model Development and Validation. Computers Fluids 24(3), 227-238, 1995

[Tsi82] Tsimbalov, S., et al. (1982), Coolant temperature distribution at VVER-440 core inlet. Atomnaya Energiya 52 (5), 304-308

[Tuo87] Tuomisto, H.: "Thermal-hydraulics of the Loviisa reactor pressure vessel overcooling transients", Imatran Voima Oy, Research report IVO-A-01/87, 1987.

[Ul83] Ulrych, G., Weber, E., Neuere Ergebnisse zur Kühlmittelströmung in Druckwasserreaktoren, Atomkernenergie-Kerntechnik 42 4, 217-223.

[Ul98] Ul'yanovsky V.N., Bezrukov Yu.A., Logvinov S.A., Sali L.A.: "A Study on Mixing of Flows with Different Boron Concentration at the Core Inlet", Proceedings of the International Conference on Thermophysical Aspects of VVER-Type Reactor Safety Volume 1, Obninsk, May 26-29, 1998, p.p. 37-46.